

# **PART I**

---

## **RHEOLOGY**

COPYRIGHTED MATERIAL



---

# 1

---

## NEWTONIAN VISCOSITY OF DILUTE, SEMIDILUTE, AND CONCENTRATED POLYMER SOLUTIONS

ALEXANDER M. JAMIESON AND ROBERT SIMHA

*Department of Macromolecular Science and Engineering, Case Western Reserve University, Cleveland, OH, USA*

- 1.1 Background
- 1.2 Introduction
  - 1.2.1 Rheology in steady shear flow: shear viscosity
  - 1.2.2 Concentration-dependent regimes of viscometric behavior
  - 1.2.3 Measurement of shear viscosity
- 1.3 Viscometric contribution of isolated macromolecules: intrinsic viscosity
  - 1.3.1 Intrinsic viscosity and hydrodynamic volume
  - 1.3.2 Intrinsic viscosity and molecular weight
- 1.4 Intrinsic viscosity and the structure of rigid particles
  - 1.4.1 Effect of particle shape
  - 1.4.2 Effect of particle porosity
- 1.5 Intrinsic viscosity and the structure of linear flexible polymers
  - 1.5.1 Role of hydrodynamic interactions
  - 1.5.2 Flory–fox equation
  - 1.5.3 Two-parameter and quasi-two-parameter theories
- 1.6 Intrinsic viscosity and the structure of branched polymers
  - 1.6.1 Branched polymers in theta solvents
  - 1.6.2 Branched polymers in good solvents
- 1.7 Intrinsic viscosity of polyelectrolyte solutions
  - 1.7.1 Role of electrostatic interactions
  - 1.7.2 Effect of ionic strength

- 1.7.3 Experiment versus theory
- 1.8 Intrinsic viscosities of liquid-crystal polymers in nematic solvents
  - 1.8.1 Intrinsic Miesowicz viscosities
  - 1.8.2 Intrinsic Leslie viscosities
- 1.9 Viscosity of semidilute and concentrated solutions
  - 1.9.1 Empirical concentration and molecular-weight scaling laws
  - 1.9.2 Predictive models for solutions of flexible neutral polymers
  - 1.9.3 Viscosity of branched polymers in semidilute and concentrated regimes
  - 1.9.4 Predictive models for solutions of stiff and semi-stiff neutral polymers
  - 1.9.5 Concentration scaling laws for polyelectrolyte solutions
- 1.10 Summary, conclusions, and outlook

## 1.1 BACKGROUND

We review current understanding of the molecular hydrodynamic origin of the shear viscosity of polymer solutions. Viscometric measurements have played an important historical role in advancing our knowledge of macromolecular structure and dynamics in solution. For example, the anomalously large viscosities of dilute polymer solutions were a key component of the arguments espoused by Hermann Staudinger in advancing the macromolecular hypothesis. Robert Simha's theoretical analysis of the viscosity of impermeable ellipsoidal particles enabled the application of viscometric measurements to determine the native molecular shapes of proteins in solution. Determination of intrinsic viscosities remains a widely used technique to obtain information about macromolecular structure in solution. The concentration dependence of polymer solution viscosity is influenced by thermodynamically-driven changes in molecular conformation, as well as intermolecular interactions, which may be direct (hard core, van der Waals, dipolar, electrostatic, hydrogen bonding) or indirect (hydrodynamic). Understanding the role of these interactions and their relationship to polymer structure is basic to controlled processing of polymers in the solution state.

## 1.2 INTRODUCTION

### 1.2.1 Rheology in Steady Shear Flow: Shear Viscosity

Figure 1.1 illustrates schematically a shear strain,  $\gamma$ , produced by applying a force  $F$  to the upper face of a cubic volume of a fluid. Relative to the three axes shown in Figure 1.1 (i.e., 1 = direction of flow, 2 = shear gradient, 3 = vorticity axis), one may define three materials parameters relating the shear stress tensor,  $\sigma$ , to the shear rate,  $\dot{\gamma}$  [Macosko, 1994]:

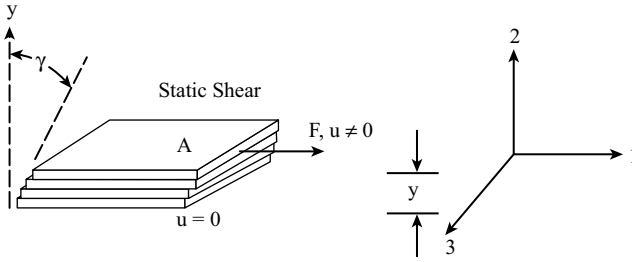


**FIGURE 1.1** Schematic of a shear deformation:  $\gamma$  = shear strain,  $\dot{\gamma}$  ( $\text{s}^{-1}$ ) = rate of shear =  $du/dy = u(\text{velocity})/y(\text{thickness})$ ,  $\sigma_{12}$  ( $\text{dyn/cm}^2$ ) = shear stress =  $F(\text{force})/A(\text{area})$ .

Steady shear viscosity:

$$\eta(\dot{\gamma}) = \frac{\sigma_{12}(\dot{\gamma})}{\dot{\gamma}} \quad (1.1)$$

First normal stress coefficient:

$$\psi_1(\dot{\gamma}) = \frac{N_1}{\dot{\gamma}^2} = \frac{\sigma_{11} - \sigma_{22}}{\dot{\gamma}^2} \quad (1.2)$$

Second normal stress coefficient:

$$\psi_2(\dot{\gamma}) = \frac{N_2}{\dot{\gamma}^2} = \frac{\sigma_{22} - \sigma_{33}}{\dot{\gamma}^2} \quad (1.3)$$

In general, each of these parameters depends on the shear rate. This dependence is associated with the fact that the macromolecule rotates around the vorticity axis in the shear flow, and if flexible, at sufficiently high shear rate becomes distorted and oriented in the direction of flow [Hsieh and Larson, 2004; Teixeira et al., 2005]. However, at sufficiently low shear rates, there is a regime where any distortion and orientation of the macromolecular structure by the flow field is erased by Brownian motion on a time scale much faster than the flow rate. Here we focus on this Newtonian regime, where  $\eta(\dot{\gamma})$ ,  $\psi_1(\dot{\gamma})$ , and  $\psi_2(\dot{\gamma})$  become independent of  $\dot{\gamma}$ , and we can expect that the viscometric behavior is related to the equilibrium macromolecular structure.

## 1.2.2 Concentration-Dependent Regimes of Viscometric Behavior

Our discussion of viscometric properties of polymer solutions is organized into four concentration regimes: isolated chains (the limit of infinite dilution) and dilute, semidilute, and concentrated solutions. The first two refer to situations where the chains are, respectively, noninteracting and weakly interacting via direct as well as indirect (hydrodynamic) interactions. The latter two regimes refer to concentrations where topological interactions of polymer molecules (i.e., chain entanglements, restricted rotational and translational degrees of freedom) may become important. The

boundary between dilute and semidilute regimes is the overlap concentration, often defined to be  $c^* = M/N_A R_g^3$ , where  $M$  is the molar mass of the macromolecule,  $R_g$  its radius of gyration, and  $N_A$  is Avogadro's number. Numerically,  $c^*$  defined in this way is close to the concentration where the hydrodynamic volumes,  $V_H$ , of the macromolecule begin to overlap each other; that is,  $(cN_A/M)V_H \sim 1$ , which corresponds to  $c \sim 2.5/[\eta]$ , where  $[\eta]$  is a viscometric parameter called the intrinsic viscosity, which is discussed below.

The boundary  $c^{**}$  between the semidilute and concentrated regimes is defined by the appearance of phenomena related to bulk properties of the polymeric solute (e.g., glass transition, liquid-crystal transition, gelation). At a concentration substantially above  $c^*$ , which may be above or below  $c^{**}$ , there is a well-established change in the viscometric properties of solutions of flexible polymers, associated with a change in macromolecular dynamics, which is referred to as the entanglement concentration,  $c_e$ . The transition from nonentangled to entangled behavior requires a minimum molecular weight,  $M_e$ , independent of concentration but dependent on polymer structure: The more flexible the polymer, the smaller is  $M_e$ .  $M_e$  is the molecular weight where the entanglement transition occurs in the bulk polymer, and as the molecular weight increases beyond  $M_e$ , the entanglement transition in solution occurs at a progressively lower concentration. Based on a theoretical argument that the transition to entanglement dynamics occurs when the number of entanglements per chain exceeds a critical value, determined to be  $\sqrt{18\pi^2}$ , Klein [1978] proposed the following expression relating the entanglement concentration to the molar mass of the polymer:

$$\log M = \log \frac{(18\pi^2)^{1/2} M_0 C_\infty}{j(\bar{v})^n \sin^2(\theta/2)} - n \log c_e \quad (1.4)$$

where  $M_0$  is the monomer molar mass,  $\bar{v}$  the monomer partial specific volume,  $j$  the number of backbone units per monomer,  $\theta$  the polymer backbone bond angle, and  $C_\infty$  the asymptotic characteristic ratio of the polymer:

$$C_\infty = \lim_{M \rightarrow \infty} \frac{6R_g^2}{j(M/M_0)\ell^2} \quad (1.5)$$

where  $\ell$  is the backbone bond length. In Eq. (1.4), the scaling parameter  $n = 1/(3\nu - 1)$ , where  $\nu$  is the exponent characterizing the molar mass dependence of  $R_g$  (i.e.,  $R_g \sim M^\nu$ ). Thus, in the semidilute and dilute concentration regimes, we may identify two possibilities: semidilute unentangled and semidilute entangled, and concentrated unentangled and concentrated entangled.

### 1.2.3 Measurement of Shear Viscosity

Three geometric arrangements are commonly used to measure fluid viscosity: capillary, coquette, and cone and plate. For a more complete discussion of the principles

of rheometry, the reader should consult a suitable textbook, such as that by Macosko [1994]. Here we limit ourselves to a simplified treatment for illustrative purposes. In capillary instruments, the fluid is forced through the capillary by application of pressure. The basis for viscosity determination is Poiseuille's equation for steady-state laminar flow. For dilute solutions, this may be written

$$\eta = \frac{\pi r_c^4 \Delta P t}{8VL_c} \quad (1.6)$$

where  $r_c$  and  $L_c$  are the radius and length of the capillary,  $\Delta P$  is the pressure drop,  $V$  is the volume of fluid that passes through the capillary, and  $t$  is the flow time. The corresponding shear stress at the capillary wall is

$$\sigma = \frac{r_c P}{2L_c} \quad (1.7)$$

and the rate of shear at the wall for a Newtonian fluid is

$$\dot{\gamma} = \frac{4V}{\pi r_c^3} \frac{1}{t} \quad (1.8)$$

The Ubbelohde capillary viscometer is a simple device which allows one to determine the flow time of a fixed volume of liquid, passing through a capillary of specified length and diameter. The pressure drop is hydrostatic  $P = (h_1 - h_2)\rho g$ , where  $h_1$  and  $h_2$  are the initial and final meniscus levels,  $\rho$  is the fluid density, and  $g$  is the gravitational acceleration (standard value at sea level = 9.8066 m/s<sup>2</sup>). Frequently, it is necessary only to determine the relative viscosity,  $\eta_r = \eta/\eta_s$ , where  $\eta_s$  is the solvent viscosity (i.e., we take the ratio of flow times of solution and solvent). From Eq. (1.6),

$$\eta_r = \frac{\rho t}{\rho_s t_s} \quad (1.9)$$

where the numerator refers to solution, the denominator to solvent. Moreover, since measurement of the viscometric contribution of isolated chains involves extrapolation of experimental values of  $\eta_r$  to zero concentration, it follows that the density of the solution will extrapolate to the density of the solvent (i.e.,  $\rho \rightarrow \rho_s$ ), and hence we can neglect the small density correction and write

$$\eta_r = \frac{t}{t_s} \quad (1.10)$$

One must choose a sufficiently narrow capillary to have flow times long enough that one is in the Newtonian region (typically,  $t > 200$  s) and also to avoid a kinetic energy correction to compensate for acceleration of the fluid during the measurement.

If one needs to investigate the dependence of  $\eta$  on shear rate,  $\dot{\gamma}$ , one must have access to a rheometer, an instrument that can characterize the dependence of viscosity on shear rate, thus enabling an extrapolation to the Newtonian limit. Typically, such measurements are conducted in Couette (concentric cylinder) or cone and plate geometry. In the Newtonian limit, for Couette geometry, when the inner cylinder is rotated, and provided that the gap between the inner and outer cylinder is small (i.e.,  $R_i/R_o < 0.99$ , where  $R_i$  and  $R_o$  are the radii of the inner and outer cylinders), the shear stress on the wall of the outer (resting) cylinder is

$$\sigma_o = \frac{M_T}{2\pi R_o^2 L} \quad (1.11)$$

and the average shear rate in the gap is

$$\dot{\gamma}(R_i) = \frac{\bar{R}}{R_o - R_i} \Omega_i \quad (1.12)$$

where  $\bar{R} = (R_o + R_i)/2$  is the midpoint of the gap and  $L$  is the cylinder length. The viscosity is proportional to the torque,  $M_T$ , exerted on the resting cylinder, divided by the angular velocity of rotation,  $\Omega$ :

$$\eta = \frac{R_o - R_i}{2\pi R_o^2 \bar{R} L} \frac{M_T}{\Omega_i} \quad (1.13)$$

In this device one can either exert a constant torque,  $M_T$ , and measure the angular velocity of the rotating cylinder,  $\Omega$  (controlled stress), or impose a constant angular rotation,  $\Omega$ , and measure the torque,  $M_T$  (controlled strain).

In the capillary and Couette (as well as rotating parallel-plate) geometries, a gradient of shear exists in the radial direction. The cone and plate geometry has the advantage that constant shear strain and shear rate are applied at all radial distances. When the cone angle  $\varpi$  is very small,  $\varpi < 0.1$  rad, analysis of the equations of motion indicates that the shear stress on the plate is

$$\sigma = \frac{3M_T}{2\pi R^3} \quad (1.14)$$

where  $R$  is the cone radius. The corresponding shear rate is

$$\dot{\gamma} = \frac{\Omega}{\varpi} \quad (1.15)$$

where  $\Omega$  is the angular velocity of the cone, and hence the viscosity is

$$\eta = \frac{3M_T \varpi}{2\pi R^3 \Omega} \quad (1.16)$$

### 1.3 VISCOMETRIC CONTRIBUTION OF ISOLATED MACROMOLECULES: INTRINSIC VISCOSITY

#### 1.3.1 Intrinsic Viscosity and Hydrodynamic Volume

The basis for relating the viscosity of a polymer solution to the structure of a dissolved polymer can be traced to Albert Einstein [1906, 1911], who showed, for spherical particles dispersed in a viscous medium, that the solution viscosity,  $\eta$ , is increased relative to that of the medium,  $\eta_s$ , by

$$\eta = \eta_s(1 + 2.5\phi) \quad (1.17)$$

where  $\phi$  is the volume fraction of the spheres. This result holds for a dispersion of hydrodynamically noninteracting particles, that is, it is assumed that the shear flow of solvent around a given sphere does not perturb the flow around a neighboring sphere. Inserting an expression for  $\phi = (c/M)N_A V_H$ , where  $V_H$  is the hydrodynamic volume,  $M$  is molecular weight,  $N_A$  is Avogadro's number, and rearranging, we obtain

$$\frac{1}{c} \left( \frac{\eta}{\eta_s} - 1 \right) = 2.5 \frac{N_A V_H}{M} \quad (1.18)$$

or

$$\frac{\eta_{sp}}{c} = 2.5 \frac{N_A V_H}{M} \quad (1.19)$$

where  $\eta_{sp} = (\eta/\eta_s - 1) = \eta_r - 1$  is the specific viscosity and  $\eta_r = \eta/\eta_s$  is the relative viscosity.

In reality, at any finite concentration, flows around near-neighbor spheres are likely to interfere with each other, so to compare Eqs. (1.18) and (1.19) with experiment, we need to extrapolate to zero concentration to eliminate the contribution of such hydrodynamic interactions between particles:

$$\lim_{c \rightarrow 0} \frac{\eta_{sp}}{c} = [\eta] = \frac{2.5 N_A V_H}{M} \quad (1.20)$$

The quantity  $[\eta]$  in Eq. (1.20) is called the intrinsic viscosity. Clearly,  $[\eta]$  depends on particle structure.

#### 1.3.2 Intrinsic Viscosity and Molecular Weight

For impermeable spheres of uniform density  $\rho_p = M/N_A V_h$ ,  $[\eta]$  is small and independent of molecular weight:

$$[\eta] = \frac{2.5}{\rho_p} \quad \text{mL/g} \quad (1.21)$$

For polymer chain molecules, which expand and entrap huge numbers of solvent molecules, the hydrodynamic volume is large and generally a strong function of molecular weight:

$$V_H \sim M^\varepsilon \quad (1.22)$$

where, intuitively, one expects that the exponent,  $\varepsilon$ , will depend not only on the degree of swelling of the polymer chain [i.e., on the thermodynamic interaction with the solvent (excluded volume effect)] and on the chain stiffness (conformation), but also on the hydrodynamic behavior of the chain. For flexible chain molecules, in the nondraining limit (strong trapping of the solvent within the coil), as we discuss further below, intuition indicates that the hydrodynamic volume is that of an impermeable sphere whose radius is approximately the radius of gyration (i.e.,  $V_h \sim R_g^3$ ), and hence since  $R_g \sim M^\nu$ , where  $\nu=0.5$  under theta conditions and  $\nu=0.6$  in good solvents, one deduces that  $\varepsilon$  varies from 1.5 for theta solvents to 1.8 for very good solvents. Thus, it follows that  $[\eta]$  is very large and strongly dependent on  $M$ :

$$[\eta] = KM^{\varepsilon-1} = KM^a \quad (1.23)$$

where  $0.5 < a < 0.8$ . Equation (1.23), referred to as the Mark–Houwink–Sakurada equation, is the basis for molecular-weight determination of polymers from  $[\eta]$  via a calibration experiment in which  $K$  and  $a$  are estimated from polymer fractions of narrow polydispersity. In such a case, assuming that the calibration is based on monodisperse fractions, the molecular weight average,  $\bar{M}_v$ , of a polydisperse unknown determined via Eq. (1.23) is

$$\bar{M}_v = \left( \frac{\sum_i c_i M_i^a}{\sum_i c_i} \right)^{1/a} \quad (1.23a)$$

Graphically, two equations may be used to determine  $[\eta]$ : The Huggins equation is

$$\frac{\eta_{sp}}{c} = [\eta] + k_1[\eta]^2 c \quad (1.24)$$

The Kraemer equation is

$$\frac{\ln \eta_r}{c} = [\eta] - k'_1[\eta]^2 c \quad (1.25)$$

where  $k_1 + k'_1 = \frac{1}{2}$ . The latter follows since

$$\begin{aligned} \ln \eta_r &= \ln(1 + \eta_{sp}) \approx \eta_{sp} - \frac{\eta_{sp}^2}{2} \\ &= c[\eta] + k_1[\eta]^2 c^2 - \frac{c^2[\eta]^2}{2} \end{aligned}$$

that is,

$$\frac{\ln \eta_r}{c} = [\eta] + \left( k_1 - \frac{1}{2} \right) [\eta]^2 c \quad (1.26)$$

It is important to realize that these equations apply only to sufficiently dilute solutions. Specifically, when  $c[\eta]$  becomes comparable to or larger than unity, one has to consider the contribution of higher-order concentration terms. As discussed earlier, this is related to the fact that when  $c[\eta] \sim 1$ , the solution becomes crowded with particles, and third-order interparticle interactions strongly influence particle motion. Thus, when carrying out experiments to determine  $[\eta]$ , to ensure that one is at sufficiently high dilution, it is suggested that one perform analyses utilizing both Eqs. (1.24) and (1.25) to confirm that extrapolation yields a common intercept.

## 1.4 INTRINSIC VISCOSITY AND THE STRUCTURE OF RIGID PARTICLES

### 1.4.1 Effect of Particle Shape

Jeffrey [1923] extended Einstein's analysis to flow around an impermeable, rigid ellipsoid of revolution, and Simha [1940] further incorporated the effect of Brownian motion, deriving an equation of the form

$$\eta = \eta_s(1 + \nu\phi) \quad (1.27)$$

where the coefficient  $\nu$  depends on the shape of the ellipsoid. Simha [1940] derived explicit expressions for the coefficient  $\nu$  as a function of the axial ratio,  $J = a/b$ , for prolate and oblate ellipsoids. In the limit  $J \gg 1$ , for prolate ellipsoids (semiaxes  $a$ ,  $b$ , with  $a > b$ ), the expressions derived reduce to

$$\nu = \frac{J^2}{15(\ln 2J - 3/2)} \quad (1.28)$$

and for oblate ellipsoids (semiaxes  $a$ ,  $a$ ,  $b$ , with  $a < b$ ),

$$\nu = \frac{16}{15} \frac{J}{\tan^{-1} J} \quad (1.29)$$

Thus, from Eq. (1.29) we deduce that

$$[\eta]M = \nu N_A V_H \quad (1.30)$$

where  $V_H$  is the equivalent hydrodynamic sphere and  $\nu$  is as given in Eqs. (1.28) and (1.29).

Using the Simha formula, viscometric analysis could, for the first time, be applied to macromolecular species [Mehl et al., 1940] and subsequently has been utilized extensively to extract information about the structure of proteins and surfactant micelles [Harding and Colfen, 1995]. For such species,  $V_H$  can be expressed in terms of the specific volume of the macromolecule and a solvation number:

$$V_H = \frac{M}{N_A} (\bar{v}_2 + \delta_s v_1^0) \quad (1.31)$$

where  $\bar{v}_2$  is the partial specific volume,  $\delta_s$  is the bound solvent (grams solvent/gram polymer), and  $v_1^0$  is the molar volume of solvent. Thus, from Eqs. (1.28) and (1.29), for a particle with hydrodynamic volume  $V_H$ ,  $\nu = 2.5$  if it is of spherical shape and  $\nu > 2.5$  if it is nonspherical. The increase in viscosity is larger on dissolving nonspherical particles than spherical particles of equal hydrodynamic volume. Numerical methods have been developed to compute an equivalent ellipsoid of revolution from intrinsic viscosity data [Harding and Colfen, 1995]. However, Eqs. (1.30) and (1.31) contain two unknowns,  $\nu$  and  $\delta$ , and hence cannot be solved uniquely [Harding and Colfen, 1995] unless two samples of the same macromolecule with different molar masses are available, or if data on preferential hydration are available (e.g., via densitometry) [Timasheff, 1998]. Typical values of  $\delta$  reported for proteins range from 0.27 g/g (ribonuclease) to 0.44 g/g (deoxyhemoglobin) [Carrasco et al., 1999].

Certain macromolecular species are modeled more accurately as a cylinder rather than an ellipsoid. Examples include short DNA fragments and rodlike viruses such as tobacco mosaic virus (TMV). Extensive theoretical studies of the hydrodynamic properties of cylindrical particles have been carried out. These have been recently reviewed by Ortega and de la Torre [2003], who have extended prior calculations using the bead-shell model to short cylinders and disks. For long cylinders of length  $L$  and cross-sectional diameter  $d$ , and hence axial ratio  $J = L/d$ , such analysis leads to

$$[\eta] = \frac{2}{45} \frac{\pi N_A L^3}{M(\ln J + C_\eta)} \quad (1.32)$$

where the end-effect term  $C_\eta$  has been evaluated numerically in the limit  $L \rightarrow \infty$  as  $C_\eta = 2 \ln 2 - 25/12$  [Yamakawa, 1975]. Expressions extending to short cylinders and disks have been formulated by Ortega and de la Torre [2003] in terms of the Einstein-Simha coefficient:

$$[\eta] = \nu \frac{\pi N_A L^3}{4J^2 M} \quad (1.33)$$

where  $\nu$  may be approximated to within 1.2% by [Ortega and de la Torre, 2003]

$$\nu = \begin{cases} 2.77 - 0.2049(\ln J)^2 - 0.8287(\ln J)^3 - 0.1916(\ln J)^4 & \text{for } J < 1 \quad (1.34) \\ 2.77 + 1.647(\ln J)^2 - 1.211(\ln J)^3 + 0.6124(\ln J)^4 & \text{for } J > 1 \quad (1.35) \end{cases}$$

As noted above, for ellipsoidal particles, determination of the dimensions  $L$  and  $d$  from  $[\eta]$  data via Eqs. (1.32) to (1.35) requires prior knowledge of the molecular hydrodynamic volume [Eq. (1.31)], which requires information on the partial specific volume and the bound solvent. This requirement can be circumvented by combining information on two hydrodynamic properties: for example, the intrinsic viscosity and the translational diffusion coefficient in the limit  $c \rightarrow 0$ ,  $D_t^0$ . Thus, the Flory–Mandelkern coefficient,  $\beta_{\text{FM}}$ , given by

$$\beta_{\text{FM}} = \frac{\eta_s}{k_B T} (M[\eta])^{1/3} D_t^0 \quad (1.36)$$

should, in principle, be sensitive to particle shape. Unfortunately, this parameter is very insensitive to macromolecular conformation [McDonnell and Jamieson, 1977]. However, for cylindrical particles, Ortega and de la Torre [2003] find that a combination of the end-over-end rotational diffusion coefficient and the translational diffusion coefficient are sufficiently sensitive to allow determination of the axial ratio,  $J$ , and hence of the cylinder dimensions,  $L$  and  $d$ .

Haber and Brenner [1984] demonstrated that the scalar energy dissipation arguments used by Einstein [1906, 1911] and Simha [1940] yield results in agreement with a more complete tensorial dynamical analysis and, using the latter approach, derived analytical results for general triaxial ellipsoidal particles. For rigid particles of irregular geometry, numerical methods to predict the intrinsic viscosity have been formulated, which integrate the hydrodynamic resistance over the surface of the macromolecule. Three general approaches have been described. One method models complex particles as an agglomeration of hydrodynamic point sources (the hydrodynamic bead model) [Garcia de la Torre et al., 2000], which interact via an Oseen-type hydrodynamic interaction; a second approach (the boundary element method) solves the Stokes integral equation for a particle whose surface is constructed from an array of flat polygons [Hahn and Aragon, 2006]; and a third method (numerical path integration method) is based on an analogy between hydrodynamics and electrostatics [Hahn et al., 2004]. The accuracy of each of the finite element methods increases as the number of finite elements,  $N$ , increases, but so does the computational time. The numerical path integration method claims an advantage [Mansfield et al., 2007] since, for such objects, the computational time scales as  $O(N)$ , whereas for the other two methods, the computational time scales as  $O(N^3)$ . Each of these methods enables the introduction of microscopic surface detail into the computation, and offers, for example, the possibility of obtaining a consistent picture of protein hydration and of determining from viscometric measurements whether the solution conformation of a protein differs from that in the crystalline state.

#### 1.4.2 Effect of Particle Porosity

The question of the effect of the permeability of a particle on its hydrodynamic behavior in a continuum fluid was addressed by Debye and Bueche [1948] and Brinkman [1947]. In viscosity experiments, the penetration of the particle by the streaming fluid

may be expected to reduce the effective hydrodynamic radius and hence decrease the intrinsic viscosity. The Debye–Bueche–Brinkman theory has been utilized to relate certain anomalies in the intrinsic viscosity and translational diffusion coefficients of globular proteins to surface porosity [McCammon et al., 1975] and to predict the intrinsic viscosity of core–shell particles with an impermeable core and a permeable shell [Zackrisson and Bergenholtz, 2003], as well as the hydrodynamics of fractal aggregates with radially varying permeability [Veerapaneni and Wiesner, 1996].

We discussed above the increase in viscosity that results when rigid particles are dispersed in a low-molar-mass Newtonian fluid [Eq. (1.30)]. It should be pointed out that a similar increase in viscosity is to be anticipated when such a particle is dispersed in a polymeric liquid. Indeed, experiment indicates that such an effect is observed, but only if the size of the added particle is substantially larger than the size of the chains in the polymeric liquid. Mackay et al. [2003] report that when the size of the added particle becomes comparable to or smaller than that of the polymer chains, the viscosity of the mixture decreases with particle concentration (i.e., non-Einstein-like behavior is observed). The authors note that the precise origin of this effect is unclear but rule out that the phenomenon is due to a change in entanglement density. Instead, noting that the addition of the nanosized particles also results in a decrease in the polymer glass transition temperature, they attribute the viscosity decrease to the increase in free volume afforded by the presence of the nanosized particles, possibly coupled with a change in configuration of the polymer chains [Mackay et al., 2003]. This observation implies a negative intrinsic viscosity, a phenomenon observed earlier in solutions of flexible coils, as discussed below, and indeed requires that the dissolved macromolecule or particle create some kind of change in the structure of the solvent.

## 1.5 INTRINSIC VISCOSITY AND THE STRUCTURE OF LINEAR FLEXIBLE POLYMERS

### 1.5.1 Role of Hydrodynamic Interactions

Equations (1.28) to (1.30) do not apply to flexible chain molecules, which are not rigid and can exhibit fluctuations in conformation. Here, one approach is to ignore shape anisometry and to make the assumption  $\nu = 2.5$  in Eq. (1.30). This enables determination of an impermeable sphere-equivalent hydrodynamic volume for flexible chain macromolecules from  $[\eta]$ , provided that  $M$  is known. As noted above, the Mark–Houwink–Sakurada equation [Eq. (1.23)] is often used to relate  $[\eta]$  to  $M$  when dealing with flexible coils.

Two early theoretical models to rationalize this result were pursued: the porous-sphere model of Debye and Bueche [1948], in which spherical beads representing the monomers are distributed uniformly in a spherical volume, and the more realistic “pearl necklace” model, proposed by Kuhn and Kuhn [1943], in which the beads are linked together by infinitely thin linkages. For each of these models, the principal challenge was to describe the flow of solvent around and within the volume occupied

by the beads. Two limiting cases can be defined: one, referred to as the free-draining limit, assumes that solvent freely penetrates within the coil volume, so that each bead contributes equally to the frictional resistance. Such a case requires the beads to be far apart, and, intuitively, is more likely if the polymer chain is very stiff or highly expanded, as in a good solvent. Such a case was discussed by Kuhn and Kuhn [1943] and leads to a result of the form of Eq. (1.23) with an exponent  $a = 1$ . In the other limit, referred to as nondraining, the hydrodynamic perturbation of the solvent flow by the beads is so large that the solvent is effectively trapped within the coil, which may therefore be treated as a rigid, hydrodynamically equivalent sphere. Such behavior seems more likely if the beads are close together (i.e., if the chain is flexible and in a poor solvent). The behavior of the pearl necklace model with variable hydrodynamic interaction was discussed by Kirkwood and Riseman [1948] and leads to a result of the form of Eq. (1.30) with  $\nu = 2.5$ :

$$[\eta] = 2.5 \left( \frac{4\pi}{3} R_h^3 \right) \frac{N_A}{M} F(\Xi) \quad (1.37)$$

where

$$\Xi = \frac{4}{9\pi^{3/2}} \frac{Zf_0}{\eta_0 R_g} \quad (1.38)$$

and  $Z$  is the number of beads in the chain,  $f_0$  is the frictional coefficient of a single bead, and  $\eta_0$  is the solvent viscosity, and  $R_H$  is the radius of the equivalent sphere. In the non-draining limit,  $F(\Xi) \rightarrow 1$ , and  $R_H$  is found [Auer and Gardner, 1955] to be proportional to the radius of gyration,  $R_H = 0.87R_g$ . Thus, from Eq. (1.37), an equation of the form of Eq. (1.23) follows with  $0.5 < a < 0.8$ , which, as pointed out by Flory and Fox [1951], is quite consistent with experimental data for flexible coils, which therefore appear to conform closely to nondraining hydrodynamics. For completeness, we note that Rouse [1953] and Zimm [1956] subsequently discussed the viscoelastic behavior of solutions of flexible chain molecules, modeled as a chain of beads, connected to each other by flexible springs. They obtained predictions for the various rheological functions, expressed in terms of the spectrum of conformational relaxation times,  $\tau_i$ , which depend on the strength of the hydrodynamic interaction. For the intrinsic viscosity, their analyses lead to [Rouse, 1953; Zimm, 1956]

$$[\eta] = \frac{RT\tau_1 S}{M\eta_s} \quad (1.39)$$

where  $S = \sum \tau_i / \tau_1$  and  $\tau_1$  is the longest relaxation time. In the free-draining limit [Rouse, 1953; Ferry, 1980],  $S = \pi^2/6 = 1.645$ ; in the nondraining limit [Zimm, 1956; Ferry, 1980],  $S = 2.369$ .

In reality, Eq. (1.23), with molar mass independent values of  $K$  and  $a$  can only be applied at relatively high molecular weights,  $M$ . When examined over a broad range of  $M$ , encompassing oligomeric to high polymers, it is found that a more complex

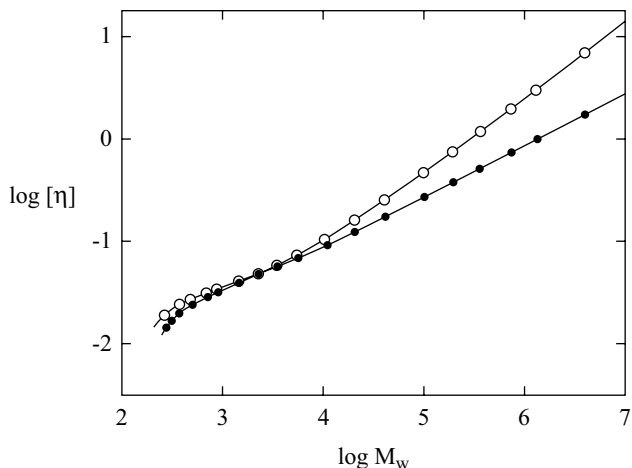


**FIGURE 1.2** Double-logarithmic plots of  $[\eta]$  (in dL/g) against  $M$ , for a-PS:  $\circ$ , in toluene at  $15.0^\circ\text{C}$ ;  $\bullet$ , in cyclohexane at  $34.5^\circ\text{C}$ . (From Abe et al. [1993a], with permission. Copyright © 1993 American Chemical Society.)

relationship generally exists. Moreover, the nature of this relationship depends not only on solvent quality, but also on the microstructure of the polymer. The most extensive studies of such issues have been carried out by Yamakawa and co-workers [Abe et al., 1993, 1994; Tominaga et al., 2002], who have determined the molecular weight dependence of the intrinsic viscosities of vinyl polymers of specified stereochemical composition (fixed fraction of racemic dyads). For example, in Figure 1.2 we show a plot of  $\log [\eta]$  versus  $\log M$  for atactic polystyrene (a-PS) in a very good solvent (toluene at  $15^\circ\text{C}$ ) and a theta solvent (cyclohexane at  $34.5^\circ\text{C}$ ). At high molecular weight,  $M_w > 5.0$  kg/mol, the  $\log [\eta]$ – $\log M$  relationship conforms to Eq. (1.23), with exponents,  $\nu$ , of 0.72 in toluene and 0.5 in cyclohexane, but deviation from Eq. (1.23) occurs at lower  $M$ . Also deduced from Figure 1.2 is the fact that at molar masses  $M_w \leq 5.0$  kg/mol, the data for either solvent coincide with each other, indicating that the unperturbed dimensions of a-PS are the same in toluene and in cyclohexane at the theta temperature. These data are consistent with earlier measurements [Abe et al., 1993a] of the radius of gyration,  $R_g$ , as a function of the weight-average degree of polymerization,  $x_w = M_w/M_m$ , shown in Figure 1.3, where they are plotted in the form of the ratio of the quantity  $R_g^2/x_w$  divided by the corresponding quantity for unperturbed chains in the limit of very high molecular weight,  $(R_{g,0}^2/x_w)_\infty$ . As shown in Figure 1.3, the ratio  $(R_g^2/x_w)/(R_{g,0}^2/x_w)_\infty$  coincides for a-PS in both solvents until the weight-average degree of polymerization,  $x_w \geq 50$ , when the values in cyclohexane reach the asymptotic value,  $(R_{g,0}^2/x_w)_\infty$ , whereas the values in toluene diverge increasingly from those in cyclohexane, due to the excluded volume effect.

As noted above, for impermeable linear flexible coils, based on the assumption that  $[\eta] \sim R_g^3/M$ , the exponent in Eq. (1.23) is expected to vary between 0.5 for

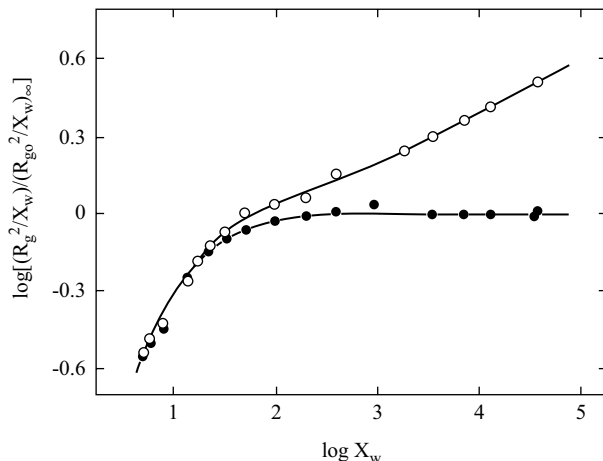


**FIGURE 1.3** Double-logarithmic plots of  $(R_g^2/x_w)/(R_{g,0}^2/x_w)_\infty$  against  $x_w = M_w/M_m$ , for a-PS samples ( $f_r = 0.59$ ):  $\circ$ , in toluene at 15.0°C;  $\bullet$ , in cyclohexane at 34.5°C. For the cyclohexane solutions,  $R_g^2/x_w$ , means  $R_{g,0}^2/x_w$ . (From Abe et al. [1993b], with permission. Copyright © 1993 American Chemical Society.)

theta solvents and 0.8 for very good solvents. In reality, experimental results such as those in Figure 1.2 indicate that whereas  $[\eta] \sim M^{0.5}$  for high-molecular-weight coils in theta solvents, typically in very good solvents at high molecular weight, the measured exponents are numerically slightly smaller than 0.8. For example, from Figure 1.2, the exponent estimated from the data for PS in toluene at  $M > 300$  kg/mol is  $\nu \sim 0.72$ . The molecular origin of this apparent discrepancy will be discussed in the next section.

### 1.5.2 Flory–Fox Equation

Based on the Kirkwood–Riseman theory, if polymer chains are nondraining, it follows [Kirkwood and Riseman, 1948; Auer and Gardner, 1955] that intrinsic viscosity data can be related to the radius of gyration,  $R_g$ , of flexible polymers. This can be expressed in an equation of the form [Flory and Fox, 1951]

$$[\eta] = \Phi_{\text{FF}} \frac{(6R_g^2)^{3/2}}{M} \quad (1.40)$$

where  $\Phi_{\text{FF}}$  is a phenomenological constant, which, in view of Eq. (1.30), is proportional to the ratio  $V_H/R_g^3$  [i.e., to  $(R_{H,\eta}/R_g)^3$ , where  $R_{H,\eta}$  is the hydrodynamic radius, determined as  $V_h = (4\pi/3)R_{H,\eta}^3$ ]. Originally, it was anticipated [Flory and Fox, 1951] that  $\Phi_{\text{FF}}$  might be a universal constant: that is, valid for polymers in good solvents and poor solvents, and insensitive to polymer architecture. However, experiment has shown that, typically,  $\Phi_{\text{FF}}$  decreases substantially for linear

coils with an increase in solvent quality. For example, for high-molecular-weight a-PS in cyclohexane and *trans*-decalin at their respective theta temperatures, experiment indicates [Konishi et al., 1991] that  $\Phi_{FF} = \Phi_{FF0} \approx 2.73 \pm 0.09 \times 10^{23} \text{ mol}^{-1}$  (when the viscosity is in mL/g and  $R_g$  is in nanometer); this contrasts with  $\Phi_{FF} \approx 2.11 \pm 0.06 \times 10^{23} \text{ mol}^{-1}$  for the same polymer in toluene at 15°C. The latter value was computed by us using  $\Phi_{FF}/\Phi_{FF0} = (\alpha_\eta/\alpha_S)^3$ , from published data [Abe et al., 1993b] on viscometric and  $R_g$  chain expansion parameters [i.e.,  $\alpha_\eta = ([\eta]/[\eta]_0)^{1/3}$  and  $\alpha_R = R_g/R_{g0}$ , where the subscript '0' refers to measurement under zero excluded-volume conditions. Similar differences in  $\Phi_{FF}$  versus  $\Phi_{FF0}$  are manifested when comparing high-molecular-weight specimens of poly(isobutylene) (PIB) [Abe et al., 1993b], poly(dimethylsiloxane) (PDMS) [Horita et al., 1995], poly( $\alpha$ -methyl styrene) (P $\alpha$ MS) [Tominaga et al., 2002], and poly(methyl methacrylate) (PMMA) [Abe et al., 1994] in good versus theta [Konishi et al., 1991] solvents. A further feature of the results above is that in the good solvents, the computed values of  $\Phi_{FF}$  typically decrease appreciably with increase in molecular weight.

The discrepancy noted above, that the Mark–Houwink–Sakurada scaling exponent  $a$  [Eq. (1.23)] does not reach its asymptotic value of 0.8 for high polymers in good solvents as quickly as does the corresponding exponent for the radius of gyration, as well as the decrease in  $\Phi_{FF}$  with solvent quality, which, as noted above, is equivalent to a decrease in the ratio  $R_{H,\eta}/R_g$ , has been interpreted in terms of an increase in solvent draining with chain expansion [Freed et al., 1988]. However, this interpretation has been disputed by Yamakawa and co-workers [Abe et al., 1994; Horita et al., 1995], who find that for most polymer–solvent systems, a self-consistent description of  $\alpha_\eta$  and  $\alpha_R$  can be achieved within the framework of a quasi-two-parameter (QTP) theory, described in more detail below, without having to incorporate a draining effect. Interestingly, however, Konishi et al. [1991] report that for certain polymers, under theta solvent conditions, small but significant differences are observed in the values of  $\Phi_{FF0}$ . For example, for PDMS in bromocyclohexane at 29.5°C, molar mass variation in  $\Phi_{FF0}$  has been reported [Konishi et al., 1991], with  $\Phi_{FF0}$  decreasing from  $2.67 \times 10^{23} \text{ mol}^{-1}$  for  $M = 1.14 \times 10^6 \text{ g/mol}$  to  $2.38 \times 10^{23} \text{ mol}^{-1}$  for  $M = 1.85 \times 10^5 \text{ g/mol}$ ; also,  $\Phi_{FF0}$  is reported [Konishi et al., 1991] to vary for atactic poly(methyl methacrylate) (a-PMMA) in two different theta solvents:  $\Phi_{FF0} = 2.34 \pm 0.06 \times 10^{23} \text{ mol}^{-1}$  in acetonitrile at 44°C, and  $2.58 \pm 0.11 \times 10^{23} \text{ mol}^{-1}$  in *n*-butyl chloride at 40.8°C, respectively. In the case of PDMS, the molar mass–dependent variation in  $\Phi_{FF0}$  is ascribed to a draining effect at lower molar masses; the origin of the smaller value of  $\Phi_{FF0}$  in a-PMMA/acetonitrile remains unclear [Konishi et al., 1991]. Here, we note, parenthetically, that the decrease in  $\Phi_{FF}$  observed with molecular weight in good solvents, alluded to above, implies an increase in draining with molecular weight, which seems physically unreasonable.

As noted above, from  $[\eta]$ , via Eq. (1.30), we can determine  $V_H$  and therefore the viscometric hydrodynamic radius,  $R_{H,\eta}$ . It is also possible to determine a frictional hydrodynamic radius,  $R_{H,f}$ , from sedimentation or translational diffusion experiments, using Stokes' law. Since the kinematics of viscosity measurement involves rotation of the macromolecule whereas that in sedimentation or diffusion involves translation,  $R_{H,\eta}$  and  $R_{H,f}$  may, in principle, differ numerically. In fact, they

coincide numerically only for macromolecules which behave hydrodynamically as rigid impermeable spheres, and differ slightly for rigid ellipsoids or flexible coils. Here we simply note that referring to the polymer–solvent systems discussed above, variations in the ratio  $\rho = R_g/R_{H,f}$  have been observed when varying solvent quality, which correlate to the corresponding variations in  $\Phi_{FF} \sim (R_g/R_{h,\eta})^3$ . For example, for high-molecular-weight polystyrenes in theta solutions,  $\rho = \rho_0 \approx 1.27$  [Konishi et al., 1991], whereas for the same polymers in toluene at 15°C, we estimate that  $\rho \approx 1.46$ , using  $\rho/\rho_0 = \alpha_R/\alpha_H$ , from published data [Arai et al., 1995] on their  $R_{H,f}$  and  $R_g$  chain expansion parameters,  $\alpha_H = R_{H,f}/R_{H,f}$  and  $\alpha_R = R_g/R_{g,0}$ .

### 1.5.3 Two-Parameter and Quasi-Two-Parameter Theories

We conclude this discussion of the viscometric behavior of  $[\eta]$  of linear coils by briefly reviewing theoretical efforts to describe all three chain expansion parameters,  $\alpha_R$ ,  $\alpha_\eta$ , and  $\alpha_H$ , formulated within the two-parameter (TP) theory of polymer solutions [Yamakawa, 1971, 1997]. In evaluating  $\alpha_R$ , note that the value of the radius of gyration in the absence of excluded volume,  $R_{g,0}$ , may or may not be equal to  $R_{g,\theta}$ , the radius of gyration measured in a specific theta solvent, depending, respectively, on whether the conformation of the chain is or is not the same in each solvent. Such questions can be resolved by comparing experimental values of  $R_g$  of oligomers for which the excluded volume effect can safely be ignored. Also, even if  $R_{g,0} = R_{g,\theta}$ , it may also happen that  $[\eta]_0 \neq [\eta]_\theta$  and  $f_0 \neq f_\theta$  if there is a “specific interaction” in one of the solvents (e.g., if a liquid structure is present in one of the solvents that is disrupted by the polymer). Indeed, such a circumstance is reported by Tominaga et al. [2002], who find that the unperturbed dimensions (i.e.,  $R_{g,0}$ ) of oligomers of P $\alpha$  MS in the good solvents toluene and *n*-butyl chloride, and in the theta solvent cyclohexane at 30.5°C, are all identical, but that the corresponding values of  $[\eta]$  of the oligomers in the good solvents are appreciably smaller than those in the theta solvent, by an amount that does not depend on molar mass, hence is attributed to a specific interaction between the polymer and the good solvents. Surprisingly, such a specific interaction is apparently not manifested in the frictional coefficients determined from the translational diffusion coefficients [Tominaga et al., 2002].

The TP theory actually formulates the average molecular dimensions of a polymer chain in terms of three parameters: the number of segments in the chain,  $n$ , the effective bond length,  $a$ , and the binary cluster integral,  $\beta$ , describing the excluded volume interaction between a pair of segments. However, these three parameters never appear separately, but only in two combinations,  $na^2$  and  $n^2\beta$ —hence the designation as a two-parameter theory [Yamakawa, 1971]. Domb and Barrett [1976] formulated a TP expression for  $\alpha_R$ , based on numerical simulations of self-avoiding walks on a lattice:

$$\alpha_R^2 = \left[ 1 + 10z + \left( \frac{70\pi}{9} + \frac{10}{3} \right) z^2 + 8\pi^{3/2} z^3 \right]^{2/15} \times \left[ 0.933 + 0.067 \exp \left( -0.85z - 1.39z^2 \right) \right] \quad (1.41)$$

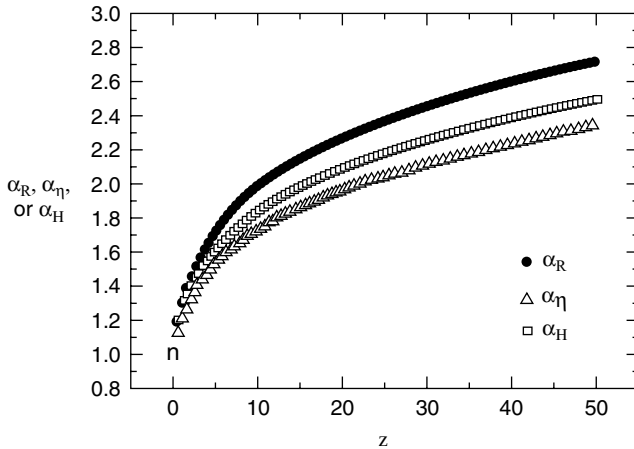


**FIGURE 1.4** Dependence of the chain expansion parameters for radius of gyration  $\alpha_R$ , intrinsic viscosity  $\alpha_\eta$ , and translational hydrodynamic radius  $\alpha_H$  on the excluded volume parameter,  $z$ , as predicted by Eqs. (1.41), (1.42), and (1.43). (From Domb and Barrett [1976], Barrett [1984].)

where  $z$  is a parameter describing the strength of the excluded volume interaction:

$$z = \left( \frac{3}{2\pi n a^2} \right)^{3/2} n^2 \beta \quad (1.41a)$$

Barrett [1984] has further proposed TP expressions for  $\alpha_\eta$  and  $\alpha_H$ , formulated within the Kirkwood–Riseman hydrodynamic theory in the nondraining limit and using approximate formulas, based on numerical simulation, for the requisite statistical averages,  $\langle R_{ij}^2 \rangle$  and  $\langle R_{ij}^{-1} \rangle$ , where  $R_{ij}$  refers to the distance between the  $i$ th and  $j$ th chain segments:

$$\alpha_\eta = \left( 1 + 3.8z + 1.9z^2 \right)^{0.1} \quad (1.42)$$

and

$$\alpha_H = \left( 1 + 6.09z + 3.59z^2 \right)^{0.1} \quad (1.43)$$

In Figure 1.4 we superimpose plots of  $\alpha_R$ ,  $\alpha_\eta$ , and  $\alpha_H$ , according to Eqs. (1.41) to (1.43). As  $z \rightarrow \infty$ , each function asymptotically approaches the strong excluded volume limit (i.e.,  $\alpha_i \sim z^{0.2} \sim M^{0.1}$ ), but  $\alpha_R$  approaches this limit more rapidly than  $\alpha_\eta$  and  $\alpha_H$ , as observed experimentally. Also, these functions predict that the ratio  $\Phi_{FF} = M[\eta]/R_g^3$  decreases, and the ratio  $\rho = R_g/R_H$  increases, with increasing  $z$ ; for example, for  $z = 10$ ,  $\Phi_{FF}/\Phi_{FF0} = \alpha_\eta^3/\alpha_R^3 = 0.657$  and  $\rho/\rho_0 = \alpha_R/\alpha_H = 1.082$ , qualitatively consistent with the above-quoted experimental results,  $\Phi_{FF}/\Phi_{FF0} \approx 2.11/2.73 \approx 0.773$  and  $\rho/\rho_0 \approx 1.46/1.27 \approx 1.15$ .

Yamakawa and co-workers developed the quasi-two-parameter (QTP) theory from the earlier two-parameter (TP) theory, to incorporate chain stiffness into the model. Specifically, the QTP theory computes  $C_\infty$  via the helical wormlike coil model (HW),

which is a refinement of the Kratky–Porod (KP) model, modified to include contributions from torsional as well as bending energy to the coil elasticity [Yamakawa and Fujii, 1976; Yamakawa, 1997]. The torsional energy becomes important when the chain exhibits helical sequences, which is viewed as likely even for atactic vinyl polymers, based on a consideration of their rotational isomeric states [Yamakawa and Fujii, 1976].

The QTP model defines a scaled excluded volume parameter,  $\bar{z}$ , related to the conventional excluded volume parameter  $z$  by

$$\bar{z} = \frac{3}{4} K(\lambda L) z \quad (1.44)$$

with  $z$  described within the HW model [Yamakawa, 1997] as

$$z = \left( \frac{3}{2\pi} \right)^{3/2} (\lambda B)(\lambda L) \quad (1.45)$$

where  $\lambda$  is the chain stiffness parameter  $= 1/2\ell_p$ ;  $\ell_p$  is the persistence length,  $L = xM_0/M_L$  is the contour length, with  $x$  the number of repeat units; and  $M_0$  and  $M_L$ , respectively, are equal to the molar mass per repeat unit and molar mass per unit contour length; and  $B$  is the excluded volume strength. Assuming that the chain consists of beads of diameter  $a$ ,  $B$  may be expressed in terms of  $\beta$ , the binary cluster integral between beads:

$$B = \frac{\beta}{a^2 C_\infty^{3/2}} \quad (1.46)$$

with the characteristic ratio  $C_\infty = \lim_{\lambda L \rightarrow \infty} (6\lambda R_{g,0}^2) / L$ . Within the framework of the HW model,  $C_\infty$  may be expressed as

$$C_\infty = \frac{4 + (\lambda^{-1}\tau_0)^2}{4 + (\lambda^{-1}\kappa_0)^2 + (\lambda^{-1}\tau_0)^2} \quad (1.47)$$

Here  $\kappa_0$  and  $\tau_0$  are, respectively, the HW bending and torsion parameters of the helix.

In Eq. (1.44),  $K(\lambda L) \equiv K(L)$ , with  $L$  expressed in units of  $\lambda^{-1}$ , is given by

$$\begin{aligned} K(L) &= 4/3 - 2.711 L^{-1/2} + (7/6)L^{-1} && \text{for } L > 6 \\ &= L^{-1/2} \exp[-6.611(L)^{-1} + 0.9198 + 0.03516\lambda L] && \text{for } L \leq 6 \end{aligned} \quad (1.48)$$

The QTP theory then assumes that  $\alpha_R$  can be described by the Domb–Barrett expression [Eq. (1.41)], with  $\bar{z}$  replacing  $z$ :

$$\begin{aligned} \alpha_R^2 &= \left[ 1 + 10\bar{z} + \left( \frac{70\pi}{9} + \frac{10}{3} \right) \bar{z}^2 + 8\pi^{3/2} \bar{z}^3 \right]^{2/15} \\ &\times \left[ 0.933 + 0.067 \exp(-0.85\bar{z} - 1.39\bar{z}^2) \right] \end{aligned} \quad (1.49)$$

and that, similarly,  $\alpha_\eta$  can be described by the expression derived by Barrett [Eq. (1.42)] in the nondraining limit:

$$\alpha_\eta = (1 + 3.8\bar{z} + 1.9\bar{z}^2)^{0.1} \quad (1.50)$$

The values of the model parameters in Eqs. (1.44) to (1.50) are determined by fitting experimental data on  $R_{g,0}^2$  of unperturbed chains to the HW theory:

$$R_{g,0}^2 = \lambda^{-2} f_s(L; \kappa_0; \tau_0) \quad (1.51)$$

where

$$f_s(L; \kappa_0, \tau_0) = \frac{\tau_0^2}{\nu^2} f_{s,KP}(L) + \frac{\kappa_0^2}{\nu^2} \left[ \frac{L}{3r} \cos\phi - \frac{1}{r^2} \cos 2\phi + \frac{2}{r^3 L} \cos 3\phi - \frac{2}{r^4 L^2} e^{-2L} \cos(\nu L + 4\phi) \right] \quad (1.52)$$

with

$$\nu = (\kappa_0^2 + \tau_0^2)^{1/2} \quad r = (4 + \nu^2)^{1/2} \quad \phi = \cos^{-1}(2/r)$$

and  $f_{s,KP}(L)$  is the Kratky–Porod function,

$$f_{s,KP}(L) = \frac{L}{6} - \frac{1}{4} + \frac{1}{4L} - \frac{1}{8L^2} (1 - e^{-2L}) \quad (1.53)$$

again with  $L$  expressed in units of  $\lambda^{-1}$ . Note that if  $\kappa_0 = 0$ , the HW theory embodied in Eq. (1.51) reduces to

$$R_{g,0}^2 = \lambda^{-2} f_{s,KP}(\lambda L) \quad (1.54)$$

which is the original KP expression for the wormlike coil.

Yamakawa and co-workers find that a universal scaling relationship exists between  $\alpha_\eta$  and  $\alpha_R$ , provided that occasional system-specific effects, such as solvent dependence of the unperturbed dimensions [Horita et al., 1993], solvent dependence of the viscosity constant  $\Phi_0$  [Konishi et al., 1991], draining effects in the theta solvent [Konishi et al., 1991], specific solvent interactions, and solvent dependence of the hydrodynamic bead diameter [Tominaga et al., 2002], are taken into account. Thus, in Figure 1.5 we reproduce a plot of  $\log \alpha_\eta^3$  versus  $\log \alpha_R^3$ , which superimposes values generated for six polymer–good solvent systems: atactic P $\alpha$ MS (a-P $\alpha$ MS) in toluene at 25.0°C, a-P $\alpha$ MS in 4-*tert*-butyltoluene at 25.0°C, a-P $\alpha$ MS in *n*-butyl chloride at 25.0°C, atactic polystyrene (a-PS) in toluene at 15.0°C, atactic PMMA (a-PMMA) in acetone at 25.0°C, and isotactic PMMA (i-PMMA) in acetone at 25.0°C. Evidently, the data for different systems superpose very well. The solid line is the prediction of the QTP theory, combining Eqs. (1.49) and (1.50). In generating  $\alpha_\eta$  values for a-P $\alpha$ MS in toluene and *n*-butyl chloride, account is taken [Tominaga et al., 2002] of

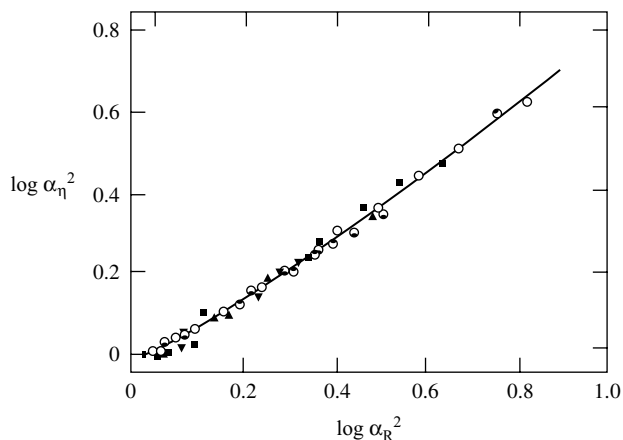


**FIGURE 1.5** Double-logarithmic plots of  $\alpha_\eta^3$  against  $\alpha_R^3$ :  $\circ$ , a-P $\alpha$ MS in toluene at 25.0°C;  $\bullet$ , data for a-P $\alpha$ MS in 4-*tert*-butyltoluene at 25.0°C;  $\circ$ , data for a-P $\alpha$ MS in *n*-butyl chloride at 25.0°C;  $\blacksquare$ , a-PS in toluene at 15.0°C;  $\blacktriangle$ , a-PMMA in acetone at 25.0°C;  $\blacktriangledown$ , i-PMMA in acetone at 25.0°C. The solid curve represents the QTP theory values calculated from Eq. (1.11) with Eq. (1.14) (see the text). (From Tominaga et al. [2002b], with permission. Copyright © 1993 American Chemical Society.)

a specific interaction, designated  $\eta^\dagger$ , not present in the theta solvent system, a-P $\alpha$ MS in cyclohexane at 30.5°C:

$$[\eta] - \eta^\dagger = [\eta]_0 \alpha_\eta^3 \quad (1.55)$$

Also, for a-P $\alpha$ MS in 4-*tert*-butyltoluene, when comparing the oligomer data against the theta solvent, a difference is observed, which decreases with molecular weight, a signature of a difference in the hydrodynamic bead diameter between the two systems; hence, only data above 3.0 kg/mol, for which the effect is negligible, are included in Figure 1.5. A similar effect is observed for a-PMMA, so data below 7.77 kg/mol are excluded from Figure 1.5. Finally, for the a-PMMA and i-PMMA systems, correction has been made in the data plotted in Figure 1.5 for solvent dependence of the Flory–Fox constant  $\Phi_{FF0}$ . Specifically,  $\alpha_\eta$  is computed as [Abe et al., 1994]

$$\alpha_\eta = C_\eta^{-1} \frac{[\eta]}{[\eta]_\theta} \quad (1.56)$$

where  $[\eta]_\theta$  is the intrinsic viscosity of the polymer in the theta solvent and

$$C_\eta = \frac{\Phi_{FF0}}{\Phi_{FF\theta}} \quad (1.57)$$

with  $\Phi_{FF0}$  the unperturbed (i.e., zero excluded volume) viscosity constant in the good solvent and  $\Phi_{FF\theta}$  the value in the theta solvent.  $C_\eta$  is thus treated as a uniform shift parameter required to superpose the a-PMMA and i-PMMA data on those for a-PS in toluene. Yamakawa and co-workers regard the superposition of the data evident in

Figure 1.5, which implies a universal scaling relationship between  $\alpha_\eta$  and the excluded volume parameter,  $\bar{z}$ , as proof that no draining effect is present in all of these systems [Abe et al., 1994; Horita et al., 1995]. Otherwise, values of  $\alpha_\eta$  for such a system would fall increasingly below those on the composite curve with increasing  $\alpha_R$ .

It is pertinent to point out here that a corresponding universal scaling relationship is found [Arai et al., 1995; Tominaga et al., 2002] between  $\alpha_R$  and  $\alpha_H$ , the chain expansion parameter for the hydrodynamic radius determined from translational diffusion. However, the scaling observed deviates substantially from the QTP theory when the latter is constructed using the Barrett equation for  $\alpha_H$  [Barrett, 1984]:

$$\alpha_H = \left(1 + 6.09\bar{z} + 3.59\bar{z}^2\right)^{0.1} \quad (1.58)$$

which is based on simulations using a preaveraged hydrodynamic interaction. Specifically, experimental data for  $\log \alpha_H$  when plotted versus  $\log \alpha_R$  fall systematically below the relationship predicted by the QTP theory. Yamakawa and Yoshizaki [1995] note that when the effect of a fluctuating (nonpreaveraged) hydrodynamic interaction is included,  $\alpha_H$  decreases below the value predicted by the Barrett theory, but substantial disagreement remains between experiment and theory [Arai et al., 1995]. Recently, however, self-consistent Brownian dynamics simulations of  $\alpha_R$  and  $\alpha_H$  by Sunthar and Prakash [2006], using a continuous-chain ( $N \rightarrow \infty$ ) representation of the bead-spring model [Edwards, 1965], which incorporates a fluctuating hydrodynamic interaction, produce results in excellent agreement with the experimental data of Tominaga et al. [2002]. Since these simulations lead in the  $N \rightarrow \infty$  limit to nondraining behavior, it appears these results support the conclusion that the discrepancy between experimental data and the QTP theory stems from the use of a preaveraged hydrodynamic interaction in Eq. (1.58).

To describe the intrinsic viscosity of wormlike coils in the absence of excluded volume, Yamakawa and co-workers developed theoretical descriptions based, first, on the KP model [Yamakawa and Fujii, 1974] and subsequently on its later adaptation, the HW model [Yoshizaki et al., 1988]. Using the cylindrical wormlike coil model, Yamakawa and Fujii [1974] obtained the following expressions, with  $L$  expressed in units of  $\lambda^{-1}$ :

$$[\eta] = \begin{cases} \frac{\Phi_{FF\infty}(L)^{3/2}}{M} \frac{1}{1 - \sum_{i=1}^4 C_i(L)^{-i/2}} & \text{for } L \geq 2.278 \quad (1.59a) \\ \frac{\pi N_A(L)^3}{24M \ln(L/d)} \frac{f(L)}{1 + \sum_{i=1}^4 A_i[\ln(d/L)]^{-i}} & \text{for } L \leq 2.278 \quad (1.59b) \end{cases}$$

where

$$f(L) = \left(3/2L^4\right) \left(e^{-2L} - 1 + 2L - 2L^2 + (4/3)L^3\right) \quad (1.59c)$$

the coefficients  $C_i$  are explicit functions of the cylinder diameter,  $d$ , the  $A_i$  are numerical coefficients, in each case given by Yamakawa and Fujii [1974], and  $\Phi_{\text{FF}\infty}$  is the value of the Flory–Fox constant in the limit  $\lambda L \rightarrow \infty$ . Bohdanecky [1983] determined that the term containing the numerical summation in Eq. (1.59a) can be approximated over a range of  $\lambda L$  values by a rather simple expression:

$$\frac{1}{1 - \sum_{i=1}^4 C_i (\lambda L)^{-i/2}} = \left( B_0 + \frac{A_0}{(\lambda L)^{1/2}} \right)^{-3} \quad (1.60)$$

where the coefficients  $A_0$  and  $B_0$  are functions of  $\lambda d$ :

$$A_0 = 0.46 - 0.53 \log \lambda d \quad \text{and} \quad B_0 = 1.00 - 0.0367 \log \lambda d \quad (1.60a)$$

This simplification leads to analysis of the data via the widely used simple equation

$$\left( \frac{M^2}{[\eta]} \right)^{1/3} = A_\eta + B_\eta M^{1/2} \quad (1.61)$$

where

$$A_\eta = A_0 M_L \Phi_{\text{FF}\infty}^{-1/3} \quad (1.61a)$$

and

$$B_\eta = B_0 \Phi_{\text{FF}\infty}^{-1/3} \frac{1}{\lambda M_L} = B_0 \Phi_{\text{FF}\infty}^{-1/3} \frac{2\ell_p}{M_L} \quad (1.61b)$$

As an example of the application of Eq. (1.61), we cite a study in which the stiffness of hyaluronic acid (HA) was determined, using size-exclusion chromatography (SEC) coupled to online multiangle light scattering and viscosity detectors [Mendichi et al., 2003]. Nine HA fractions were subjected to SEC analysis in 0.15 M NaCl, which generated data on molar mass, radius of gyration, and intrinsic viscosity as a function of molecular weight. A log-log plot of  $[\eta]$  versus  $M$ , superimposing nine samples, exhibits curvature characteristic of a wormlike coil, whereas the corresponding Bohdanecky plot of these data is linear, as predicted by Eq. (1.61). To interpret the parameters  $A_\eta$  and  $B_\eta$  deduced from a least squares fit to the experimental data, according to Eqs. (1.61a) and (1.61b), the authors used tabulated expressions for  $A_0$  and  $B_0$  as functions of  $\lambda d$  [cf. Eq. (1.60a)], assumed a value  $\Phi_{\text{FF}\infty} = 2.86 \times 10^{-23}$ , and used a relationship, suggested by Bohdanecky [1983], connecting the hydrodynamic diameter  $d$  to the mass per contour length  $M_L$ :

$$d = \frac{4\bar{v}_2 M_L}{\pi N_A} \quad (1.62)$$

where  $\bar{v}_2 = 0.57 \text{ mL/g}$  is the partial specific volume of HA in aqueous NaCl. With these assumptions, they obtained the results  $\ell_p = 6.8 \text{ nm}$ ,  $d = 0.8 \text{ nm}$ , and  $M_L = 480 \text{ nm}^{-1}$ . The value of  $\ell_p$  is somewhat smaller than a theoretical prediction [Bathe et al., 2005]

in 0.15 M NaCl (8.0 nm), and the value of  $M_L$  is a little higher than literature values (400 to 410 nm<sup>-1</sup>) [Mendichi et al., 2003]. The good agreement with literature results illustrates the potential power of SEC analysis coupled to online concentration and viscosity detectors for structural analysis of macromolecular species.

Yamakawa and co-workers were led to develop the HW model [Yoshizaki et al., 1980] by the observation that for some stiff-chain polymer–solvent systems, the KP model generates physically incorrect values of the characteristic parameters  $\ell_p$  and  $M_L$ . The following results were obtained [Yoshizaki et al., 1980, 1988], with  $L$  expressed in units of  $\lambda^{-1}$ :

$$[\eta] = [\eta]_{\text{a-KP}} \Gamma_\eta(L, d; \kappa_0, \tau_0) \quad (1.63)$$

where

$$[\eta]_{\text{a-KP}} = \begin{cases} \frac{C_\infty^{3/2} \Phi_{\text{FF}\infty}(L)^{3/2}}{M} \frac{1}{1 - \sum_{j=1}^4 C_\infty^{j/2} C_j L^{-j/2}} & \text{for } L \geq 2.278 C_\infty \quad (1.63a) \\ \frac{\pi N_A(L)^3}{24M} F_\eta\left(\frac{L}{d}, \varepsilon\right) f(C_\infty^{-1}L) & \text{for } L \leq 2.278 C_\infty \quad (1.63b) \end{cases}$$

In Yoshizaki et al. [1980], numerical expressions are formulated for the functions  $\Gamma_\eta$  [Eq. (1.63)],  $F_\eta$ , and  $f$  [Eq. (1.63b)], as well as the coefficients  $C_j$  in Eq. (1.63a). Yoshizaki et al., [1980] evaluated the utility of the KP and HW models in predicting the literature data on  $[\eta]$  for various polymer–solvent systems. An example is shown in Figure 1.6 pertaining to data on  $[\eta]$  obtained for cellulose acetate (CAc) samples

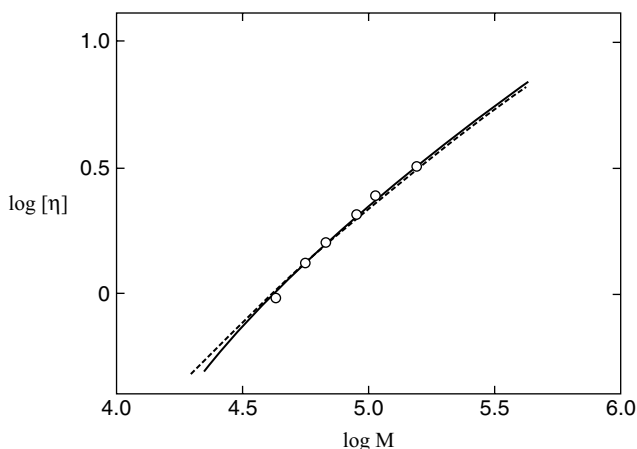


**FIGURE 1.6** Analysis of intrinsic viscosity data for cellulose acetate in trifluoroethanol at 20°C. The solid and dashed curves represent the best-fit theoretical values using the HW and KP chain models, respectively. (From Yoshizaki et al. [1980], with permission. Copyright © 1993 American Chemical Society.)

in trifluoroethanol [Tanner and Berry, 1974]. The solid and dashed lines indicate the best fits to the HW and KP models, Eqs. (1.63) and (1.63a), respectively, where values used for the ratio  $M_L/\lambda$  were determined from data on  $R_g$ , fitted to the HW and KP expressions for the unperturbed wormlike coil. Although both models provide fairly good fits, the KP model produces the results  $d=0.01$  nm,  $M_L=260$  nm<sup>-1</sup>, and  $\lambda^{-1}=2\ell_p=9.7$  nm. Yoshizaki et al., [1980] note that the values of  $d$  and  $M_L$  appear to be unrealistically small. In particular, for the fully extended CAC chain,  $M_L=506$  nm<sup>-1</sup>. Thus, they reject the KP prediction. The HW model produces the fit parameters  $d=0.52$  nm,  $M_L=540$  nm<sup>-1</sup>, and  $\lambda^{-1}=2\ell_p=37.0$  nm, which seem more reasonable.

## 1.6 INTRINSIC VISCOSITY AND THE STRUCTURE OF BRANCHED POLYMERS

### 1.6.1 Branched Polymers in Theta Solvents

Intrinsic viscosity also finds use in characterizing the presence of branching in polymers. Since a linear random walk occupies a larger volume than a random walk of an equal number of steps, which bifurcates or trifurcates at intervals, the radius of gyration of a branched polymer is smaller than that of a linear polymer of equal molecular weight:

$$R_{gb,M}^2 \leq R_{g\ell,M}^2 \quad (1.64)$$

A branching ratio may be defined as:

$$g = \frac{R_{gb,M}^2}{R_{g\ell,M}^2} \quad (1.65)$$

Thus, we expect, for branched polymers,  $g \leq 1$ , and  $g$  will decrease as the number and functionality of branch points increases. By functionality, we mean the number of chain segments attached to a branch site. Thus, a nine-arm star polymer has one branch point and a functionality of 9. The parameter  $g$  may theoretically be computed for various branch structures, usually assuming Gaussian random coil statistics for the chain segments between branch points. Different branching architectures (e.g., star versus comb structures) have been evaluated. The simplest case is that of star-branched polymers of functionality,  $p$ , assuming Gaussian statistics and equal branch lengths, for which Zimm and Stockmayer [1949] deduced

$$g = \left( \frac{3p-2}{p^2} \right) \quad (1.66)$$

Zimm and Stockmayer [1949] also derived theoretical expressions for monodisperse and polydisperse randomly branched polymers with branch functionalities of 3 and 4.

For monodisperse polymers with trifunctional branch points, they obtained

$$g = \left[ \left( 1 + \frac{B_n}{7} \right)^{1/2} + \frac{4B_n}{9\pi} \right]^{-1/2} \quad (1.67)$$

and for monodisperse polymers with tetrafunctional branch points

$$g = \left[ \left( 1 + \frac{B_n}{6} \right)^{1/2} + \frac{4B_n}{3\pi} \right]^{-1/2} \quad (1.68)$$

where  $B_n$  is the (number-average) number of branch points per chain.

Recalling the Flory–Fox equation [Eq. (1.40)] it seems reasonable to anticipate that one might determine  $g$  from intrinsic viscosity data. Specifically, we may write

$$\frac{[\eta]_{b,M}}{[\eta]_{\ell,M}} = g_\eta \quad (1.69)$$

If the Flory–Fox equation could be assumed for both linear and branched chains, it would follow that  $g_\eta = g^{3/2}$ . In fact, such a relationship is not found experimentally. Zimm and Kilb [1959] carried out a theoretical analysis of the intrinsic viscosity of star polymers, in the absence of excluded volume, which led to a prediction for  $g_\eta$ :

$$g_\eta = \frac{(2/p)^{3/2}[0.39(p-1) + 0.196]}{0.586} \quad (1.70)$$

Equation (1.70) may be approximated by a simple relation between  $g_\eta$  and  $g$  of the form  $g_\eta = g^{0.5}$ . Analysis of experimental intrinsic viscosity data on star polymers in theta solvents indicates that while substantially better than the relation based on the Flory–Fox equation, Eq. (1.70) is still inaccurate, and that a better empirical description is given by [Douglas et al., 1990]

$$g_\eta = \left( \frac{3p-2}{p^2} \right)^{0.58} \quad (1.71)$$

(i.e.,  $g_\eta = g^{0.58}$ ). Subsequent theoretical analysis [Shida et al., 2004] using Monte Carlo simulation on a cubic lattice, obtained numerical results in agreement with Eq. (1.71), suggesting that the error in the Zimm–Kilb analytical description stems from the use of a preaveraging approximation in computing the hydrodynamic interaction between chain segments. Figure 1.7 shows the agreement between the prediction of Eq. (1.71) for star polymers versus experimental data and Monte Carlo simulation [Shida et al., 2004].

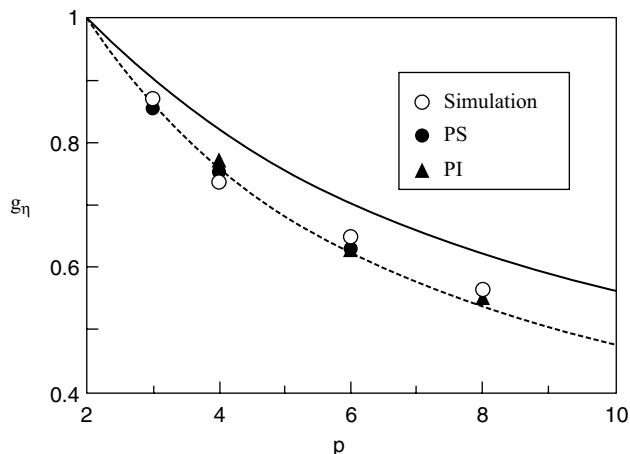


**FIGURE 1.7** Plots of viscometric branching parameter,  $g_\eta$ , versus branch functionality,  $p$ , for star chains on a simple cubic lattice (unfilled circles), together with experimental data for star polymers in theta solvents: ●, polystyrene in cyclohexane; ▲, polyisoprene in dioxane. Solid and dashed lines represent calculated values via Eqs. (1.70) and (1.71), respectively. (Adapted from Shida et al. [2004].)

## 1.6.2 Branched Polymers in Good Solvents

Reliable theoretical expressions for the  $g$ -parameter in good solvents are not yet available. However, a semiempirical equation for  $g_\eta$  has been suggested by Douglas et al. [1990] based on a fit to experimental data for polystyrene (PS), polyisoprene (PIP), and polybutadiene (PBD) star polymers. The equation is

$$g_\eta = \frac{[(3p - 2)/p^2]^{0.58} [1 - 0.276 - 0.015(p - 2)]}{1 - 0.276} \quad (1.72)$$

Further Monte Carlo simulations [Shida et al., 1998] have confirmed the accuracy of Eq. (1.72), as shown in Figure 1.8. Numerically, in the range  $p = 2$  to 20, Eq. (1.72) can be approximated by the simple power-law expression,  $g_\eta = g^{0.75}$ . Note that Eqs. (1.71) and (1.72) apply only to star polymers and are not strictly applicable to branched polymers having other types of architecture. Somewhat larger experimental values of the exponent  $\varepsilon$  in the equation  $g_\eta = g^\varepsilon$  have been reported by Farmer et al. [2006] for regular and random combs and regular centipedes in a good solvent (i.e.,  $\varepsilon \approx 0.9$ ).

It should also be noted that a similar treatment is possible for the translational hydrodynamic radius,  $R_{h,f}$ , obtained from measurements of translational diffusion coefficients or sedimentation coefficients of branched polymers. One may define a parameter  $g_H = R_{h,fb}/R_{h,fl}$ : the ratio of the hydrodynamic radius of the branched polymer relative to that of a linear polymer of the same molecular weight. Again, it is expected that  $g_H \leq 1$ . For star polymers with uniform subchain lengths having

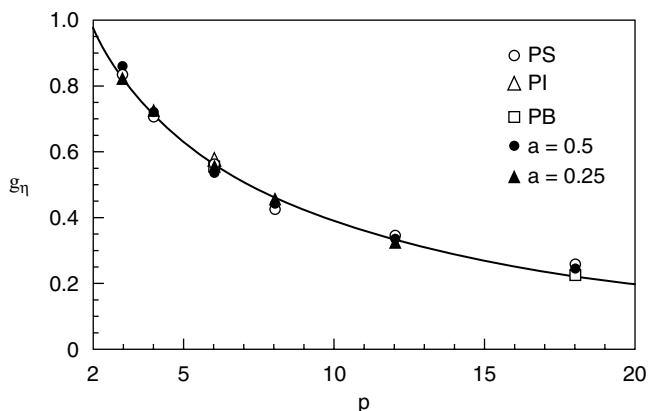


**FIGURE 1.8** Plots of the viscosity branching ratio  $g_\eta$  versus branch functionality,  $p$ : filled symbols, Monte Carlo simulations of star chains on a lattice using two bead sizes; unfilled symbols, experimental data; solid line, values calculated from Eq. (1.72). (From Shida et al. [1998], with permission. Copyright © 1998 American Chemical Society.)

Gaussian statistics, the following expression has been derived [Stockmayer and Fixman, 1953] using a preaveraging approximation:

$$g_H = \frac{p^{1/2}}{2 - p + 2^{1/2}(p - 1)} \quad (1.73)$$

Douglas et al. [1990] found substantial discrepancies between experimental data and the prediction of Eq. (1.73), and instead suggested the empirical equation

$$g_H = \frac{p^{1/4}}{[2 - p + 2^{1/2}(p - 1)]^{1/2}} \quad (1.73a)$$

which was also found to be consistent with Monte Carlo simulations which avoided the preaveraging approximation [Shida et al., 2004]. For uniform stars in a very good solvent, a semiempirical equation for  $g_H$  has been proposed by Douglas et al. [1990], based on fits to experimental data for PS, PIP, and PB stars:

$$g_H = \frac{p^{1/4}}{[2 - p + \sqrt{2}(p - 1)]^{1/2}} \frac{0.932 - 0.0075(p - 1)}{0.932} \quad (1.74)$$

Again the utility of this equation has been confirmed via Monte Carlo simulations on a lattice [Shida et al., 1998]. Comparing Eqs. (1.71) through (1.74), it turns out that  $1 \leq g_H/g_\eta \leq 1.39$ , indicating that the effect of branching is greater in the intrinsic viscosity than in the frictional coefficient.

## 1.7 INTRINSIC VISCOSITY OF POLYELECTROLYTE SOLUTIONS

### 1.7.1 Role of Electrostatic Interactions

The discussion above focused principally on nonionic polymers in organic solvents. We now consider the case of polyelectrolyte solutions. Here, one has to deal with the role of electrostatic interactions, which can be relatively strong compared to excluded volume interactions and which can therefore dramatically modify the hydrodynamic volume and concentration dependence of the solution viscosity. The impact of electrostatic interactions is affected by the density of charges on the polyelectrolyte chain and the concentration of added salt. Such effects can be discussed quantitatively in terms of two length scales. First, the Bjerrum length,  $\ell_B$ , is the scale at which the electrostatic energy of two elementary charges equals the thermal energy  $kT$ , where  $k$  is Boltzmann's constant and  $T$  is temperature (K):

$$\ell_B = \frac{e^2}{4\pi\epsilon_s\epsilon_0k_B T} \quad \text{m} \quad (1.75)$$

Here  $e$  ( $=1.602 \times 10^{-19}$  C) is the elementary charge,  $\epsilon_0$  ( $=8.854 \times 10^{-12}$  C<sup>2</sup>/N. m<sup>2</sup>) is the vacuum permittivity, and  $\epsilon_s$  is the solvent dielectric constant. At  $T = 25^\circ\text{C}$ , water has  $\epsilon_s = 78$ , and hence  $\ell_B = 0.72$  nm. According to Manning's counterion condensation theory [Manning, 1969], all counterions are mobile if the charge spacing along the chain exceeds  $\ell_B$ . However, if the spacing becomes smaller than  $\ell_B$ , counterions condense on the chain to lower the charge repulsion until the distance between effective charges equals  $\ell_B$ . Quantitatively, if the polyelectrolyte has a contour length  $L$  and  $N$  monomers each having an ionizable group with valency  $\nu_p$ , with counterions having valency  $\nu_c$ , the counterion condensation criterion is [Manning, 1969]

$$\frac{\nu_p\nu_c\ell_B}{a} \geq 1 \quad (1.76)$$

where  $a = L/N$  is the monomer length. It therefore follows that the fraction,  $\chi_m$ , of monomers bearing an effective charge is given by  $\chi_m = \alpha$ , where  $\alpha$  is the degree of dissociation of the polyelectrolyte, when  $\ell_B/a \leq (\nu_p\nu_c)^{-1}$ , and  $\chi_m = a/\lambda_B\nu_p\nu_c$ , when  $\ell_B/a > (\nu_p\nu_c)^{-1}$ . In practice, if the conformation of the polyelectrolyte chain is not known (i.e., if  $a = L/N$  is unknown),  $\chi_m$  must be determined by osmotic pressure [Pochard et al., 2001] or conductimetric measurements [Beyer and Nordmeier, 1995].

### 1.7.2 Effect of Ionic Strength

The strength of electrostatic interactions between two ionic groups is diminished by the addition of salt to a polyelectrolyte solution, since the added ions are attracted to ionic groups of opposite charge, forming an ion atmosphere surrounding them. Here the length scale of importance is the Debye screening length,

$$\ell_D = (8000\pi N_A \ell_B I)^{-1/2} \quad \text{m} \quad (1.77)$$

where  $N_A$  is Avogadro's number and  $I = \frac{1}{2} \sum C_i Z_i^2$  is the ionic strength, where  $C_i$  is the molar concentration (mol/L) of ionic species  $i$ ,  $Z_i$  is the valency of the ion, and the summation is taken over all mobile ions in the solution.  $\ell_D$  is a measure of the distance beyond which the interaction between two charges is screened out by the presence of added small ions. For a 1 : 1 charged group ( $\nu_p = 1 = \nu_c$ ) [Eisenberg and Pouyet, 1954],

$$I = \begin{cases} \alpha \frac{C}{2} + C_s + C_r & \text{when } \alpha \leq \frac{a}{\ell_B} \\ \frac{a}{\ell_B} \frac{C}{2} + C_s + C_r & \text{when } \alpha > \frac{a}{\ell_B} \end{cases} \quad (1.78)$$

where  $C$  is the molar concentration of polyelectrolyte,  $C_s$  is the molar concentration of added (1 : 1) salt, and  $C_r$  is the molar concentration of residual (1 : 1) ions in the water used to make the solution ( $10^{-7}$  M in ideal pure water). For a 0.1 M ( $10^{-7}$  mol/m<sup>3</sup>) solution of a 1 : 1 electrolyte in water,  $\ell_D = 1$  nm and decreases with increase in salt concentration (increase of  $I$ ). Thus, the electrostatic energy between two elementary charges separated by a distance  $\ell_B$  will decrease below  $k_B T$  when salt is added to the medium, and since the strength of the interaction decreases essentially as  $\exp(-\ell_B/\ell_D)$ , will be approximately  $0.5kT$  when  $I = 0.1$ .

### 1.7.3 Experiment Versus Theory

The viscosity of a polyelectrolyte solution is affected by electrostatic interactions in two ways. First, intramolecular repulsions between like charges will increase the chain dimensions; attractive intramolecular forces between unlike charges will contract the chain. Second, intermolecular repulsions may lead to intermolecular ordering of charged coils. Based on the discussion above, it is clear that the strength of such interactions will be determined by factors influencing counterion condensation [Eq. (1.76)]: the number of charged groups on the polyelectrolyte (influenced strongly, for polyacids and polybases, by the solution pH), the valency of the charges, and the monomer length, as well as the ionic strength. In the absence of added salt, the sole contribution to the ionic strength comes from the counterions, and therefore, as the solution is diluted, the ionic strength decreases, the electrostatic repulsions increase in strength, and the ensuing chain expansion and strong intermolecular interaction may lead to a dramatic increase in the reduced viscosity  $\eta_{sp}/c$  and the appearance of a maximum in the very dilute concentration range [Eisenberg and Pouyet, 1954; Cohen and Priel, 1990; Borsali et al., 1992; Nishida et al., 2001, 2002]. An example, taken from the recent study by Nishida et al. [2002] on aqueous solutions of the sodium salt of partially sulfuric acid-esterified sodium polyvinyl alcohol, is shown in Figure 1.9. A pronounced peak is evident in the absence of added salt, the intensity of which decreases considerably, and the location of which,  $c_{\max}$ , moves to higher concentration, with the addition of increasing amounts of salt. Experiments indicate [Cohen and Priel, 1990] that  $c_{\max}$  increases linearly with  $c_s$  at fixed polyelectrolyte molecular weight,  $M$ , and temperature,  $T$ . Similarly, results indicate [Cohen and Priel, 1990] that  $c_{\max}$  increases linearly with  $M$ , at fixed  $c_s$  and  $T$ . At fixed  $c_s$  and  $M$ ,

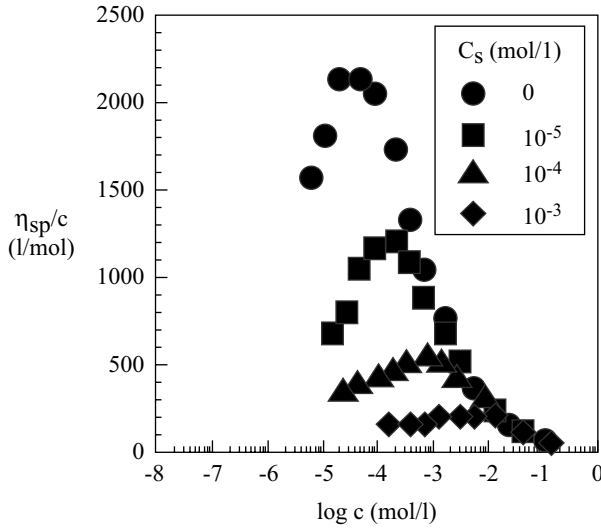


**FIGURE 1.9** Plot of  $\eta_{sp}/c$  versus  $c$  for the sodium salt of partially sulfuric acid-esterified sodium polyvinyl alcohol (degree of substitution  $\alpha = 0.31$ , and degree of polymerization = 2500) in water with added molar concentrations of NaCl as indicated. (Adapted from Nishida et al. [2002].)

Arrhenius dependence of  $c_{max}$  on temperature was observed [Cohen and Priel, 1990]:  $c_{max} = A \exp(-E/RT)$ .

The highly nonlinear concentration dependence evident in Figure 1.9 makes determination of the intrinsic viscosity by extrapolation of  $\eta_{sp}/c$  data via Eqs. (1.24) and (1.25) impossible. Cohen and Priel [1990] report observing that linear concentration dependence is observed at concentrations substantially below  $c_{max}$ , allowing determination of  $[\eta]$ . Theoretical analysis [Nishida et al., 2001, 2002] suggests that the dominant contribution responsible for the appearance of the peak in the  $\eta_{sp}/c$  versus  $c$  plots comes from the intermolecular electrostatic repulsions between polyions. Based on this idea, Nishida et al. [2002] propose a method to determine the intrinsic viscosity of polyelectrolyte solutions at very low ionic strength, by assuming additivity in the contributions of intra- and intermolecular interactions; that is,

$$\frac{\eta_{sp}}{c} = \frac{\eta_{intra}}{c} + \frac{\eta_{inter}}{c} \quad (1.79)$$

These authors adopt an expression for the viscosity of polyion solutions derived by Rice and Kirkwood [1959]:

$$\eta = \frac{M\rho^2}{30\xi} \int_V r^2 \left( \frac{\partial^2 U}{\partial r^2} + \frac{4}{r} \frac{\partial U}{\partial R} \right) g(r) dr \quad (1.80)$$

where  $M$ ,  $\rho$ ,  $\xi$ , and  $g(r)$  are, respectively, the molecular weight, number density, segmental friction coefficient, and pair distribution function of polyions. They assume

[Nishida et al., 2001] that the conformation of polyions at low ionic strength is rodlike, and hence the polyions adopt a simplified mean-field expression for  $g(r) = g(r, \theta) = \exp[-U(r, \theta)/k_B T]$ , where the intermolecular potential  $U(r, \theta)$  is a function not only of the interparticle distance,  $r$ , but the orientation angle,  $\theta$ , between the rods. Computation of the intermolecular contribution to the viscosity then proceeds, using Eq. (1.80), via

$$\eta_{\text{inter}} = \int_0^{2\pi} \eta d\theta \quad (1.81)$$

and results in a computed function that reproduces the characteristic peak observed in polyelectrolyte solutions (Figure 1.9). The resulting function,  $\eta_{\text{inter}}/c$ , may then be subtracted from the experimental values of  $\eta_{\text{sp}}/c$  to determine  $\eta_{\text{intra}}/c$  [cf. Eq. (1.79)]. The authors find [Nishida et al., 2002] that the resulting  $\eta_{\text{intra}}/c$  increases with dilution, reflecting the chain expansion due to the decrease in electrostatic screening with dilution, and then levels off at a constant value, which corresponds to the intrinsic viscosity of the polyelectrolyte. The results further indicate [Nishida et al., 2002] that  $[\eta]$  increases with decrease in concentration of added salt, and levels off when the overall ionic strength,  $I$ , falls below  $10^{-4}$ , indicating that flexible polyions cannot expand indefinitely.

## 1.8 INTRINSIC VISCOSITIES OF LIQUID-CRYSTAL POLYMERS IN NEMATIC SOLVENTS

### 1.8.1 Intrinsic Miesowicz Viscosities

We conclude this discussion of dilute solution viscosity by describing some recent studies of the viscometric behavior of liquid-crystal polymers (LCPs) in low-molar-mass nematic solvents. Earlier studies in this area have been reviewed by Jamieson et al. [1996]. When dealing with the viscosity of nematic fluids, several different shear viscosity coefficients can be accessed experimentally [Brochard, 1979]. These include the Miesowicz viscosities,  $\eta_a$ ,  $\eta_b$ , and  $\eta_c$ , in which the nematic director is pinned, respectively, along the vorticity direction, parallel to the direction of flow and along the shear gradient (i.e., directions 1, 2, and 3 in Figure 1.1, respectively). One may also perform shear flow experiments in which the director is allowed to rotate [Brochard, 1979]. In such a case, the orientation of the director is determined by two of the six Leslie viscosity coefficients,  $\alpha_2$  and  $\alpha_3$ . Specifically, the director orients preferentially at an angle close to the flow direction, when  $\alpha_2 < 0$  and  $\alpha_3 < 0$ ; in contrast, when  $\alpha_2 < 0$  but  $\alpha_3 > 0$ , the nematic exhibits tumbling flow, the director rotating continuously around the vorticity axis; when both  $\alpha_2 > 0$  and  $\alpha_3 > 0$ , the nematic again exhibits aligning flow, but in this case, the director is oriented along the vorticity axis. The initial impetus for studies in this area was a theoretical analysis by Brochard [1979], who derived expressions for the increments in various nematic viscosity coefficients due to the dissolution of polymer chains in nematic media. In

particular, the following expressions were obtained [Brochard, 1979] for increments in the Miesowicz viscosities  $\eta_b$  and  $\eta_c$ :

$$\delta\eta_c = \frac{ck_B T \tau_R}{N} \frac{R_{\parallel}^2}{R_{\perp}^2} \quad (1.82)$$

$$\delta\eta_b = \frac{ck_B T \tau_R}{N} \frac{R_{\perp}^2}{R_{\parallel}^2} \quad (1.83)$$

Here  $R_{\parallel}$  and  $R_{\perp}$  are the rms (root mean square) end-to-end distances of the polymer chain parallel and perpendicular to the director, respectively,  $\tau_R$  is the conformational relaxation time of the polymer,  $c$  the polymer concentration,  $N$  is the degree of polymerization, and  $T$  the temperature (K). These results are interesting, because they predict that if the dissolved polymer stretches along the director, because of an interaction with the nematic field, the increment in  $\eta_c$  will be much larger than that in  $\eta_b$ . Specifically, from Eqs. (1.82) and (1.83), the ratio of the two scales as

$$\frac{\delta\eta_c}{\delta\eta_b} = \frac{R_{\parallel}^4}{R_{\perp}^4} \quad (1.84)$$

This prediction can be tested in a relatively straightforward way, using a nematic solvent that has positive dielectric anisotropy. Such a solvent will orient in an electric field with the director oriented along the direction of the electric field. Thus, in an electrorheological (ER) experiment, with the applied field oriented along the shear gradient, one measures  $\eta_c$ ; when the field is switched off (provided that  $\alpha_2 < 0$  and  $\alpha_3 < 0$ ), the director rotates very close to the flow direction, and therefore one measures approximately  $\eta_b$ . Hence, the Brochard theory predicts a large enhancement of the ER effect in such a nematic fluid if we dissolve in it a polymer whose conformation stretches along the nematic director, and the magnitude of the enhancement should be very sensitive to the conformational anisotropy of the polymer [Eq. (1.84)].

In reality, it is very difficult to dissolve a flexible polymer chain in a nematic fluid, because of the entropic penalty. However, it is relatively easy to dissolve liquid-crystal polymers in such media, because of the favorable contribution from the nematic interaction between the mesogenic groups of polymer and solvent. Thus, the predictions of the Brochard theory have been confirmed qualitatively by ER experiments [Chiang et al., 1997a] in which LCPs of differing architectures [i.e., (1) a main-chain LCP (MCLCP) consisting of mesogenic groups connected linearly by flexible spacers; (2) an end-on side-chain LCP (SCLCP) having mesogens attached end-on to a flexible backbone; and (3) a side-on SCLCP having mesogens attached side-on (i.e., parallel to the backbone)] were dissolved in low-molar-mass nematic solvents such as pentylcyanobiphenyl (5CB), octylcyanobiphenyl (8CB), and the corresponding alkyloxycyanobiphenyls (5OCB and 8OCB). The magnitude of the ratio of the increment in field-on viscosity to the increment in field-off viscosity (i.e.,  $\delta\eta_{\text{on}}/\delta\eta_{\text{off}}$ ) was largest for the MCLCP, smallest for the end-on SCLCP, and

intermediate for the side-on SCLCP. Identifying  $\delta\eta_{\text{on}} = \delta\eta_c$  and  $\delta\eta_{\text{off}} \sim \delta\eta_b$ , this result is consistent with Eq. (1.84), taking account of the theoretical expectation [Carri and Muthukumar, 1998] that the MCLCP and the side-on SCLCP will each be strongly stretched along the nematic director ( $R_{\parallel} \gg R_{\perp}$ ), while the end-on SCLCP will have a globular conformation ( $R_{\parallel} \sim R_{\perp}$ ), which might be slightly prolate or oblate, depending on the strength of the coupling to the nematic field.

Subsequently, more detailed studies were conducted on nematic solutions of a MCLCP [Chiang et al., 1997b, 2000] and an end-on SCLCP [Yao and Jamieson, 1997; Chiang et al., 2002]. First, we note that Eqs. (1.82) and (1.83) apply strictly only in the limit of infinite dilution; hence, the experimental values of  $\delta\eta_{\text{on}}/c$  and  $\delta\eta_{\text{off}}/c$  must be extrapolated to  $c = 0$ . With this modification, Eqs. (1.82) and (1.83) may be rewritten:

$$\lim_{c \rightarrow 0} \frac{\delta\eta_c}{c} = \frac{k_B T \tau_R}{N} \frac{R_{\parallel}^2}{R_{\perp}^2} \quad (1.85)$$

$$\lim_{c \rightarrow 0} \frac{\delta\eta_b}{c} = \frac{k_B T \tau_R}{N} \frac{R_{\perp}^2}{R_{\parallel}^2} \quad (1.86)$$

Hence,

$$\frac{\lim_{c \rightarrow 0} \delta\eta_c/c}{\lim_{c \rightarrow 0} \delta\eta_b/c} = \frac{R_{\parallel}^4}{R_{\perp}^4} \quad (1.87)$$

Moreover, we point out that when one has determined the ratio  $R_{\parallel}/R_{\perp}$  via Eq. (1.87), it becomes possible to determine the conformational relaxation time  $\tau_R$  via the following equation, obtained by subtracting Eq. (1.86) from Eq. (1.85):

$$\lim_{c \rightarrow 0} \frac{\delta\eta_c}{c} - \lim_{c \rightarrow 0} \frac{\delta\eta_b}{c} = \frac{k_B T \tau_R}{N} \left( \frac{R_{\parallel}^2}{R_{\perp}^2} - \frac{R_{\perp}^2}{R_{\parallel}^2} \right) \quad (1.88)$$

ER experiments were conducted [Chiang et al., 1997b, 2000] on a MCLCP designated TPBn which has mesogenic groups, 1-(4-hydroxy-4-O-bisphenyl)-2-(4-hydroxyl phenyl)butane, linearly linked by flexible oligomethylene ( $n$ -mer) spacers. For TPB10 dissolved in 5OCB at several temperatures in the nematic range, the Mark–Houwink relation  $[\eta_c] = kL_w^a$ , where  $L_w$  is the weight-average contour length of the polymer, was determined. The results indicate [Chiang et al., 1997b] a relatively high exponent,  $a = 1.06$  at  $T = 52^\circ\text{C}$  ( $\Delta T = T_{\text{NI}} - T = 15^\circ\text{C}$ ), decreasing slightly to  $a = 0.92$  at  $62^\circ\text{C}$  ( $\Delta T = 5^\circ\text{C}$ ). Combination of  $\delta\eta_b$  and  $\delta\eta_c$  data led, via Eqs. (1.87) and (1.88) [Chiang et al., 1997b], to values of  $R_{\parallel}/R_{\perp}$  and  $\tau_R$  listed in Table 1.1. The results show that with increasing molecular weight,  $\tau_R$  increases dramatically,  $\tau_R \sim L^b$ , with  $b = 1.99$  at  $T = 52^\circ\text{C}$ , decreasing slightly to  $b = 1.94$  at  $T = 52^\circ\text{C}$ , whereas  $R_{\parallel}/R_{\perp}$  shows no clear trend with molar mass. Based on earlier studies of the twist viscosity of TPBn polymers [Chen and Jamieson, 1994], which encompassed oligomers to high

**TABLE 1.1 Conformational Anisotropy ( $R_{\parallel}/R_{\perp}$ ) and Conformational Relaxation Time ( $\tau_R$ ) of TPB10 in Nematic 5OCB**

Contour Length (nm)	$T = 52^{\circ}\text{C}$		$T = 57^{\circ}\text{C}$		$T = 62^{\circ}\text{C}$	
	$R_{\parallel}/R_{\perp}$	$\tau_R$ (m)	$R_{\parallel}/R_{\perp}$	$\tau_R$ (m)	$R_{\parallel}/R_{\perp}$	$\tau_R$ (m)
62.99	2.46	2.97	2.43	2.36	2.33	1.90
118.15	3.16	7.80	2.94	6.90	2.60	6.06
215.66	3.17	21.5	2.93	17.0	2.47	15.0
354.86	2.99	106	2.75	84.5	2.38	63.4

polymers and which indicate that we are in the long polymer limit for TPB10, when  $L \geq 62.99$  nm, we have tentatively interpreted [Chiang et al., 1997b, 2000] the strong molecular-weight dependence of  $\tau_R$  to indicate that TPB10 behaves as a free-draining Gaussian coil. Specifically, from the Brochard model [Brochard, 1979],

$$\tau_R = \frac{\lambda_{\parallel}\lambda_{\perp}R_{\parallel}^2R_{\perp}^2}{\lambda_{\perp}R_{\perp}^2 + \lambda_{\parallel}R_{\parallel}^2} \frac{1}{k_B T} \quad (1.89)$$

where  $\lambda_{\parallel}$  and  $\lambda_{\perp}$  are the translational frictional coefficients for motion parallel and perpendicular to the director, respectively. When  $R_{\parallel} \gg R_{\perp}$ , this simplifies to  $\tau_R \sim 1/\lambda_{\perp}R_{\perp}^2 \sim M^2$ , when  $\lambda_{\perp} \sim M$  (free-draining hydrodynamics) and  $R_{\perp} \sim M^{0.5}$  (Gaussian statistics). Alternatively, some combination of partial draining and non-Gaussian (wormlike-coil) statistics may also give an exponent  $b \sim 2$ . Table 1.1 indicates further that an increase in temperature results in a slight decrease in both  $R_{\parallel}/R_{\perp}$  and  $\tau_R$ . The latter observation is consistent with the dual theoretical expectation (see below) that the strength of the nematic interaction will decrease, and the flexibility of the polymer chain will increase, with increasing temperature.

To obtain a more quantitative picture of the temperature dependence of  $\tau_R$  and  $R_{\parallel}/R_{\perp}$ , specimens of TPB10 were dissolved in a proprietary mixture of low-molar-mass nematics, designated E5, which has a broad nematic temperature range [Chiang et al., 2000]. Experimental results for two TPB10 specimens having DP = 18 and 63 are shown in Figure 1.10. First, the temperature dependence of  $R_{\parallel}$  and  $R_{\perp}$  may be considered in the context of pertinent statistical theories. An analysis by Halperin and William [1992] of the conformation of main-chain LCPs using an Ising chain model led to the conclusion that the chain dimensions,  $R_{\parallel}$  and  $R_{\perp}$ , each exhibit exponential temperature dependence:

$$R_{\parallel} = \left(\frac{a}{\ell_p}\right)^{4/5} \exp\left(\frac{2U_h}{5k_B T}\right) R_{g,0} \quad (1.90a)$$

$$R_{\perp} = \left(\frac{a}{\ell_p}\right)^{7/10} \exp\left(\frac{-U_h}{10k_B T}\right) R_{g,0} \quad (1.90b)$$

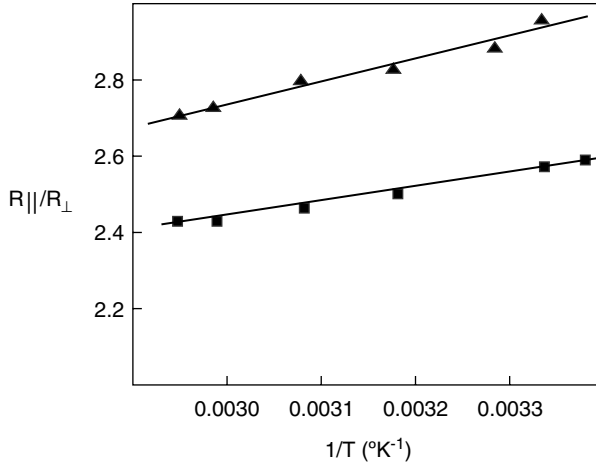


**FIGURE 1.10** Conformational anisotropy of main-chain LCP TPB10 dissolved in nematic solvent E48: ■, DP = 18; ▲, DP = 63. (Adapted from Chiang et al. [2000].)

where  $a$  is the monomer length,  $\ell_p$  the persistence length,  $R_{g,0}$  the Flory phantom-chain radius of gyration of the LCP, and  $U_h$  the energy required to form a hairpin turn in the flexible spacer groups of the MCLCP. These equations predict that  $R_{||}$  will decrease with increasing  $T$  and  $R_{\perp}$  will increase with increasing  $T$ . Examining Eq. (1.90), it is clear that the conformational anisotropy,  $R_{||}/R_{\perp}$  is predicted to decrease with increasing temperature, in agreement with the experimental data:

$$\frac{R_{||}}{R_{\perp}} = \left(\frac{a}{\ell_p}\right)^{1/10} \exp\left(\frac{U_h}{2k_B T}\right) \quad (1.91)$$

In addition, the hairpin activation energy  $U_h$  can be calculated from the Arrhenius fit to the data in Figure 1.10, from which we obtain a value  $U_h = 3.6$  kJ/mol. Noting that hairpin formation in the decamethylene spacer requires two *trans-to-gauche* transformations, each of which involves an energy expenditure of about 1 kJ/mol [Morrison and Boyd, 1983], it appears that the experimental result is of the correct order of magnitude.

Our results for  $R_{||}/R_{\perp}$  can also be interpreted within the theoretical description of Carri and Muthukumar [1998]. In the limit of long polymers, these authors derive the equation

$$\left(\frac{R_{||}}{R_{\perp}}\right)^2 = \frac{1}{1 + D} \quad (1.92)$$

where  $D$  is a coupling strength parameter that describes the strength of the nematic interaction between the mesogenic groups on the polymer and the nematic solvent. For TPB10, a MCLCP that has mesogens parallel to the polymer backbone, theory implies

**TABLE 1.2 Conformational Relaxation Time ( $\tau_R(\mu\text{s})$ ) of TPB10 Samples in Nematic E48**

Temperature ( $^{\circ}\text{C}$ )	23	27	32	42	52	62	67
TPB10 (DP = 18)	24.9	18.4	9.76	5.71	2.58	1.80	1.61
TPB10 (DP = 63)	240	173	99.7	37.4	24.7	19.1	15.8

that the polymer segments will align strongly with the director (i.e., the conformation will be strongly prolate,  $D \ll 0$ , and  $R_{\parallel}/R_{\perp} \gg 1$ ), as indeed is found experimentally (Figure 1.10). Moreover, Figure 1.10 indicates that  $R_{\parallel}/R_{\perp}$  decreases with temperature (i.e.,  $|D|$  decreases with temperature), presumably reflecting an increase in flexibility of the decamethylene spacer, and a decrease in the nematic order parameter, at higher temperatures. Also, from the temperature dependence of the conformational relaxation time (data shown in Table 1.2), we can determine the activation energy,  $U_c$ , associated with conformational dynamics. We find that  $U_c = 52.2$  kJ/mol. This result appears to be relatively insensitive to the structure or flexibility of the LCP, consistent with the idea [Pashkovskii and Litvina, 1992a, b] that  $U_c$  is determined principally by the viscous activation energy of the solvent, which is on the order of 50 kJ/mol.

Similar studies were carried out on two end-on SCLCPs: one having a polysiloxane backbone and a 4'-methoxyphenyl-4''-oxybenzoate mesogen [Yao and Jamieson, 1997; Chiang et al., 2002], the other having a polyacrylate backbone and a cyanobiphenyl mesogen [Chiang et al., 2002], in each case with an undecylmethylene spacer connecting the mesogen to the polymer backbone. Analysis of the increments in Miesowicz viscosities  $\delta\eta_b$  and  $\delta\eta_c$  indicated that for the polysiloxane SCLCP [Yao and Jamieson, 1997; Chiang et al., 2002], dissolved in 5OCB at  $T = 62^{\circ}\text{C}$ ,  $R_{\parallel}/R_{\perp}$  decreased from 1.18 to 1.03, and  $\tau_R$  increased from 1.67  $\mu\text{s}$  to 10.4  $\mu\text{s}$  ( $\tau_R \sim N^{0.8}$ ), as the degree of polymerization,  $N$ , increased from 45 to 198; in contrast, for the polyacrylate SCLCP [Chiang et al., 2002], dissolved in E48, at  $52^{\circ}\text{C}$ ,  $R_{\parallel}/R_{\perp}$  decreased from 1.54 to 1.20 and  $\tau_R$  increased from 0.37  $\mu\text{s}$  to 19.01  $\mu\text{s}$  ( $\tau_R \sim N^{1.5}$ ), as  $N$  increases from 9 to 100. In both cases, while  $R_{\parallel}/R_{\perp}$  is substantially smaller than that of the main-chain LCP, the conformation is prolate rather than the oblate conformation theoretically predicted for side-chain LCPs [Cotton and Hardouin, 1997]. Such a discrepancy with theory has been attributed [Cotton and Hardouin, 1997] to a dominant contribution from excluded interactions of the spacer, which is relatively long for the polymers under discussion here. In previous work [Yao and Jamieson, 1997], oblate conformations were indeed found for a polysiloxane SCLCP with a short ( $n = 3$ ) spacer. The larger anisotropy and stronger molecular weight dependence of  $\tau_R$  of the acrylate versus the siloxane SCLCP suggests a difference in conformation, perhaps reflecting the more rigid backbone and/or weaker influence of the nematic field in the case of the acrylate polymer.

## 1.8.2 Intrinsic Leslie Viscosities

In addition to the Miesowicz viscosities, the Brochard model also enables one to predict how dissolution of a polymer in a nematic solvent will modify the Leslie

viscosity coefficients. Specifically, the theory predicts that [Brochard, 1979]

$$\delta\alpha_2 = \frac{ck_B T \tau_R}{N} \frac{R_\perp^2 - R_\parallel^2}{R_\perp^2} \quad (1.93)$$

$$\delta\alpha_3 = \frac{ck_B T \tau_R}{N} \frac{R_\perp^2 - R_\parallel^2}{R_\parallel^2} \quad (1.94)$$

These results are interesting because they predict that the sign of the coefficients can change if a sufficient quantity of a polymer with a particular conformational shape is added. As indicated by Eqs. (1.93) and (1.94), a flow-aligning nematic solvent ( $\alpha_2 < 0$  and  $\alpha_3 < 0$ ) such as 5CB or 5OCB will transform to a flow-tumbling solution ( $\alpha_2 < 0$ ,  $\alpha_3 > 0$ ) on dissolution of a sufficient amount of a SCLCP with an oblate conformation ( $R_\perp > R_\parallel$ ), since  $\alpha_3$  will increase positively faster than  $\alpha_2$ . It follows from Eqs. (1.93) and (1.94) that continued addition of the oblate polymer may lead to the situation  $\alpha_2 > 0$  and  $\alpha_3 > 0$ , in which case the solution will experience a second transition back to flow aligning, this time with the director aligned along the vorticity axis. As a corollary, Eqs. (1.93) and (1.94) predict that addition of a sufficient quantity of a MCLCP ( $R_\parallel > R_\perp$ ) to a tumbling-flow nematic solvent such as 8CB ( $\alpha_2 < 0$ ,  $\alpha_3 > 0$ ) will produce a flow-aligning mixture ( $\alpha_2 < 0$  and  $\alpha_3 < 0$ ), since both  $\alpha_2$  and  $\alpha_3$  increase negatively.

These predictions have been tested using experiments in which the transient stress response of a homeotropic nematic monodomain subjected to shear deformation is monitored [Gu et al., 1993; Gu and Jamieson, 1994a; Kempe and Kornfield, 2003]. A flow-aligning nematic ( $\alpha_2 < 0$  and  $\alpha_3 < 0$ ) shows [Gu et al., 1993; Gu and Jamieson, 1994a, b] a characteristic stress overshoot followed by decay to a steady value, corresponding to a viscosity numerically close to  $\eta_b$ ; a flow-aligning nematic ( $\alpha_2 > 0$  and  $\alpha_3 > 0$ ) shows [Kempe and Kornfield, 2003] a characteristic rise to a steady stress corresponding to a viscosity numerically close to  $\eta_c$ ; a tumbling nematic ( $\alpha_2 < 0$ ,  $\alpha_3 > 0$ ) shows [Gu et al., 1993; Gu and Jamieson, 1994a, b; Mather et al., 1997] a characteristic damped oscillatory viscosity signature. Using this technique, addition of a SCLCP to a flow-aligning solvent was observed to induce a transition to tumbling flow [Gu et al., 1993]; in addition, the observation of a second transition to aligning flow with the director along the vorticity axis was demonstrated [Kempe and Kornfield, 2003] on dissolution of a SCLCP with a highly oblate conformation. The addition of a MCLCP to a tumbling nematic solvent was demonstrated to induce a transition to aligning flow [Gu and Jamieson, 1994a].

On detailed analysis of the transient stress signatures, certain numerical discrepancies were noted [Gu et al., 1993; Gu and Jamieson, 1994a] between the experimental increments in Leslie viscosities  $\delta\alpha_2$  and  $\delta\alpha_3$  versus the Brochard prediction. Specifically, for the side-chain LCP, assuming an oblate conformation, the theory [Eqs. (1.55)] predicts that both  $\delta\alpha_2$  and  $\delta\alpha_3$  should be positive, whereas we found [Gu et al., 1993; Gu and Jamieson, 1994a] that  $\delta\alpha_2 < 0$  and  $\delta\alpha_3 > 0$ . Also, the magnitude and signs of these viscosity increments were found to be strictly inconsistent with

electrorheological (ER) measurements [Yao and Jamieson, 1998] of the Miesowicz viscosity increments  $\delta\eta_b$  and  $\delta\eta_c$ .

Finally, in addition to predictions for the increments in Miesowicz and Leslie viscosities, the Brochard theory predicts [Brochard, 1979] the increment  $\delta\gamma_1$  in the viscosity associated with the twist distortion of a nematic solvent on dissolution of a polymeric solute:

$$\delta\gamma_1 = \frac{ck_B T \tau_R}{N} \frac{R_{||}^2 - R_{\perp}^2}{R_{||}^2 R_{\perp}^2} \quad (1.95)$$

Using dynamic light-scattering measurements [Jamieson et al., 1996],  $\delta\gamma_1$  was determined for nematic solutions of a SCLCP, which had a weakly prolate or oblate conformation (i.e.,  $R_{||}/R_{\perp} \sim 1$ ), based on ER measurements of  $\delta\eta_b$  and  $\delta\eta_c$ , and indicated [Liu et al., 1999] that  $\delta\gamma_1 \sim ck_T \tau_R / N$ , whereas the Brochard model predicts [via Eq. (1.95)] that  $\delta\gamma_1 \sim 0$ .

An explanation for these various discrepancies was suggested [Yao and Jamieson, 1998], based on the notion that when the nematic director of the solvent is allowed to rotate, one must take account of the coupling between the solvent director and the LCP director. This induces an additional viscous dissipation mechanism which contributes to the Leslie viscosities and the twist viscosity, but not to the Miesowicz viscosities:

$$\delta\gamma_1 = \frac{ck_B T \tau_R}{N} \left( \frac{R_{||}^2 - R_{\perp}^2}{R_{||}^2 R_{\perp}^2} \right)^2 + \frac{ck_B T \tau_R}{N} \quad (1.96)$$

As a test of the revised theory, further experiments were conducted [Zhao et al., 2005] on nematic solutions of a SCLCP. ER measurements indicated, via application of the Brochard hydrodynamic model, a slightly prolate conformation,  $R_{||}/R_{\perp} = 1.17 \pm 0.02$ , consistent with small-angle neutron scattering measurements, which indicated, that  $R_{g,||}/R_{g,\perp} = 1.12 \pm 0.06$ . Observations of the shear stress transient response of a homeotropic monodomain indicated that at a concentration between 0.01 and 0.02 g/mL, the solution exhibited a transition from director-aligning to director-tumbling behavior. The latter result is inconsistent with the original Brochard model [see Eq. (1.94)], which predicts such a transition (i.e.,  $\delta\alpha_3 > 0$ ) only for a polymer with an oblate shape but agrees with the modified theory [Eq. (1.96)].

## 1.9 VISCOSITY OF SEMIDILUTE AND CONCENTRATED SOLUTIONS

### 1.9.1 Empirical Concentration and Molecular-Weight Scaling Laws

The concentration dependence of the Newtonian viscosity of dilute polymer solutions may be expressed in the form of a polynomial:

$$\eta_r = 1 + [\eta]c + k_1[\eta]^2 c^2 + k_2[\eta]^3 c^3 + \dots \quad (1.97)$$

where each term of order  $c^n$  reflects  $n$ th-order interparticle direct and indirect (hydrodynamic) interactions. An empirical equation often useful to fit experimental data encompassing the dilute and semidilute concentration regimes is the Martin equation [Martin, 1951; Wetzal et al., 1953]:

$$\eta_r = 1 + c[\eta] \exp(K_M c[\eta]) \quad (1.98)$$

Indeed, data for a wide variety of polymer–solvent systems [Hager and Berry, 1982; Durand, 2007] can be described by Eq. (1.98), but such agreements provide little insight into the molecular origin of solution viscosity. As concentration increases above the overlap value,  $C^* \sim M/N_A R_g^3 \sim 2.5/[\eta]$ , a contraction of the chain dimensions occurs for flexible polymers in a good solvent, due to screening of the intersegmental excluded volume interactions, as the coils interpenetrate. Similarly, screening of the hydrodynamic interactions between the segments occurs, resulting in an increase in relaxation times for molecular motion. As concentration increases further above  $c^*$ , and chains become more deeply entangled with each other, various pieces of experimental evidence indicate that a discrete change occurs in the molecular dynamics of polymer solutions when the polymer molecular weight is sufficiently high. In particular, the molar mass dependence of molecular relaxation times increases from  $\tau \sim M$  to  $\tau \sim M^{3.5}$ , and a plateau appears in the shear storage modulus. As noted earlier, the transition occurs at a concentration referred to as the entanglement concentration and is generally interpreted as signaling a crossover from Rouse-like to reptative (snakelike) molecular dynamics. The drastic increase in relaxation times leads in turn to a correspondingly enhanced increase in solution viscosity as concentration increases. Empirically, experimental data are often expressed in terms of a power-law expression of the form [Onogi et al., 1966, 1967]

$$\eta = K_T \phi^m M^n \quad (1.99)$$

where  $K_T$  is a temperature-dependent constant,  $\phi$  is a polymer volume fraction, and  $m$  and  $n$  are constants such that  $n = 3.5 \pm 0.1$  and the ratio  $n/m$  varies from 0.5 for theta solvents to 0.7 for good solvents. The correlation between the ratio  $n/m$  and the Mark–Houwink–Sakurada exponent is often consistent with a concentration scaling of the form  $\phi/\phi^* \sim c/c^* \sim c[\eta]$ .

### 1.9.2 Predictive Models for Solutions of Flexible Neutral Polymers

Several attempts have been made to derive predictive relationships for the Newtonian viscosity of semidilute and concentrated polymer solutions. Simha and co-workers [Simha, 1952; Utracki and Simha, 1963; Simha and Somcynsky, 1965; Simha and Chan, 1971; Utracki and Simha, 1981] explored the possibility of developing a principle of corresponding states based on the  $(c, M)$  scaling equivalent to the packing of hard spheres:

$$\tilde{\eta} = \frac{\eta_{sp}}{c[\eta]} = f(c[\eta]) \quad (1.100)$$

Comparison of experiment versus a scaling analysis according to Eq. (1.100) indicates that hard-sphere scaling works reasonably well for theta and subtheta conditions [Simha, 1952; Simha and Chan, 1971; Utracki and Simha, 1981], but breaks down for good solvents. For these systems, a molecular weight–dependent scaling concentration can be defined of the form [Utracki and Simha, 1963; Simha and Somcynsky, 1965]

$$\gamma_{ss} = K_1 M^{-\alpha_1} = \frac{KK_1 M^{a-\alpha_1}}{[\eta]} \quad (1.101)$$

Experimentally, as the solvent quality approaches the theta condition, the exponent  $\alpha_1$  approaches the Mark–Houwink–Sakurada exponent,  $a$ , which, in turn, approaches the limiting value 0.5. The applicability of Eqs. (1.100) and (1.101) was found to extend to concentrations in excess of the entanglement concentration.

To proceed further (i.e., to extend the treatment to encompass temperature dependence and the crossover from semidilute to concentrated solution regime, it is necessary to incorporate information regarding the free-volume characteristics of polymer and solvent. Utracki and Simha [1981] find that a scaling equation of the form

$$\ln \tilde{\eta} = D_0 + D_1 Y_\phi \quad (1.102)$$

provides a means of generating a universal dependence of  $\eta$  as a function of the independent reduced variables, molecular weight,  $\tilde{M}$ , concentration,  $\tilde{c}$ , and temperature  $\tilde{T}$ . In Eq. (1.102),  $D_1 = -D_0$ , where

$$D_0 = \frac{-6(D_0^1 - 2)^2}{(D_0^1)^2 - 12D_0^1 + 12} \quad (1.103)$$

where  $D_0^1 = d_1 h_s / f_{h,s} H_s$ , with  $f_{h,s} = (h_s V - V_0) / V_0$  the hydrodynamically accessible free volume of the pure solvent,  $V$  and  $V_0$  the specific volumes of the solvent at  $T$  and  $T = 0$  K, respectively,  $h_s \leq 1$  a hydrodynamic shielding parameter of the pure solvent,  $H_s$  the corresponding shielding parameter of the solvent in the solution, and  $d_1$  a coefficient in the Doolittle equation,  $\ln \eta = d_0 + d_1 / f_h$ . Also, in Eq. (1.102),

$$Y_\phi = \frac{1}{1 + D_2^\dagger \tilde{\phi}} \quad (1.104)$$

where  $\tilde{\phi} = \phi / \phi^*$  and  $\phi^*$  is the scaling volume fraction. The parameter  $D_2^\dagger$  is explicitly defined in the theory as

$$D_2^\dagger = \frac{D_2^1 (D_0^1 - 2)}{2D_0} \quad (1.105)$$

where  $D_2^1 = (H_p / H_s) U - 1$ , and  $U = \exp b(X_p - X_s)$ , with  $X_i$  the temperature, scaled by the glass transition temperature of polymer ( $i = p$ ) and solvent ( $i = s$ ).

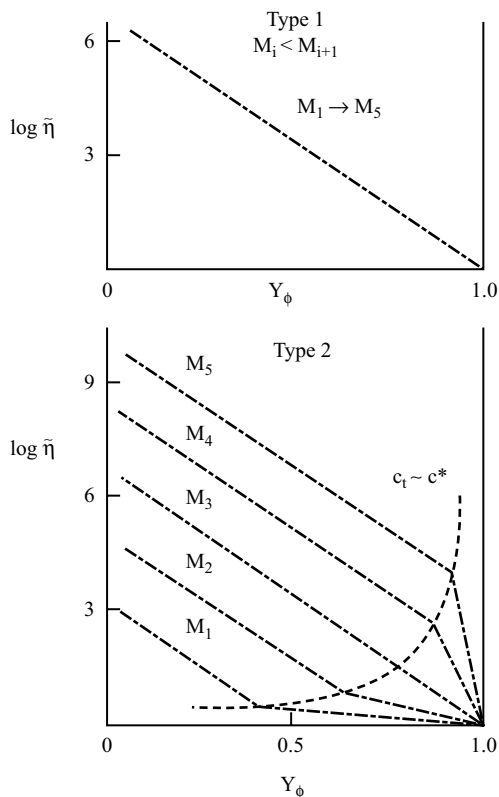


**FIGURE 1.11** Schematic representation of the two types of viscosity–concentration scaling behavior seen in polymer solutions: (a) type 1, linear superposition of data for solutions having different polymer molecular weights,  $M_i < M_{i+1}$ , according to Eq. (1.61) with  $D_2^\dagger$  as a fitting parameter; (b) type 2, superposition failure indicating molecular weight dependence of  $D_2^\dagger$  and a break in the plots at the overlap concentration. (Adapted from Utracki and Simha [1981].)

Experimentally,  $D_2^\dagger$  is determined by iteration to linearize the data according to Eq. (1.102), using as a starting value  $D_2^\dagger/\phi^* = 1/\gamma_{ss}$ , the characteristic scaling concentration defined in Eq. (1.101).

Applying, Eq. (1.102) to scale viscosity data, two types of behavior are observed [Utracki and Simha, 1981], as shown schematically in Figure 1.11. Most systems show a linearization according to Eq. (1.102) over the full range of concentration and molecular weight (Figure 1.11a), representing a scaling in terms of corresponding states characterized by the reduced concentration,  $\tilde{\phi}$ . In some systems, a second type of behavior is observed (Figure 1.11b), in which superposition, according to Eq. (1.102), of data for samples of different molecular weight fails and a break occurs in the plots, at concentrations  $c_l$  which turn out to be comparable to the concentration  $c^* \approx 1.1/[\eta]$ , at which coil overlap occurs. Superposition of the data at  $c > c^*$

can be achieved by a horizontal shift, which, within the framework of the theoretical model, corresponds [Eqs. (1.104) and (1.105)] to incorporating the molecular weight dependence of the glass transition temperatures of polymer and solvent. The origin of the break in the plots of  $\ln \tilde{\eta}$  versus  $Y_\phi$  is still not understood [Utracki and Simha, 1981] but apparently indicates some change in the flow mechanism near  $c_f$ .

As noted earlier, for polymers of sufficiently high molecular weight, at a concentration substantially in excess of the overlap concentration, there is a distinct transition in the viscoelastic behavior of polymer solutions, attributed to the point at which topological restrictions to translational and rotational mobility appear due to interchain entanglements. Efforts have been made to model the viscometric behavior of polymer solutions through this entanglement transition. First, Phillies [Phillies, 1995, 2002a; Phillies and Quinlan, 1995] has derived a pseudovirial expansion of the form Eq. (1.97), describing the concentration dependence of polymer solution viscosity by evaluating interchain hydrodynamic interactions to third order via an extension of the Kirkwood–Riseman model. Such an analysis neglects chain-crossing constraints, so may be expected to be valid until chain entanglements play a dominant role. Extrapolation to higher concentrations can be performed via a renormalization group, which leads to an expression of the stretched exponential form:

$$\eta = \eta_0 \exp(\alpha_p c^s M^t) \quad (1.106)$$

where  $\alpha_p$ ,  $s$ , and  $t$  are scaling exponents. Phillies notes that Eq. (1.106) is in agreement with experimental data for many polymer–solvent systems [Phillies, 1995; Phillies and Quinlan, 1995] and finds that the parameter  $\alpha_p$  varies with solvent quality as  $\alpha_p \sim \alpha_\eta^3 = [\eta]/[\eta]_\theta$ , predicted by the hydrodynamic scaling model. Phillies further suggests [Phillies, 1995; Phillies and Quinlan, 1995] that the limit of applicability of Eq. (1.106) may be used to identify the concentration at which entanglement constraints become dominant in determining chain mobility. Thus, as shown in Figure 1.12, using data of Dreval et al. [1973] on hydroxypropylcellulose solutions in water, Phillies and Quinlan [1995] find a crossover from stretched-exponential to power-law concentration dependence,  $\eta \sim c^\epsilon$ , signifying what they term a solutionlike–meltlike transition in polymer dynamics. As shown in Figure 1.12, the crossover occurs at the concentration  $c[\eta] \sim 20$  (i.e., considerably in excess of the overlap concentration,  $c^*[\eta] \sim 1.0$ ). Phillies [2002b] has further demonstrated self-consistency between his hydrodynamic scaling model for viscosity and a similar analysis of the self-diffusion coefficient of polymer chains in semidilute solution, which also leads to stretched-exponential concentration dependence, in agreement with experiment.

Berry [1996] has developed a formalism designed to describe the viscosity of isotropic solutions of flexible, semiflexible, and rodlike polymer chains over a range of concentrations encompassing dilute solutions to the undiluted polymer. The expression is formulated to account for the separate effects of screening of thermodynamic and hydrodynamic interactions, as well as the onset of intermolecular chain entanglements, under a range of solvent quality extending from theta to “good”

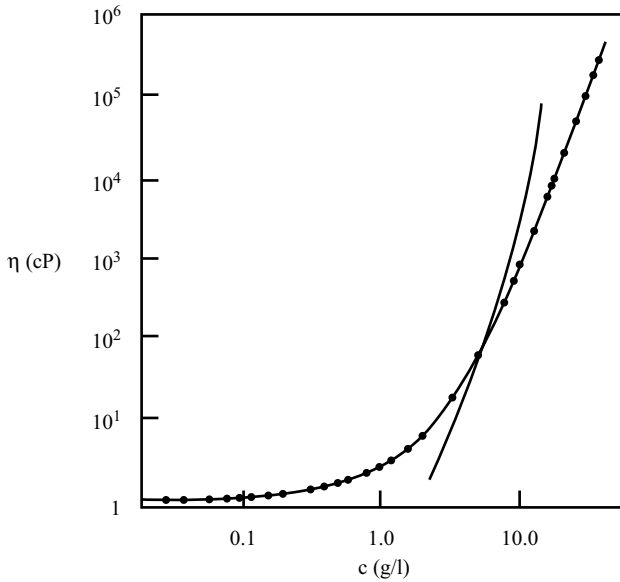


**FIGURE 1.12** Viscosity of hydroxypropylcellulose (nominal molecular weight  $M = 10^6$  g/mol) in water and fits to stretched exponential and power-law concentration dependence. (From Phillis and Quinlan [1995], with permission. Copyright © 1995 American Chemical Society.)

solvents:

$$\frac{\eta}{\eta_{\text{LOC}}^{(c)}} = 1 + \left[ \left\{ c[\eta] \left( \frac{\alpha^{(c)}}{\alpha} \right)^3 \left( 1 + c[\eta] \left( \frac{\alpha^{(c)}}{\alpha} \right)^3 \right)^{k'} \right\}^2 + \left\{ H^{(c)} X \mathfrak{E} \left( \frac{X}{X_c} \right) \right\}^2 \right]^{1/2} \quad (1.107)$$

where  $X$  is a revised dimensionless Fox parameter,  $X = \pi N_A c (R_g^{(c)})^2 / M_L$ , which, experiment suggests, has a quasiuniversal value for flexible polymers at the onset of entanglement, (i.e.,  $X_c = 100$ ) and  $k'$  is the Huggins coefficient. The function  $\mathfrak{E}(X/X_c)$  incorporates the effect of chain entanglements:

$$\mathfrak{E}(y) = 1 + [y^2 m(y)]^{2^{1/2}} \quad (1.108)$$

where  $m(y) \sim (1 - \mu y^{-1/2})^3$ , with  $\mu$  a constant of order unity, is a function that tends to unity for  $X/X_c > 100$  and equals  $y^{0.4}$  for  $X/X_c < 100$ . The effect of thermodynamic interactions is described by the concentration-dependent chain expansion parameter:

$$\alpha^{(c)} = \text{Max} \left\{ 1; \alpha (1 + c[\eta])^2 \right\}^{-1/16} \quad (1.109)$$

where the function  $\text{Max}\{x; y\}$ , which specifies the maximum of the two arguments, ensures that  $\alpha \geq \alpha^{(c)} \geq 1$  for finite excluded volume,  $z \geq 0$ . The concentration-dependent radius of gyration is thus given by  $R_g^{(c)} = R_g \alpha^{(c)} / \alpha$ . The influence of hydrodynamic interactions is described by the hydrodynamic screening function:

$$H^{(c)} = 1.156 \left( \frac{c}{\rho} \right)^\beta (\alpha^{(c)})^4 \left\{ 1 - \exp \left[ -2 \left( \frac{c}{\rho} \right)^\beta \right] \right\} \quad (1.110)$$

where the parameter  $\beta = 0.5$  for flexible coils. In Eq. (1.107),  $\eta_{\text{LOC}}^{(c)}$  represents a local viscosity, expected to depend on temperature and polymer concentration but to be nearly independent of molecular weight;  $\eta_{\text{LOC}}^{(c)}$  is proportional to the segmental friction factor appearing in other treatments. For infinitely dilute solutions,  $\eta_{\text{LOC}}^{(c)} = \eta_{\text{solvent}}$ . In the opposite extreme of undiluted polymer,  $\eta_{\text{LOC}}^{(c)}$  is given by  $\eta_{\text{repeat}}^{(c)}$ , representing the viscosity needed to compute the segmental friction factor for the undiluted polymer from the segment dimensions, using Stokes' law. For solutions it seems reasonable to approximate  $\eta_{\text{LOC}}^{(c)}$  in terms of  $\eta_{\text{solvent}}$  and  $\eta_{\text{repeat}}$  by relations similar to those used for the viscosity of mixtures of small molecules [Berry, 1996]. For example, one might use the empirical approximation

$$\eta_{\text{LOC}}^{(c)} = \eta_{\text{solvent}}^{1-f(\phi)} \eta_{\text{repeat}}^{f(\phi)} \quad (1.111)$$

with  $f(\phi)$  determined principally by, but not necessarily equal to, the polymer volume fraction  $\phi = c/\rho$ . Berry [1996] demonstrates that Eq. (1.107) can be conveniently used to correlate viscometric data, and to estimate  $\eta/\eta_{\text{LOC}}^{(c)}$  as a function of  $c$  and  $M$ , provided that sufficient structural information about the polymer and solvent can be obtained.

The Newtonian viscosity of polymer solutions, encompassing the dilute and semi-dilute concentration regimes, has been discussed [Jamieson and Telford, 1982; Takahashi et al., 1985] within the context of the de Gennes scaling description, using the reptation model [de Gennes, 1976a, b], in which the chain is assumed to execute a snakelike motion (i.e., reptation) within a tube whose length is equal to the contour length of the polymer and whose width is determined by repulsive contacts with its neighbors. Within this model, the elastic modulus of an entangled polymer network is

$$G \propto \frac{k_B T}{\xi^3} \quad (1.112)$$

and the reptation time is

$$\tau_{\text{rep}} \propto \frac{\eta_s (M/M_e)^3 \xi^3}{k_B T} \quad (1.113)$$

where  $\xi$  is the monomer–monomer correlation length and  $M_e$  is the entanglement molecular weight. Scaling arguments [de Gennes, 1976a, b] lead to the conclusion that  $\xi \sim R_g (c/c^*)^{-\nu/(3\nu-1)}$ , and hence, in good solvents  $\xi \sim c^{-3/4}$ , and in theta solvents  $\xi \sim c^{-1}$ . Combining Eqs. (1.112) and (1.113), the zero-shear viscosity is

$$\eta = G \tau_{\text{rep}} \propto \eta_s \left( \frac{M}{M_e} \right)^3 \quad (1.114)$$

and is determined by the number of entanglements in solution, as in the polymer melt state. Noting the experimental result in the melt,  $\eta \sim M^{3.4}$ , Takahashi et al. [1985] suggest replacing this result by

$$\eta \propto \eta_s \left( \frac{M}{M_e} \right)^{3.4} \quad (1.115)$$

Scaling arguments imply that

$$\frac{M}{M_e} \propto \left( \frac{c}{c^*} \right)^{1/(3\nu-1)} \quad (1.116)$$

where  $\nu$  is the excluded volume exponent, ( $R_G^2 \sim M^{2\nu}$ ),  $0.5 < \nu < 0.6$ , and  $c^* = M/N_A R_G^3$  is the overlap concentration. This leads to scaling predictions for the viscosity:

$$\eta_r \propto \left( \frac{c}{c^*} \right)^{3/(3\nu-1)} \quad (1.117a)$$

if one accepts Eq. (1.114), or

$$\eta_r \propto \left( \frac{c}{c^*} \right)^{3.4/(3\nu-1)} \quad (1.117b)$$

if one accepts Eq. (1.115). These results lead to molecular weight- and concentration-scaling laws of the form

$$\eta_{\text{sp}} \propto M^3 c^{3/(3\nu-1)} \quad (1.118a)$$

and

$$\eta_{\text{sp}} \propto M^{3.4} c^{3.4/(3\nu-1)} \quad (1.118b)$$

respectively. Thus, according to Eq. (1.118b), the reptation model of entanglement dynamics leads to values of the concentration exponent that fall in the range 4.25 (good solvent) to 6.8 (theta solvent).

Conflicting conclusions are found in the literature as to the accuracy of these predictions. Takahashi et al. [1985] tested these scaling predictions against experimental data on  $\eta_r$  for polystyrene in theta, marginal, and good solvents, encompassing the

dilute and semidilute regimes and found that Eqs. (1.117) and (1.118) superpose data in dilute and semidilute solutions, respectively, for theta and marginal solvents but not for good solvents. Systematic deviations are observed in the latter, which increase as the molecular weight of the polymer decreases. These findings seem consistent with those of Utracki and Simha [1981] when considering that  $c/c^*$  scaling is essentially equivalent to  $c[\eta]$  scaling. On the other hand, viscosity measurements of Adam and Delsanti [1982, 1983] for various polymers in good solvents scale with  $c/c^*$ , whereas corresponding measurements in theta solvents did not [Adam and Delsanti, 1984; Roy-Chowdhury and Deuskar, 1986]. Accepting the latter data, Colby and Rubinstein [1990] argue that the breakdown in  $c/c^*$  scaling in theta solvents arises because in contrast to the situation in good solvents, the correlation length,  $\xi$ , and the tube diameter,  $\delta$ , depend on concentration differently. Specifically, the concentration scaling of  $\delta$  is determined by the density of binary contacts between monomers. In good solvents, the density of intermolecular binary contacts scales as  $c^{9/4}$ , and hence  $\delta \sim (c^{-9/4})^{1/3} \sim c^{-3/4}$  (i.e., the same dependence as  $\xi$ ); however, in theta solvents, the density of binary contacts scales as  $c^2$ , and the chain may be modeled in semidilute solution as a random walk of  $N/N_\xi$  blobs of size  $\xi$ . The associated volume in which  $kT$  is stored is  $(N_e/N_\xi)\xi^3$ , with  $N_e/N_\xi$  given by the random walk result,  $N_e/N_\xi \sim (\delta/\xi)^2$ . It follows that [Colby and Rubinstein, 1990; Colby et al., 1994]

$$G = \frac{k_B T}{(N/N_\xi)\xi^3} = \frac{k_B T}{(\delta/\xi)^2 \xi^3} = \frac{k_B T}{\delta^2 \xi} \quad (1.119)$$

This result, which contrasts with Eq. (1.112), leads to the same concentration scaling as Eq. (1.112) in good solvents,  $G \sim c^{9/4}$ , but differs from Eq. (1.112) in theta solvents,  $G \sim c^{7/3}$ , since  $\delta \sim c^{-3/4}$ , and  $\xi \sim C^{-1}$ . The reptation time is calculated on the assumption that relaxation is Zimm-like inside the blobs and Rouse-like between entanglements:

$$k_B T \tau_{\text{rep}} \sim \eta_s \xi^3 \left( \frac{N_e}{N_\xi} \right)^2 \left( \frac{N}{N_e} \right)^3 \sim \frac{\eta_s \delta^4 (N/N_e)^3}{\xi} \quad (1.120)$$

Thus,

$$\eta = G \tau_{\text{rep}} = \eta_s \left( \frac{\delta}{\xi} \right)^2 \left( \frac{N}{N_e} \right)^3 \quad (1.121)$$

It follows that for semidilute solutions in a good solvent,  $\delta \sim \xi$ ,  $N_e \sim \delta^{1/\nu} \sim c^{1/(1-3\nu)}$ , and therefore Eq. (1.121) leads to the de Gennes result, Eq. (1.114), whereas for theta solutions,  $\xi \sim c^{-1}$ ,  $\delta \sim c^{-2/3}$ , and  $N_e \sim \delta^2 \sim c^{-4/3}$ , and hence from Eq. (1.121):

$$\eta \sim \eta_s N^3 c^{14/3} \sim \eta_s M^{2/3} (c/c^*)^{14/3} \quad (1.122)$$

Thus, Colby and Rubinstein [1990] predict that  $\eta_r \sim (c/c^*)^{3/(3\nu-1)}$  in good solvents, whereas  $\eta_r/M^{2/3} \sim (c/c^*)^{14/3}$  in theta solvents, and they further demonstrate that the

data of Adam and Delsanti [1984] and Roy-Chowdhury and Deuskar [1986] are consistent with the latter scaling prediction.

The blob model offers another insight [Raspaud et al., 1995; Heo and Larson, 2005], in which a semidilute solution may be viewed, on a length scale larger than the blob size, as a melt of chains of blobs. Within the blob, the chain does not know that it is in a melt, and its dynamics are determined by the Zimm theory, in which hydrodynamic interactions dominate. On length scales larger than the blob, hydrodynamic interactions are screened and Rouse dynamics operate. From this point of view, one can expect that the  $c[\eta]$  or  $c/c^*$  scaling of the solution viscosity in dilute solution will extend into the semidilute regime until the concentrated solution regime is reached, or if the molecular weight of the polymer is high enough, until the number of blobs per chain exceeds the number needed for the chain to become entangled, at which point the entanglement concentration becomes an additional scaling variable (semidilute entangled regime). In the melt, the scaling prediction of the reptation theory [Eq. (1.115)] may be expressed instead as [Raspaud et al., 1995]

$$\frac{\eta}{\eta_{\text{Rouse}}} \sim \left( \frac{M}{M_e} \right)^{2.4} \quad (1.123)$$

where  $\eta_{\text{Rouse}}$  is the melt viscosity at the molecular weight selected, if entanglements are absent. Eq. (1.123) follows since Rouse theory implies that  $\eta_{\text{Rouse}} \sim M$ . Following the melt analogy, in the semidilute entangled regime, this suggests [Raspaud et al., 1995; Heo and Larson, 2005] a scaling treatment of the form

$$\eta/\eta_{\text{Rouse}} \sim \left[ \left( \frac{N}{N_\xi} \right) / \left( \frac{N}{N_\xi} \right)_e \right]^{2.4} \sim \left( \frac{n_b}{n_{be}} \right)^{2.4} \quad (1.124)$$

where  $n_b$  is the number of blobs per chain at concentration  $c$  and  $n_{be}$  is the critical number of blobs per entanglement, assumed independent of concentration. Since in semidilute solutions  $n_b/n_{be} = (c/c_e)^{1/(3\nu-1)}$ , the equivalent concentration scaling treatment is

$$\frac{\eta}{\eta_{\text{Rouse}}} = k \left( \frac{c}{c_e} \right)^{2.4/(3\nu-1)} \quad (1.125)$$

This scaling prediction has been tested against experimental data and appears to be successful for both flexible and semiflexible polymers in good solvents. When plotting a reduced viscosity versus a reduced concentration, the best collapse of the data onto a universal curve was found if two different definitions of  $c^*$  were chosen [Raspaud et al., 1995]:  $\eta_{\text{Rouse}} = \eta_s(N/N_\xi) = \eta_s(c/c^*)^{1/(3\nu-1)}$  with  $c^* = 1/[\eta]$ , and  $c_e = c^* n_{be}^{3\nu-1}$  with  $c^* = 1/M_w A_2$ . The latter definition assumes that the appropriate scaling for concentration is based not on hydrodynamic volume but on the thermodynamic

equivalent hard-sphere volume. Specifically, Heo and Larson [2005] find that

$$\frac{\eta}{\eta_{\text{Rouse}}} = (45 \pm 2) \left( \frac{c}{c_e} \right)^{2.95 \pm 0.07} \quad (1.126)$$

which is in good agreement with Eq. (1.125) when one chooses  $\nu = 0.588$ .

In summary, results to date suggest that the concentration dependence of viscometric data may be treated distinctly in three regimes: dilute, semidilute, and concentrated. In the dilute and semidilute unentangled regimes, the concentration dependence derives from indirect (hydrodynamic) and direct intermolecular interactions, and can be described by  $c[\eta]$  or  $c/c^*$  scaling via a virial type of equation [Eq. (1.119)] or the stretched-exponential description of Phillis [2002a, b]). In the semidilute entangled regime, a scaling treatment according to reptation theory seems to work well [Eq. (1.118) or (1.126) in good solvents, Eq. (1.122) in theta solvents]. In the concentrated regime, one has to resort to a treatment such as that of Utracki and Simha [1981] or that of Berry [1996], which incorporates the concentration, temperature, and solvent dependence of the segmental frictional coefficient.

### 1.9.3 Viscosity of Branched Polymers in Semidilute and Concentrated Regimes

The concentration dependence of solutions of branched polymers has also been studied in the semidilute and concentrated regimes. Intuitively, one expects that at concentrations and molecular weights below the entanglement transition, the viscosity should be smaller than that of linear polymers, because the hydrodynamic volume of a branched polymer is smaller than that of a linear polymer of the same molecular weight. Above the entanglement transition, the situation becomes more complicated, and if the molecular weight of the branches is larger than the entanglement molecular weight, the viscosity rises more rapidly than that of a linear polymer of the same molar mass. This can be explained using the reptation model, in which the entanglement network constrains translational motion of chain segments to a confining tube. However, the branch points block reptative motion of the entire macromolecule, and hence the only way in which the chain can translate is by retraction of the arms from their tubes at the branch points and reinsertion into different tubes in new directions. This leads to a substantial increase in the longest relaxation time,  $\tau_r$ , and hence a large increase in viscosity, since the entanglement density, and hence the plateau modulus,  $G$ , remain unchanged [see Eq. (1.114)]. Such an expectation has been confirmed experimentally for the melt [Kraus and Gruver, 1965] and for solutions [Lee et al. 2006], and is illustrated in Figure 1.13, which compares shear viscosity data [Lee et al., 2006] for solutions of a linear 1,4-polyisoprene (PIP;  $M_n = 256.9$  kg/mol) versus a three-arm star PIP ( $M_n = 299.8$  kg/mol), each dissolved in a low-molar-mass linear PIP ( $M_n = 3.22$  kg/mol). The latter  $M_n$  is smaller than the entanglement molecular weight for PIP ( $M_e = 4.2$  kg/mol) [Lee et al., 2006]. A second feature manifested in Figure 1.13 is that a simple power-law scaling versus concentration no longer works. Instead, reptation theory applied to star polymers in

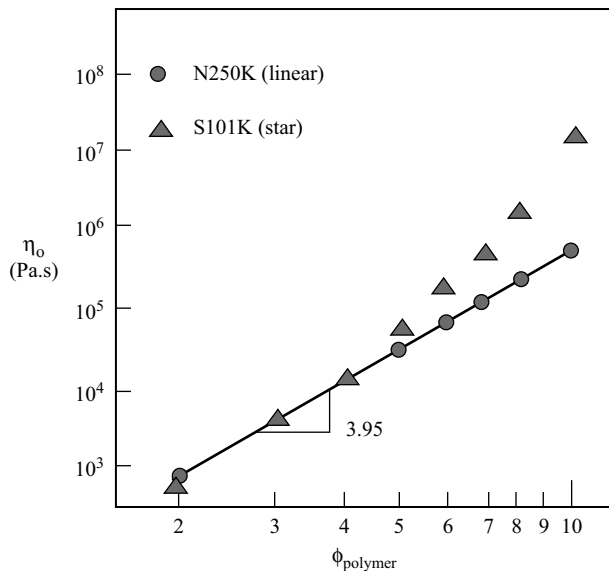


**FIGURE 1.13** Concentration dependence of the zero-shear viscosity of 1,4-polyisoprene linear (N250K,  $M_n = 256,900$  g/mol), three-arm symmetric star (S101K,  $M_{n,\text{arm}} = 101,000$  g/mol), and three-arm asymmetric star ( $A_2B73K$ ,  $M_{n,A} = 73,000$  g/mol,  $M_{n,B} = 33,000$  g/mol and  $A_2B182K$ ,  $M_{n,A} = 182,000$  g/mol,  $M_{n,B} = 33,000$  g/mol) polymer solutions. (Adapted from Lee et al. [2006].)

the melt state predicts an exponential dependence on arm molecular weight,  $M_a$  [Vega et al., 2002]:

$$\eta \sim \left( \frac{M_a}{M_e} \right)^\beta \exp \left( \frac{kM_a}{M_e} \right) \quad (1.127)$$

where  $\beta$  and  $k$  are constants. For example, Vega et al. [2002] deduce that the theory of Milner and McLeish [1997] predicts that  $\beta = 0.68$  and  $k = 0.48$ . Following the suggestion of Lee et al. [2006], a corresponding result for the concentration dependence of viscosity of star polymer solutions may be derived by defining the appropriate concentration dependence of  $M_a/M_e$ . For concentrated solutions (above 40 to 50%), assumption of theta solution scaling appears to describe experimental data successfully [Lee et al., 2006]: that is,  $M_a/M_e(\phi_p) = (M_a/M_e^0)\phi_p^{4/3} = (M_a/M_e^0)(c_p\bar{v}_p)^{4/3}$ , where  $\phi_p$  is the polymer volume fraction,  $M_e^0$  is the entanglement molecular weight of the melt, and  $c_p$  and  $\bar{v}_p$  are the polymer concentration and partial specific volume, respectively. At lower concentrations, the model predictions deviate systematically from the experimental data, for reasons that remain unclear at this date.

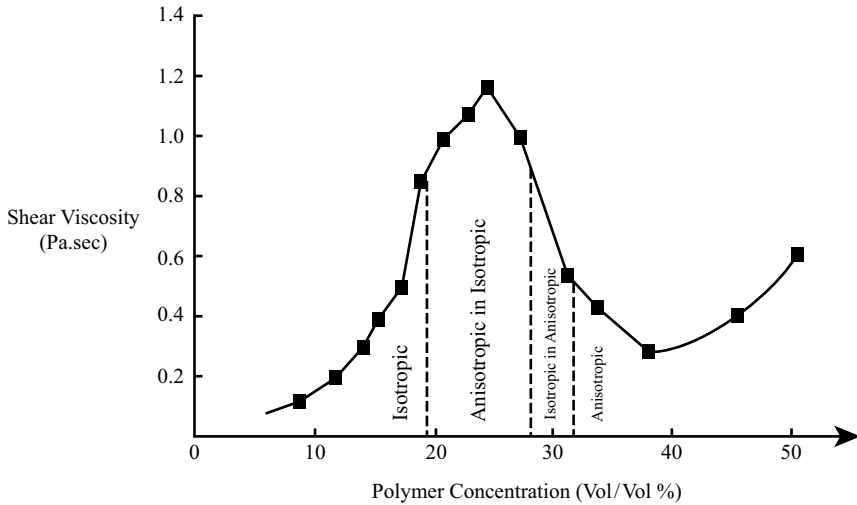


**FIGURE 1.14** Viscosity as a function of polymer concentration of a solution of a 50 : 50 random copolymer, poly(*n*-hexylisocyanate-*co*-*n*-propylisocyanate) ( $M_w = 41,000$  g/mol) in toluene, encompassing the isotropic, biphasic, and anisotropic (liquid crystal) regimes. (Adapted from Aharoni [1980a].)

#### 1.9.4 Predictive Models for Solutions of Stiff and Semi-stiff Neutral Polymers

The concentration and molecular weight dependence of solutions of rodlike polymers (length  $\times$  diameter =  $L \times d$ ) has been studied experimentally and theoretically. Owing to their rodlike shape, which can lead to liquid-crystal formation, the viscosity behavior of rodlike polymer solutions is greatly different from that of flexible polymer solutions. On the experimental side, as illustrated in Figure 1.14, for concentrated solutions of a poly(*n*-hexylisocyanate) (PnHIC) of  $M_w = 41$  kg/mol in toluene, when concentration is increased above the overlap concentration,  $c^* = M/N_A L^3$  (g/mL), the viscosity rises steeply, as  $c^5 \rightarrow c^8$ , until at a particular concentration,  $c^{**} = M/N_A d L^2$  (g/mL), transition to a lyotropic liquid-crystal phase occurs [Aharoni, 1979, 1980a, b]. At this point, droplets of a liquid-crystal polymer phase are dispersed in a continuous isotropic solution phase, the rate of increase of viscosity slows, until the viscosity reaches a maximum value and then decreases. With further increase in polymer concentration, the volume fraction of liquid-crystal phase increases until it becomes, first, the continuous phase and then completely liquid crystalline, the viscosity continues to decrease, reaches a minimum value, and then begins to increase again as the liquid-crystal phase becomes more concentrated in polymer molecules. In addition to PnHIC solutions, similar behavior has been documented for concentrated solutions of xanthan, a rigid ionic double-helical polysaccharide in aqueous NaCl [Lee and Brant, 2002].

Theoretical discussion of the concentration and molecular weight dependence of the viscosity of semidilute solutions of rigid-rod macromolecules has been reported. Doi and Edwards [1978] derived the well-known result

$$\eta = \frac{\beta k_B T L^6}{10 D_R^0} \left( \frac{c N_A}{M} \right)^3 = \frac{\beta \pi \eta_s L^9}{30 \ln(L/d)} \left( \frac{c N_A}{M} \right)^3 \quad (1.128)$$

where  $D_R^0$  is the rotational diffusion coefficient of the rod at infinite dilution and  $\beta$  is a numerical constant. Note that neglecting the weakly length-dependent term  $\ln(L/d)$ , this result conforms to the frequently observed scaling of flexible polymers,  $\eta \sim f(c/c^*)$ , where  $c^* \sim M/N_A R_g^3 \sim M/N_A L^3$ . Subsequently, Doi [1975, 1981] extended this prediction to higher concentrations, where the finite diameter of the rods imposes increased restrictions on rod mobility:

$$\eta = \frac{\beta \pi \eta_s L^9}{30 \ln(L/d)} \left( \frac{c N_A}{M} \right)^3 \left( \alpha_{DE} - \frac{c N_A}{M d L^2} \right)^{-2} \quad (1.129)$$

where  $\alpha_{DE}$  is a numerical coefficient. This equation may be written in terms of the crossover concentrations  $c^*$  and  $c^{**}$ , where  $c^{**} \sim 1/dL^2$  is the concentration at the onset of liquid-crystal formation:

$$\eta = \frac{\beta \pi \eta_s}{30 \alpha_{DE}^2 \ln(L/d)} \left( \frac{c}{c^*} \right)^3 \left( 1 - \frac{c}{\alpha_{DE} c^{**}} \right)^{-2} \quad (1.130)$$

Comparisons of experimental data on various highly rigid polymers against the predictions of this equation have been reported [Chu et al., 1981; Jamieson, 1983; Enomoto et al., 1985]. Chu et al. [1981] report failure of Eq. (1.130) to superimpose data on semirigid polyimide chains in sulfonic acids. Enomoto et al. [1985] report superposition of viscometric data of diverse semirigid polymers provided that the contribution of entanglement dynamics to the viscosity is isolated by subtracting the contribution of interchain hydrodynamic interactions to the total viscosity. Their analysis indicates that the prefactor  $\beta$  is substantially smaller than unity ( $\beta \sim 0.03$ ), traceable to the fact that the onset of entanglement dynamics occurs at a concentration substantially higher than the overlap value,  $c^* = M/N_A L^3$ . Jamieson [1983] pointed out that the failure of Eq. (1.130) in the approximate form  $\eta/\eta_s \sim (c/c^*)^3 f(c/c^{**})$  to superimpose viscometric data in the regime  $c \gg c^*$  can be improved by using scaling of the form  $(\eta/\eta_s)(c^*/c^{**})^3 \sim (c/c^{**})^3 f(c/c^{**})$ . In all these analyses, it seems clear that the parameter  $\alpha_{DE}$  varies substantially among different polymer systems, presumably reflecting system-specific variations in polydispersity, interchain association, differing degrees of chain stiffness, and the direct (nonhydrodynamic) intermolecular interactions.

Indeed, Teramoto and co-workers [Sato et al., 1991, 2003; Ohshima et al. 1995] have pointed out that the viscosity of stiff-chain polymers is affected dramatically by chain flexibility. To illustrate this, in Figure 1.15, Sato et al. [2003] compare

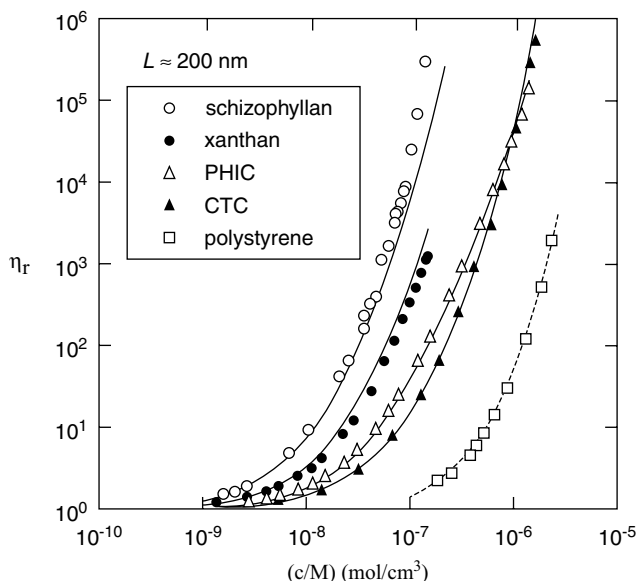


**FIGURE 1.15** Relative viscosities  $\eta_r$  of five polymer solution systems with different chain stiffness, plotted against the molar concentration,  $c/M$ :  $\circ$ , schizophyllan (a triple-helical polysaccharide) in water at 25°C ( $q = 200$  nm;  $L = 210$  nm);  $\bullet$ , xanthan (double-helical ionic polysaccharide) in 0.1 M aqueous NaCl at 25°C ( $q = 100$  nm;  $L = 190$  nm);  $\Delta$ , poly(*n*-hexyl isocyanate) (PHIC) in toluene at 25°C ( $q = 37$  nm;  $L = 210$  nm);  $\blacktriangle$ , CTC in tetrahydrofuran at 25°C ( $q = 10.5$  nm;  $L = 220$  nm);  $\square$ , polystyrene in cyclohexane at 34.5°C ( $q = 1$  nm;  $L = 340$  nm). Solid curves, fuzzy-cylinder theory; dashed curve for polystyrene solutions, eye guide. (From Sato et al. [2003], with permission. Copyright © 2003 American Chemical Society.)

the concentration-dependent viscosities of several stiff-chain polymer species, each of which have comparable contour lengths,  $L \sim 200$  nm, but which differ in their persistence lengths,  $\ell_p$ . Of these polymers, all of which are stiff enough to form a liquid-crystal phase at high concentrations, the stiffest, schizophyllan ( $\ell_p = 200$  nm), has the highest viscosity, and the others have lower viscosities in increasing order of chain flexibility: xanthan ( $\ell_p = 100$  nm) > poly(*n*-hexylisocyanate) (PnHIC;  $\ell_p = 37$  nm) > cellulose tris(phenyl carbamate) (CTC;  $\ell_p = 10.5$  nm). Also shown for comparison is the viscosity of polystyrene ( $\ell_p = 1$  nm), a non-liquid-crystal-forming polymer. To describe such systems, Sato et al. [1991] developed a variant of the Doi–Edwards model in which the chain segments can execute rapid motions orthogonal to the axis of the tube in which the chain is confined. Thus, the chain configuration may be approximated as a cylindrically smoothed segmental density (fuzzy cylinder model). The average cylinder length,  $L_e$ , and diameter,  $d_e$ , are then given by

$$L_e = \langle h^2 \rangle \quad \text{and} \quad d_e = \left( \langle H^2 \rangle + d^2 \right)^{1/2} \quad (1.131)$$

where  $\langle h^2 \rangle$  and  $\langle H^2 \rangle$  and  $d$  are, respectively, the mean-square end-to-end distance, the mean-square distance between the chain midpoint and the end-to-end axis, and the diameter of the chain.

The fuzzy cylinders are assumed to interact dynamically through a hard-core potential. The rotational diffusion coefficient of the rods is computed as

$$\frac{D_R}{D_R^0} = \left[ 1 + B \frac{cN_A}{M} \left( \frac{D_{||0}}{D_{||}} \right)^{1/2} \right]^{-2} \quad (1.132)$$

Here  $D_{||}$  and  $D_{||0}$  are longitudinal diffusion coefficients at finite concentration  $c$  and infinite dilution, respectively. The parameter  $B$  is given by

$$B = 1350^{-1/2} L_e^3 f_R \left( \frac{L_e}{d_e} \right) \left( \frac{L_e^2 D_R^0}{6D_{||0}} \right)^{1/2} \quad (1.133)$$

where  $f_R(L_e/d_e)$  describes the effect of segment fluctuation inside the cylinder on the entanglement dynamics:

$$f_R(x) = (1 + Cx)^3 \left( 1 - \left( \frac{1}{5} \right) Cx \right) \quad (1.134)$$

with the coefficient  $C$  expressed empirically as

$$C = \frac{1}{2} \left( \tanh \frac{N - N^*}{\Delta} + 1 \right)$$

in terms of  $N = L/2\ell_p$ , and two adjustable parameters,  $N^*$  and  $\Delta$ . The ratio  $D_R^0/D_{||0}$  is determined using the wormlike coil model, and the ratio  $D_{||0}/D_{||}$  is computed by assuming that longitudinal diffusion needs the formation of a critical hole whose size and shape are assumed to be equal to that of the fuzzy cylinder [Sato et al., 1991]:

$$\frac{D_{||0}}{D_{||}} = \exp \left( \frac{V_{\text{ex}}^* c N_A}{M} \right) \quad (1.135)$$

where  $V_{\text{ex}}^*$  is the excluded volume between the critical hole and a neighboring polymer chain.

The shear viscosity is computed as

$$\eta_0 = \eta_s \left\{ 1 + [\eta]c \left[ 1 + \frac{3}{4} \gamma_I \chi_h^2 \left( \frac{D_R^0}{D_R} - 1 \right) \right] \right\} \quad (1.136)$$

where  $\gamma_I$  and  $\chi_h$  are hydrodynamic factors that can be calculated from the axial ratio of the chain. Thus, to determine  $\eta_0$  for isotropic solutions of a stiff-chain polymer,

the parameters,  $L_e$ ,  $d_e$ ,  $L$ , and  $\ell_p$  are needed as well as the experimental values of  $[\eta]$  and  $\eta_s$ . The hydrodynamic parameters  $\gamma_1$  and  $\chi$  are calculated from  $L/d$  and  $L/\ell_p$ . The parameters  $N^*$  and  $\Delta$ , as well as a scaling coefficient,  $\lambda^*$ , which defines the size of  $V_{\text{ex}}^*$ , are the only adjustable parameters [Sato et al., 1991, 2003; Ohshima et al., 1995, 1999]. The curves shown in Figure 1.15 are fits of experimental data to the fuzzy cylinder theory. As noted by Sato et al. [2003], the fuzzy cylinder theory becomes less accurate for low and high molecular weights. The former problem can be rectified [Sato et al., 2003] by including in Eq. (1.136) an intermolecular hydrodynamic interaction term which can be a first- or second-order Huggins expression,  $h_\eta(c)$ :

$$\eta_0 = \eta_s \left\{ 1 + [\eta]c \left[ 1 + \frac{3}{4} \gamma_I \chi_h^2 \left( \frac{D_R^0}{D_R} - 1 \right) \right] h_\eta(c) \right\} \quad (1.137)$$

where

$$h_\eta(c) = 1 + k'_{\text{HI}}[\eta]c + k''_{\text{HI}}([\eta]c)^2 \quad (1.138)$$

The problem at higher molecular weights probably signals the onset of reptative motions in the system [Sato et al., 2003]. Sato et al. [2003] note that based on the fuzzy cylinder model, the viscosity inversion apparent in Figure 1.15 at high concentrations when comparing CTC versus PnHIC is due to a stronger intermolecular hydrodynamic interaction for CTC.

### 1.9.5 Concentration Scaling Laws for Polyelectrolyte Solutions

The concentration dependence of the viscosity of polyelectrolyte solutions has been discussed by several authors [Cohen et al., 1988; Cohen and Priel, 1990; Borsali et al., 1992, 1994; Antonietti et al., 1997]. Several groups [Borsali et al., 1992, 1994; Antonietti et al., 1997] have used the mode–mode coupling approximation of Hess and Klein [1983]. In the weakly charged polyelectrolyte limit, the latter formulation leads to an expression for the time-dependent viscosity of the form [Borsali et al., 1992]

$$\eta_s(t) = \frac{k_B T c N_A}{16\pi^3 M_0} \int d^3 q I^2(q, t) \left[ \frac{q}{I^2(q)} \right]^2 \left[ \frac{\partial H(q)}{\partial q} \right]^2 \quad (1.139)$$

where  $q$  and  $t$  are the scattering vector and time, respectively,  $c$  is polyion concentration,  $M_0$  is the monomer molecular weight,  $I(q, t)$  is the time-dependent scattering intensity, and  $H(q)$  is the pair correlation function, expressed in terms of the solution structure factor,  $S(q)$ , as  $S(q) = 1 + (cN_A/M_0)H(q)$ .  $I(q, t)$  is assumed to be an exponential decay,

$$I(q, t) = I(q) \exp(-\Gamma(q)t) \quad (1.140)$$

where  $\Gamma(q)$  is the decay constant. The mean scattered intensity,  $I(q) = (cN_A M/M_0^2)P(q)S(q)$ , where  $P(q)$  is the polyion scattering function and  $S(q)$  is given by

$$S(q) = \frac{1}{1 + (cN_A M/M_0^2)[P(q) + (v + \alpha(q))]} \quad (1.141)$$

where  $v$  and  $\alpha(q)$  are the neutral and electrostatic contributions to the excluded volume parameter, respectively. Via Eqs. (1.139) to (1.141), the reduced viscosity can be computed as

$$\frac{\eta_{sp}}{c} = \frac{\eta - \eta_0}{\eta_0 c} = \frac{1}{\eta_0 c} \int_0^\infty \eta_s(t) dt \quad (1.142)$$

Cohen et al. [1988] evaluated Eqs. (1.139) to (1.142) using a strong coupling approximation:

$$S(q, t) = S(q) \exp \left[ -\frac{D_t^0 q^2 t}{S(q)} \right] \quad (1.143)$$

with

$$S(q) = \frac{1}{1 - cH(q)} \quad (1.143a)$$

$D_t^0$  is the polyion translational diffusion coefficient ( $D_t^0 \sim 1/R_H$ ) and

$$H(q) = -\frac{\tilde{U}(q)f(q)}{k_B T} \quad (1.143b)$$

where  $\tilde{U}(q)$  is the Fourier transform of the potential of mean force between polyions, for which an expression of the Debye–Hückel form is assumed [Cohen et al., 1988]:

$$\tilde{U}(q) = \frac{4\pi Z_{\text{eff}}^2 e^2}{\epsilon_o(q^2 + \kappa^2)} \quad (1.143c)$$

$$f(q) = \left[ \frac{J_1(qR)}{qR} \right]^2 \quad (1.143d)$$

where  $J_1$  is a spherical Bessel function,  $Z_{\text{eff}}$  the effective charge on the polyion, and  $R$  the mean polyion separation. Examining the analytical form of  $S(q)$  and  $H(q)$ , Cohen et al. [1988] further assume that  $P(q) = 1$  and argue that  $S(q)$  can be set equal to unity

and  $H(q)$  approximated as

$$H(q) = \frac{c\tilde{U}(q)}{Z_{\text{eff}}k_B T} \quad (1.143e)$$

With these assumptions, integration according to Eqs. (1.139) to (1.143) leads to the following result:

$$\eta \sim \frac{R_H \ell_B^2 c^2}{\kappa^3} \quad (1.144)$$

Cohen et al. note that this equation is in agreement with their experimental results [Cohen et al., 1988; Cohen and Priel, 1990], including the existence of a maximum in concentration dependence of  $\eta_{\text{sp}}/c$  as well as the dependence of  $c_{\text{max}}$  on salt concentration and molecular weight. Moreover, once the (omitted) multiplicative constant in Eq. (1.144) is set by matching the experimental and theoretical values of  $\eta_{\text{sp}}/c_{\text{max}}$  for a single salt concentration, the theory does not have any adjustable parameters.

Borsali et al. [1992] note that the formulation of Cohen et al. [1988] above is strictly valid only for point-charged particles and have presented a more physically realistic treatment developed within the framework of the Rouse dynamical model, and valid for weakly charged polyions. They find that Eqs. (1.139) to (1.142) reduce to [Borsali et al., 1992]

$$\eta - \eta_0 = \frac{(M/M_0)\zeta}{8\pi^2} \int_0^\infty dq q^2 \frac{P(q)}{S(q)} \left[ \frac{\partial S(q)}{\partial q} \right]^2 \quad (1.145)$$

where  $\zeta$  is the friction coefficient per monomer. Evaluating this result numerically and assuming Gaussian behavior of the polyion coil, Borsali et al. [1992] were also able to reproduce the viscosity maximum observed in the concentration dependence of dilute polyelectrolyte solutions and to investigate the dependence of  $c_{\text{max}}$  on system variables. They found that (1) in agreement with experiment and theory by Cohen and co-workers [Cohen et al., 1988; Cohen and Priel, 1990], adding salt reduces  $\eta_{\text{sp}}/c$  and moves the position of  $c_{\text{max}}$  to higher concentration, specifically  $c_{\text{max}} \sim c_s$ , but it is noted [Borsali et al., 1992] that this relationship is expected to depend on the fractional charge on the polyion; (2) increasing the effective charge on the polyion,  $Z_{\text{eff}}$ , enhances the polyelectrolyte effect by shifting  $c_{\text{max}}$  to lower concentrations (i.e.,  $c_{\text{max}} \sim Z_{\text{eff}}^{-x}$ , with  $x \approx 2$ ), which differs from the prediction of Cohen et al. [1988],  $c_{\text{max}} \sim Z_{\text{eff}}^{-1} c_s$ ; and (3) for the molecular-weight dependence, Borsali et al. [1992] found that  $C_{\text{max}} \sim M^y$  with  $y = 1$ . This result is quite different from that reported experimentally [Cohen and Priel, 1990] and predicted [Cohen et al., 1988] for fully charged polyelectrolytes. Subsequent analysis [Borsali et al., 1994], which incorporated screening of hydrodynamic interactions, indicates that the qualitative behavior of  $\eta_{\text{sp}}/c$  does not change; that is, it still shows a peak at  $c_{\text{max}}$ , but its value decreases significantly and there is a slight shift in  $c_{\text{max}}$  toward higher concentrations.

To our knowledge, experimental investigations of weakly charged polyelectrolyte solutions to test these predictions have not been explored.

Antonietti et al. [1997] have carried out experimental studies of the viscosity of solutions of spherical polyelectrolyte microgel particles in aqueous solution in the absence of added salt. They note that such microgel particles are not expected to undergo the large ionic strength-driven conformational changes exhibited by linear flexible polyions on dilution. Since these solutions, like those of linear polyions (Figure 1.11), exhibit a large increase in  $\eta_{sp}/c$  on dilution, they conclude that the origin of this effect is an increase in intermolecular repulsions with decreasing concentration, not a coil-rod transition. They offer an interpretation of their observations based on a theoretical expression of the form

$$\frac{\eta_{sp}}{c} = [\eta]_0 + k_H[\eta]_0^2 c + \frac{1}{160} R_H \left( \frac{4\pi e^2}{M\epsilon\epsilon_0 k_B T} \right)^{1/2} \frac{Z_{eff}^4 c}{\left[ 2 \frac{M}{M_s} C_S + Z_{eff} c \right]^{3/2}} \quad (1.146)$$

with

$$[\eta]_0 = \frac{10\pi}{3} \frac{N_A}{M} (R_{H,\eta} + R_B)^3 \quad (1.146a)$$

where the hydrodynamic radius of the polyion,  $R_H = R_{H,\eta} + R_B$ , is the sum of  $R_{H,\eta}$ , the radius of the uncharged polyion, and  $R_B$ , the Bjerrum radius which reflects the intermolecular electrostatic interactions,  $R_B = Z_{eff}^2 \ell_B / 2$ . Equation (1.146) accurately describes their experimental data, which can be divided into three distinct concentration regimes: (1) a very low concentration regime,  $c < c_{max}$ , where the viscosity is determined by single-particle properties; (2) an intermediate concentration regime, bounded by  $c_{max}$  and the overlap concentration,  $c^*$ , where  $\eta_{sp}/c \sim c^{-0.25}$ ; and (3)  $c > c^*$ , where electrostatic interactions are largely screened and intermolecular hydrodynamic interactions become dominant. Near  $c^*$ , a minimum in the concentration dependence of  $\eta_{sp}/c$ , is observed. Below  $c^*$ , Antonietti et al. [1997] find only a very weak dependence of  $\eta_{sp}/c$  on polyion molecular weight, and note that this can be explained in terms of the Hess–Klein mode–mode coupling model [Eq. (1.146)] which in the limit of low salt concentration ( $c/c_s \gg 1$ ) reduces to

$$\frac{\eta_{sp}}{c} = \frac{R_H Z_{eff}^{5/2}}{M_w^{0.5}} \quad (1.147)$$

Since, experimentally,  $R_H \sim M_w^{0.47}$ , it follows that  $\eta_{sp}/c \sim Z_{eff}^{5/2}$ . Thus, from fits to the data,  $Z_{eff}$  is found to be slightly dependent on molecular weight, a counterintuitive result, but consistent with previous results.

The experimental data above have focused on polyelectrolyte solutions in aqueous media. Dou and Colby [2006] have pointed out that studies of weakly charged polyions in aqueous solutions are limited because of poor solubility. They have reported [Dou and Colby, 2006] an extensive study of the effect of charge density using random copolymers of 2-vinylpyridine and *N*-methyl-2-vinylpyridinium chloride (PMVP-Cl)

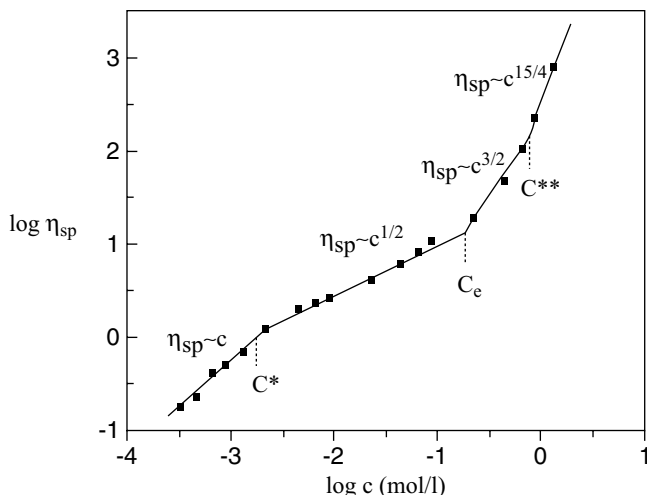


**FIGURE 1.16** Determination of the chain overlap concentration  $c^*$ , the entanglement concentration  $c_e$ , the electrostatic blob overlap concentration  $c^{**}$  from the concentration dependence of specific viscosity for a 17%-quaternized P2VP copolymer (17PMVP-Cl) in solution in ethylene glycol at 25°C. Symbols are experimental data and solid lines represent the power laws predicted from scaling theory. (Adapted from Dou and Colby [2006].)

in anhydrous ethylene glycol (EG) as solvent. Since EG is a good solvent for poly-2-vinylpyridine, solubility of random copolymers of any charge density is possible. An added bonus, pointed out by Dou and Colby [2006], is that EG has a very low residual ion contamination. Experimental results for a series of copolymers, with percent quaternization varying from 3 to 55%, were studied. Results for the copolymers having percent quaternization of 17% are shown in Figure 1.16, plotted as  $\log \eta_{sp}$  versus  $\log(c/c^*)$ . Here  $c^*$  was estimated as the average value of  $c/\eta_{sp}$  for dilute solution data for each polymer (i.e.,  $c^* = c/\eta_{sp} \approx 1/[\eta]$ ). Dou and Colby [2006] found that all polymers with a degree of quaternization higher than 10% gave essentially identical plots of  $\eta_{sp}$  versus  $c$ . This was explained on the basis that counterion condensation on the copolymers begins at this percent quaternization. While the effective charge continues to increase in the strongly charged polyions, its effect in stretching the chain is counterbalanced by a dipolar attraction from the condensed counterion/charged monomer pairs which acts to contract the chain. In interpreting their viscometric data, Dou and Colby [2006] utilize scaling arguments which are reproduced below. First, in dilute solution, electrostatic repulsions stretch the chain into a directed random walk of electrostatic blobs of size  $\xi_e$  containing  $g_e$  monomers, a fraction,  $f$ , of which are charged.  $\xi_e$  is determined by the balance between the electrostatic repulsion and thermal energy:

$$\frac{(fg_e e^2)}{\varepsilon \xi_e} \approx k_B T \Rightarrow fg_e \ell_B \approx 1 \quad (1.148)$$

Also, within the blob, the chain exhibits self-avoiding walk statistics, hence

$$\xi_e \approx b g_e^{3/5} \quad (1.149)$$

where  $b$  is the monomer size. Combining Eqs. (1.148) and (1.149) leads to

$$\xi_e \approx b^{10/7} \ell_B^{-3/7} f^{-6/7} \quad \text{and} \quad g_e \approx \left( \frac{b}{\ell_B} \right)^{5/7} f^{-10/7} \quad (1.150)$$

Thus, the contour length of the chain, having  $N/g_e$  blobs, is

$$L \approx \xi_e \left( \frac{N}{g_e} \right) \approx b N \left( \frac{\ell_B}{b} \right)^{2/7} f^{4/7} \approx \frac{b N}{B} \quad (1.151)$$

where  $B$  may be viewed as a stretching parameter, since it is the ratio of the maximum contour length,  $Nb$  to the experimental value,  $L$ . Since each blob repels its neighbors,  $L$  is also the end-to-end distance of the chain in dilute solution. Thus, in dilute solution,

$$\eta_{\text{sp}} = [\eta]c \sim L^3 c \quad \text{for} \quad c < c^* \quad (1.152)$$

The overlap concentration,  $c^*$ , can be expressed as

$$c^* \approx \frac{N}{L^3} \approx \frac{B^3}{b^3 N^2} \approx b^{-3} N^{-2} \left( \frac{b}{\ell_B} \right)^{6/7} f^{-12/7} \quad (1.153)$$

Above the overlap concentration,  $c^* \approx 1/[\eta] \sim c/\eta_{\text{sp}}$ , electrostatic repulsions are partially screened by other chains. Here, one defines the correlation length  $\xi$ , which characterizes the average intermonomer separation, and it is assumed that  $\xi$  depends only on concentration when  $c > c^*$  [i.e.,  $\xi \approx R_g(c/c^*)^m$ ]. Since in dilute solution  $R_g \approx L$ ,  $c^* \approx N/R_g^3 = N/L^3$ , and  $L \sim N$ , it follows that  $m = -\frac{1}{2}$ , that is,

$$\xi \approx L \left( \frac{c}{c^*} \right)^{-1/2} \approx \left( \frac{B}{cb} \right)^{1/2} \quad \text{for} \quad c > c^* \quad (1.154)$$

Above  $c^*$ , on scales smaller than  $\xi$ , the chain is a directed random walk, but on scales larger than  $\xi$ , it is a random walk of steps of size  $\xi$ . Hence, the radius of gyration decreases from its dilute solution value as

$$R_G \approx L \left( \frac{c}{c^*} \right)^{-1/4} \approx \left( \frac{b}{cB} \right)^{1/4} N^{1/2} \quad \text{for} \quad c > c^* \quad (1.155)$$

The scaling model predicts the chain in semidilute solution exhibits Rouse-like dynamics, with a relaxation time given by

$$\tau = \frac{\tau_0 N^2}{(cb^3 B^3)^{1/2}} \quad \text{for } c^* < c < c_e \quad (1.156)$$

where  $\tau_0 = \eta_s b^3 / k_B T$  is the relaxation time of a monomer. This result holds for concentrations between  $c^*$  and the entanglement concentration,  $c_e$ . The terminal modulus is equal to the number of chains times  $k_B T$ :

$$G = \frac{c}{N} k_B T \quad \text{for } c < c_e \quad (1.157)$$

Since  $\eta = G\tau$ , it follows that

$$\eta_{sp} \approx \frac{G\tau}{\eta_s} \approx \left( \frac{cb^3}{B^3} \right)^{1/2} N \approx \left( \frac{c}{c^*} \right)^{1/2} \quad \text{for } c^* < c < c_e \quad (1.158)$$

Thus, recalling that in dilute solution ( $c < c^*$ ),  $\eta_{sp} \approx c/c^*$ , Eq. (1.158) indicates that for  $c < c_e$ ,  $\eta_{sp}$  should depend only on  $c/c^*$ . Clearly, this is consistent with the experimental data shown in Figure 1.16.

The entanglement concentration,  $c_e$ , is assumed to be proportional to  $c^*$ . From Eq. (1.158), we have

$$c_e \propto c^* \approx \frac{B^3}{b^3 N^2} \approx b^{-3} N^{-2} \left( \frac{b}{\ell_B} \right)^{6/7} f^{-12/7} \quad (1.159)$$

with the constant of proportionality  $\approx 1000$ . A third characteristic concentration in polyelectrolyte solutions is the overlap concentration of electrostatic blobs, designated  $c^{**}$ :

$$c^{**} \approx \frac{ge}{\xi_e^3} \approx b^{-3} \left( \frac{\ell_B f^2}{b} \right)^{4/7} \sim \frac{1}{b^3 B^2} \quad (1.160)$$

For  $c > c^{**}$ , electrostatic interactions no longer perturb the chain conformation, and the solution properties are expected to be similar to that of a semidilute solution of neutral polymers in a good solvent [Colby et al., 1994] In the semidilute entangled neutral polymer regime [Colby et al., 1994],

$$\tau \sim c^{3/2}; G \sim c^{9/4}; \quad \text{and } \eta_{sp} \sim c^{15/4} \quad \text{for } c > c^{**} \quad (1.161)$$

If  $c^{**}$  is greater than  $c_e$ , there will be a semidilute regime of entangled polyelectrolyte solution rheology. Here, the terminal relaxation time is predicted to be [Colby et al.,

1994; Dou and Colby, 2006]

$$\tau \sim \tau_0 \left( \frac{c^*}{c_e} \right)^{1/2} \left( \frac{N}{B} \right)^3 \quad \text{for } c_e < c < c^{**} \quad (1.162)$$

The plateau modulus is

$$G \approx \frac{k_B T}{b^3} \left( \frac{c^*}{c_e} \right)^{1/2} \left( \frac{cb^3}{B} \right)^{3/2} \quad \text{for } c_e < c < c^{**} \quad (1.163)$$

and hence the specific viscosity is

$$\eta_{sp} \approx \frac{\tau G}{\eta_s} \approx \left( \frac{c^*}{c_e} \right) \left( \frac{cb^3}{B^3} \right)^{3/2} N^3 \quad \text{for } c_e < c < c^{**} \quad (1.164)$$

Thus, the scaling theory predicts a crossover in the concentration dependence of  $\eta_{sp}$  from  $\eta_{sp} \sim c$  [Eq. (1.152)] to  $\eta_{sp} \sim c^{1/2}$  at  $c^*$  [Eq. (1.158)], and from  $\eta_{sp} \sim c^{1/2}$  to  $\eta_{sp} \sim c^{3/2}$  [Eq. (1.164)] at  $c_e$ , and finally from  $\eta_{sp} \sim c^{3/2}$  to  $\eta_{sp} \sim c^{15/4}$  [Eq. (1.161)] at  $c^{**}$ . Dou and Colby [2006] find that their viscometric data are in good agreement with these predictions, as illustrated in Figure 1.16.

## 1.10 SUMMARY, CONCLUSIONS, AND OUTLOOK

Substantial progress has been achieved in our understanding of the molecular origin of shear viscosity of colloidal dispersions and polymer solutions, although certain issues remain to be resolved. For dilute colloidal dispersions, the seminal work of Einstein and Simha has culminated in the development of numerical methods to compute the intrinsic viscosity of impermeable particles of irregular geometry as a tool for structural analysis [Garcia de la Torre et al., 2000; Hahn et al., 2004; Hahn and Aragon, 2006; Mansfield et al., 2007]. The effect of particle permeability can be incorporated via the Debye–Bueche–Brinkman theory [Veerapaneni and Wiesner, 1996; Zackrisson and Bergenholtz, 2003]. In dilute polymer solutions, the extensive experimental studies of the Yamakawa group have illuminated the molecular weight dependence of the intrinsic viscosity of linear flexible chain molecules, encompassing oligomers to high polymers. Provided that certain system-specific effects are taken into account, as indicated in Figure 1.5, universal scaling is found between the viscometric chain expansion parameter,  $\alpha_\eta = ([\eta]/[\eta]_0)^{1/3}$ , and the configurational chain expansion parameter,  $\alpha = (R_g^2/R_{g,0}^2)^{1/2}$ , the former computed in the nondraining limit, suggesting that draining effects can usually be neglected in solutions of neutral linear polymers [Tominaga et al., 2002]. The experimental results are well described by an extension of the classical two-parameter theory, designated the quasi-two-parameter (QTP) theory [Yamakawa, 1997], which explicitly incorporates the chain stiffness into the excluded volume parameter, using the helical wormlike coil model.

It should be noted that since  $\alpha_\eta^3/\alpha^3 = \Phi_{\text{FF}}/\Phi_{\text{FF}0} = (R_{h,\eta}/R_g)^3/(R_{h,\eta 0}/R_{g,0})^3$ , the variation with solvent quality of the ratio  $R_g/R_{h,\eta}$ , proportional to the Flory–Fox viscosity constant,  $\Phi_{\text{FF}}$ , can be traced within the QTP theory to the adoption of the Domb–Barrett [1976] and Barrett [1984] expressions for  $\alpha$  and  $\alpha_\eta$ , respectively, and therefore conflicts with suggestions by Douglas et al. [1990], based on renormalization group calculations that such variations are due to an increase in solvent draining with chain expansion in good solvents. A similar universal scaling of  $\alpha_R$  versus  $\alpha_H$ , the chain expansion parameter for the translational hydrodynamic radius is found experimentally, but a problem exists that, to date, the corresponding relationship cannot be predicted accurately by the QTP theory [Tominaga et al., 2002] when  $\alpha_H$  is calculated using the Barrett equation for  $\alpha_H$  [Barrett, 1984]. Recent Brownian dynamics simulations [Sunthar and Prakash, 2006] conclude that this deficiency is due to the use of a preaveraged hydrodynamic interaction in the calculation of  $\alpha_H$ .

The intrinsic viscosity can be applied to determine the molecular hydrodynamic volume of a polymer, via the Einstein equation (1.20), and also, in principle, the radius of gyration, via the Flory–Fox equation (1.40), using an appropriate value of the Flory–Fox constant  $\Phi_{\text{FF}}$ . However,  $\Phi_{\text{FF}}$  decreases uniformly from a value  $\Phi_{\text{FF}0} \sim 2.73 \times 10^{23} \text{ mol}^{-1}$  in theta solvents to a value  $\Phi_{\text{FF}} \sim 2.11 \times 10^{23} \text{ mol}^{-1}$  in the good solvent limit, and there appears to be sufficient variation in the numerical value of  $\Phi_{\text{FF}}$  even in the theta solvent limit to render uncertain a precise determination of  $R_G$  [Konishi et al., 1991].  $R_{h,\eta}$  and  $R_G$  are sensitive to polymer structure and conformation, and well-tested theory exists to extract information regarding the molecular architectures of branched polymers and persistence lengths of linear semiflexible chains from  $[\eta]$  data. The development of online viscosity detectors for size-exclusion chromatography (SEC) enables the separation and online size characterization of individual species in multicomponent polymer solutions. SEC coupled to concentration and viscosity detectors enables universal calibration of elution volume against molecular weight, and hence the technique becomes a powerful method for rapid generation of information on the molecular weight dependence of the hydrodynamic volume [see Eqs. (1.20) and (1.23)], and hence enables online determination of persistence lengths of semiflexible polymers via wormlike coil theory [Eq. (1.61)] or characterization of chain branching in synthetic polymers [Eq. (1.72)]. Theoretical and experimental progress has been made in understanding the intrinsic viscosity of polyelectrolytes under conditions of low ionic strength and high charge density, where electrostatic interactions dominate. New ground has been broken in extending intrinsic viscosity measurements to liquid-crystal polymers in nematic solvents, as a probe for the effect of the nematic field on LCP conformation.

Progress has also been made in understanding the concentration dependence of shear viscosity of polymer solutions, which may be treated in three distinct regimes: dilute, semidilute, and concentrated. In the dilute and semidilute unentangled regimes, the concentration dependence derives from indirect (hydrodynamic) and direct intermolecular interactions and can be described by  $c[\eta]$  or  $(c/c^*)$  scaling via a virial type of equation [Eq. (1.119)] or the stretched-exponential description of Phillis [2002a, b]. In the semidilute entangled regime, a scaling treatment according to reptation theory seems to work well [Eq. (1.118) or (1.126) in good solvents, Eq. (1.122) in

theta solvents]. Theoretical formalisms have been developed in the semidilute concentration regime for stiff chains [Doi and Edwards, 1978, 1981], semi-stiff chains [Sato et al., 1991, 2003], and polyelectrolyte chains [Cohen et al., 1988; Borsali et al., 2006; Antonietti et al., 1997; Dou and Colby, 2006]. In the concentrated regime, one has to resort to a treatment such as that of Utracki and Simha [1981] or Berry [1996] which incorporates the concentration, temperature, and solvent dependence of the segmental frictional coefficient.

## REFERENCES

- Abe, F., Einaga, Y., Yoshizaki, T., and Yamaka, H., Excluded volume effects on the mean-square radius of gyration of oligo- and polystyrenes in dilute solutions, *Macromolecules*, **26**, 1884–1890 (1993a).
- Abe, F., Einaga, Y., and Yamakawa, H., Excluded volume effects on the intrinsic viscosity of oligomers and polymers of styrene and isobutylene, *Macromolecules*, **26**, 1891–1897 (1993b).
- Abe, F., Horita, K., Einaga, Y., and Yamakawa, H., Excluded volume effects on the mean-square radius of gyration and intrinsic viscosity of oligo- and poly(methyl methacrylate), *Macromolecules*, **27**, 725–732 (1994).
- Adam, M., and Delsanti, M., Viscosity of semi-dilute polymer solutions, *J. Phys. (Paris)*, **43**, 549–557 (1982).
- Adam, M., and Delsanti, M., Viscosity and longest relaxation time of semi-dilute polymer solutions: I. Good solvent, *J. Phys. (Paris)*, **44**, 1185–1193 (1983).
- Adam, M., and Delsanti, M., Viscosity and longest relaxation time of semi-dilute polymer solutions: II. Theta solvent, *J. Phys. (Paris)*, **45**, 1513–1521 (1984).
- Aharoni, S. M., Rigid backbone polymers: II. Polyisocyanates and their liquid-crystal behavior, *Macromolecules*, **12**, 94–103 (1979).
- Aharoni, S. M., Rigid backbone polymers: XV. Phase transitions in polyisocyanate solution, *Ferroelectrics*, **30**, 227–235 (1980a).
- Aharoni, S. M., Rigid backbone polymers: XVII. Solution viscosity of polydisperse systems, *Polymer*, **21**, 1413–1422 (1980b).
- Antonietti, M., Briel, A., and Forster, S., Quantitative description of the intrinsic viscosity of branched polyelectrolytes, *Macromolecules*, **30**, 2700–2704 (1997).
- Arai, T., Abe, F., Yoshikazi, T., Einaga, Y., and Yamakawa, H., Excluded volume effects on the hydrodynamic radius of oligo- and polystyrenes in dilute solution, *Macromolecules*, **28**, 3609–3616 (1995).
- Auer, R. L., and Gardner, C. S., Solution of the Kirkwood–Riseman integral equation in the asymptotic limit, *J. Chem. Phys.*, **23**, 1546–1547 (1955).
- Barrett, A. J., Intrinsic viscosity and friction coefficients for an excluded volume polymer in the Kirkwood approximations, *Macromolecules*, **17**, 1566–1572 (1984).
- Bathe, M., Rutledge, G. C., Grodzinsky, A. J., and Tidor, B. A., Coarse-grained molecular model for glycosaminoglycans: application to chondroitin sulfate, chondroitin and hyaluronic acid, *Biophys. J.*, **88**, 3870–3887 (2005).
- Berry, G. C., Crossover behavior in the viscosity of semi-flexible polymers: intermolecular interactions as a function of concentration and molecular weight, *J. Rheol.*, **40**, 1129–1154 (1996).

- Beyer, P., and Nordmeier, E., Some phenomena of counterion condensation on dextran sulphate, *Eur. Polym. J.*, **31**, 1031–1036 (1995).
- Bohdanecky, M., New method for estimating the parameters of the wormlike chain model from the intrinsic viscosity of stiff-chain polymers, *Macromolecules*, **16**, 1483–1492 (1983).
- Borsali, R., Vilgis, T. A., and Benmouna, M., Viscosity of weakly-charged polyelectrolyte solutions: the mode-mode coupling approach, *Macromolecules*, **25**, 5313–5317 (1992).
- Borsali, R., Vilgis, T. A., and Benmouna, M., Viscosity of weakly-charged polyelectrolyte Solutions: the screening of hydrodynamic interactions, *Macromol. Theory Simul.*, **3**, 73–77 (1994).
- Brinkman, H. C., A calculation of the viscous force exerted by a flowing fluid on a dense swarm of particles, *Appl. Sci. Res.*, **A1**, 27–34 (1947).
- Brochard, F., Viscosities of dilute polymer solutions in nematic liquids, *J. Polym. Sci. Polym. Phys. Ed.*, **17**, 1367–1374 (1979).
- Carrasco, B., de la Torre, J. G., Byron, O., King, D., Walters, C., Jones, S., and Harding, S. H., Novel size-independent modeling of the dilute solution conformation of the immunoglobulin IgG Fab' Domain using Solpro and Ellipse, *Biophys. J.*, **77**, 2902–2910 (1999).
- Carri, G. A., and Muthukumar, M., Configurations of liquid crystal polymers in nematic solvents, *J. Chem. Phys.*, **109**, 11117–11128 (1998).
- Chen, F. L., and Jamieson, A. M., Molecular weight-dependent behavior of the twist distortion in a nematic monodomain containing a main-chain liquid crystal polymer, *Macromolecules*, **27**, 1943–1948 (1994).
- Chiang, Y. C., Jamieson, A. M., Campbell, S., Lin, T., O'Sidocky, N. D., Chien, L. C., Kawasumi, M., and Percec, V., The effect of molecular architecture on the electrorheological response of liquid crystal polymers in nematic solvents, *Rheol. Acta*, **36**, 505–512 (1997a).
- Chiang, Y. C., Jamieson, A. M., Kawasumi, M., and Percec, V., Electrorheological behavior of main-chain liquid crystal polymers in nematic solvents, *Macromolecules*, **30**, 1992–1996 (1997b).
- Chiang, Y. C., Jamieson, A. M., Campbell, S., Tong, T. H., Sidocky, N. D., Chien, L. C., Kawasumi, M., and Percec, V., Electro-rheological behavior of liquid crystal polymers (LCPs) dissolved in a nematic solvent: dependence on temperature and LCP structure, *Polymer*, **41**, 4127–4135 (2000).
- Chiang, Y. C., Jamieson, A. M., Zhao, Y., Kasko, A. M., and Pugh, C., Effect of molecular weight on the electrorheological behavior of side-chain liquid crystal polymers in nematic solvents, *Polymer*, **43**, 4887–4894 (2002).
- Chu, S. G., Venkatraman, S., Berry, G. C., and Einaga, Y., Rheological properties of rodlike polymers in solution: 1. Linear and nonlinear steady-state behavior, *Macromolecules*, **14**, 939–946 (1981).
- Cohen, J., and Priel, Z., Viscosity of dilute polyelectrolyte solutions: temperature dependence, *J. Chem. Phys.*, **93**, 9062–9068 (1990).
- Cohen, J., Priel, Z., and Rabin, Y., Viscosity of dilute polyelectrolyte solutions, *J. Chem. Phys.*, **88**, 7111–7116 (1988).
- Colby, R. H., and Rubinstein, M., Two-parameter scaling for polymers in  $\Theta$  solvents, *Macromolecules*, **23**, 2753–2757 (1990).
- Colby, R. H., Rubinstein, M., and Daoud, M., Hydrodynamics of polymer solutions via 2-parameter scaling, *J. Phys. II*, **4**, 1299–1310 (1994).

- Cotton, J. P., and Hardouin, F., Chain conformation of liquid-crystalline polymers studied by small-angle neutron scattering, *Prog. Polym. Sci.*, **22**, 795–828 (1997).
- de Gennes, P. G., Dynamics of entangled polymer solutions: I. The Rouse model, *Macromolecules*, **9**, 587–593 (1976a).
- de Gennes, P. G., Dynamics of entangled polymer solutions: II. Inclusion of hydrodynamic interactions, *Macromolecules*, **9**, 594–598 (1976b).
- Debye, P., and Bueche, A. M., Intrinsic viscosity, diffusion, and sedimentation rate of polymers in solution, *J. Chem. Phys.*, **16**, 573–579 (1948).
- Doi, M., Rotational relaxation time of rigid rod-like macromolecule in concentrated solution, *J. Phys.*, **36**, 607–611 (1975).
- Doi, M., Molecular dynamics and rheological properties of concentrated solutions of rodlike polymers in isotropic and liquid crystalline phases, *J. Polym. Sci. Polym. Phys. Ed.*, **19**, 229–243 (1981).
- Doi, M., and Edwards, S. F., Dynamics of rod-like macromolecules in concentrated solution: Part 2, *J. Chem. Soc. Faraday Trans. 2*, **74**, 918–932 (1978).
- Domb, C., and Barrett, A. J., Universality approach to expansion factor of a polymer-chain, *Polymer*, **17**, 179–184 (1976).
- Dou, S., and Colby, R. H., Charge density effects in salt-free polyelectrolyte solutions, *J. Polym. Sci. Polym. Phys.*, **44**, 2001–2013 (2006).
- Douglas, J. F., Roovers, J., and Freed, K. F., Characterization of branching architecture through “universal” ratios of polymer solution properties, *Macromolecules*, **23**, 4168–4180 (1990).
- Draval, V. E., Malkin, A. Y., and Botvinnik, G. O., Approach to generalization of concentration dependence of zero-shear viscosity in polymer solutions, *J. Polym. Sci. Polym. Phys. Ed.*, **11**, 1055–1076 (1973).
- Durand, A., Semiempirical equations for the viscosity of amphiphilic polymer solutions: a critical examination, *Polym. Eng. Sci.*, **47**, 481–488 (2007).
- Edwards, S. F., The statistical mechanics of polymers with excluded volume, *Proc. Phys. Soc.*, **85**, 613–624 (1965).
- Einstein, A., Eine neue Bestimmung der Molekldimensionen, *Ann. Phys.*, **324**, 289–306 (1906).
- Einstein, A., Berichtigung zu meiner Arbeit: Eine neue Bestimmung der Molekldimensionen, *Ann. Phys.*, **339**, 591–592 (1911).
- Eisenberg, H., and Pouyet, J., Viscosities of dilute aqueous solutions of a partially quaternized poly-4-vinylpyridine at low gradients of flow, *J. Polym. Sci.*, **13**, 85–91 (1954).
- Enomoto, H., Einaga, Y., and Teramoto, A., Viscosity of concentrated solutions of rodlike polymers, *Macromolecules*, **18**, 2695–2702 (1985).
- Farmer, B. S., Terao, K., and Mays, J. W., Characterization of model branched polymers by multi-detector SEC in good and theta solvents, *Int. J. Polym. Anal. Char.*, **11**, 3–19 (2006).
- Ferry, J. D., *Viscoelastic Properties of Polymers*, 3rd ed., Wiley, New York, 1980.
- Flory, P. J., and Fox, T. G., Treatment of intrinsic viscosities, *J. Am. Chem. Soc.*, **73**, 1904–1908 (1951).
- Freed, K. F., Wang, S. Q., Roovers, J., and Douglas, J. F., Partial draining and universality of dilute solution polymer dynamics: comparison of theory and experiment, *Macromolecules*, **21**, 2219–2224 (1988).

- Garcia de la Torre, J., Huertas, M. L., and Carrasco, B., Calculation of hydrodynamic properties of globular proteins from their atomic-level structure, *Biophys. J.*, **78**, 719–730 (2000).
- Gu, D., and Jamieson, A. M., Rheological characterization of director dynamics in a nematic monodomain containing mesogenic polymers of differing architectures, *Macromolecules*, **27**, 337–347 (1994a).
- Gu, D., and Jamieson, A. M., Shear deformation of homeotropic monodomains: temperature dependence of stress response for flow-aligning and tumbling nematics, *J. Rheol.*, **38**, 555–571 (1994b).
- Gu, D., Jamieson, A. M., and Wang, S. Q., Rheological characterization of director tumbling induced in a flow-aligning nematic solvent by dissolution of a side-chain liquid crystal polymer, *J. Rheol.*, **37**, 985–1001 (1993).
- Haber, S., and Brenner, H., Rheological properties of dilute suspensions of centrally symmetric Brownian particles at small shear rates, *J. Colloid Interface Sci.*, **97**, 496–514 (1984).
- Hager, B. L., and Berry, G. C., Moderately concentrated solutions of polystyrene: I. Viscosity as a function of concentration, temperature, and molecular weight, *J. Polym. Sci. Polym. Phys. Ed.*, **20**, 911–928 (1982).
- Hahn, D. K., and Aragon, S. R., Intrinsic viscosity of proteins and platonic solids by boundary element methods, *J. Chem. Theory Comput.*, **2**, 1416–1428 (2006).
- Hahn, E.-H., Mansfield, M. L., and Douglas, J. F., Numerical path integration method for the calculation of the transport properties of proteins, *Phys. Rev. E*, **69**, 031918 (2004).
- Halperin, A., and Williams, D. R. M., Liquid crystalline polymers as ising chains: stretching and swelling, *Europhys. Lett.*, **20**, 601–606 (1992).
- Harding, S. E., and Colfen, H., Inversion formulae for ellipsoid of revolution macromolecular shape functions, *Anal. Biochem.*, **228**, 131–142 (1995).
- Heo, Y., and Larson, R. G., The scaling of zero-shear viscosities of semi-dilute polymer solutions with concentration, *J. Rheol.*, **49**, 1117–1128 (2005).
- Hess, W., and Klein, R., Generalized hydrodynamics of systems of Brownian particles, *Adv. Phys.*, **32**, 173–283 (1983).
- Horita, K., Abe, F., Einaga, Y., and Yamakawa, H., Excluded volume effects on the intrinsic viscosity of oligostyrene and polystyrenes–solvent effects, *Macromolecules*, **26**, 5067–5072 (1993).
- Horita, K., Sawatari, N., Yoshizaki, T., Einaga, Y., and Yamakawa, H., Excluded volume effects on the transport coefficients of oligo(dimethylsiloxane) and poly(dimethylsiloxane) in dilute solution, *Macromolecules*, **28**, 4455–4463 (1995).
- Hsieh, C. C., and Larson, R. G., Modeling hydrodynamic interaction in Brownian dynamics: simulations of extensional and shear flows of dilute solutions of high molecular weight polystyrene, *J. Rheol.*, **48**, 995–1021 (2004).
- Jamieson, A. M., General discussion, *Faraday Symp. Chem. Soc.*, **18**, 223–224 (1983).
- Jamieson, A. M., and Telford, D., Newtonian viscosity of semi-dilute solutions of polystyrene in tetrahydrofuran, *Macromolecules*, **15**, 1329–1332 (1982).
- Jamieson, A. M., Gu, D., Chen, F. L., and Smith, S. R., Viscoelastic behavior of nematic liquid crystal monodomains containing liquid crystal polymers, *Prog. Polym. Sci.*, **21**, 981–1033 (1996).
- Jeffery, G. B., The motion of ellipsoidal particles immersed in a viscous fluid, *Proc. R. Soc. London Ser. A*, **102**, 161–179 (1923).

- Kempe, M. D., and Kornfield, J. A., Shear alignment behavior of nematic solutions induced by ultralong side-group liquid crystal polymers, *Phys. Rev. Lett.*, **90**, 115501 (2003).
- Kirkwood, J. G., and Riseman, J., The intrinsic viscosities and diffusion constants of flexible macromolecules in solution, *J. Chem. Phys.*, **16**, 565–573 (1948).
- Klein, J., The onset of entangled behavior in semidilute and concentrated polymer solutions, *Macromolecules*, **11**, 852–858 (1978).
- Konishi, T., Yoshizaki, T., and Yamakawa, H., On the universal constants  $\rho$  and  $\Phi$  of flexible polymers, *Macromolecules*, **24**, 5614–5622 (1991).
- Kraus, G., and Gruver, J. T., Rheological properties of multichain polybutadienes, *J. Polym. Sci. A*, **3**, 105–122 (1965).
- Kuhn, W., and Kuhn, H., Die Frage nach der Aufrollung von Fadenmolekeln in strömenden Lösungen, *Helv. Chim. Acta*, **26**, 1394–1465 (1943).
- Lee, H. C., and Brant, D. A., Rheology of concentrated isotropic and anisotropic xanthan solutions: 1. A rod-like low molecular weight sample, *Macromolecules*, **35**, 2212–2222 (2002).
- Lee, J. H., Goldberg, J. M., Fetters, L. J., and Archer, L. A., Linear viscoelastic behavior of symmetric and asymmetric star polymer solutions, *Macromolecules*, **39**, 6677–6685 (2006).
- Liu, P. Y., Yao, N., and Jamieson, A. M., Twist viscosity of side-chain liquid-crystalline polysiloxanes in a nematic solvent, *Macromolecules*, **32**, 6587–6594 (1999).
- Mackay, M. E., Tien, T. D., Tuteja, A., Ho, D. L., Van Horn, B., Kim, H. C., and Hawker, C. J., Nanoscale Effects leading to non-Einstein-like decrease in viscosity, *Nat. Mater.*, **2**, 762–766 (2003).
- Macosko, C. W., *Rheology: Principles, Measurements, and Applications*, Wiley-VCH, New York, 1994, Chap. 4.
- Manning, G. S., Limiting laws and counterion condensation in polyelectrolyte solution: I. Colligative properties, *J. Chem. Phys.*, **51**, 924–933 (1969).
- Mansfield, M. L., Douglas, J. F., Irfan, S., and Kang, E.-H., Comparison of approximate methods for calculating the friction coefficient and intrinsic viscosity of nanoparticles and macromolecules, *Macromolecules*, **40**, 2575–2589 (2007).
- Martin, A. F., Toward a referee viscosity method for cellulose, *Tappi J.*, **34**, 363–366 (1951).
- Mather, P. T., Pearson, D. S., Larson, R. G., Gu, D., and Jamieson, A. M., The origin of stress-oscillation damping during start-up and reversal of torsional shearing of nematics, *Rheol. Acta*, **36**, 485–497 (1997).
- McCammon, J. A., Deutsch, J. M., and Bloomfield, V., Low values of the Scheraga–Mandelkern  $\beta$  parameter for proteins: an explanation based on porous sphere hydrodynamics, *Biopolymers*, **14**, 2479–2486 (1975).
- McDonnell, M. E., and Jamieson, A. M., The molecular weight average obtained by combining quasielastic light scattering and intrinsic viscosity measurements, *J. Appl. Polym. Sci.*, **21**, 3261–3267 (1977).
- Mehl, J. W., Oncley, J. L., and Simha, R., Viscosity and the shape of protein molecules, *Science*, **92**, 132–133 (1940).
- Mendichi, R., Soltes, L., and Schieroni, A. G., Evaluation of radius of gyration and intrinsic viscosity molar mass dependence and stiffness of hyaluronan, *Biomacromolecules*, **4**, 1805–1810 (2003).
- Milner, S. T., and McLeish, T. C. B., Parameter-free theory for stress relaxation in star polymers, *Macromolecules*, **30**, 2159–2166 (1997).

- Morrison, R. T., and Boyd, R. N., *Organic Chemistry*, Allyn & Bacon, Boston, 1983, p. 85.
- Nishida, K., Kaji, K., and Kanaya, T., Theoretical calculation of reduced viscosity of polyelectrolyte solutions, *Polymer*, **42**, 8657–8662 (2001).
- Nishida, K., Kaji, K., Kanaya, T., and Fanjat, N., Determination of intrinsic viscosity of polyelectrolyte solutions, *Polymer*, **43**, 1295–1300 (2002).
- Ohshima, A., Kudo, H., Sato, T., and Teramoto, A., Entanglement effects in semiflexible polymer solutions: 1. Zero-shear viscosity of poly(*n*-hexyl isocyanate) solutions, *Macromolecules*, **28**, 6095–6099 (1995).
- Ohshima, A., Yamagata, A., Sato, T., and Teramoto, A., Entanglement effects in semiflexible polymer solutions: 3. Zero-shear viscosity and mutual diffusion coefficient of poly(*n*-hexyl isocyanate) solutions, *Macromolecules*, **32**, 8645–8654 (1999).
- Onogi, S., Kimura, S., Kato, T., Masuda, T., and Miyanaga, N., Effects of molecular weight and concentration on flow properties of concentrated polymer solutions, *J. Polym. Sci. C*, **15**, 381–406 (1966).
- Onogi, S., Masuda, T., Miyanaga, N., and Kimura, Y., Dependence of viscosity of concentrated polymer solutions upon molecular weight and concentration, *J. Polym. Sci. A-2*, **5**, 899–913 (1967).
- Ortega, A., and de la Torre, J., Hydrodynamic properties of rodlike and disklike particles in dilute solution, *J. Chem. Phys.*, **119**, 9914–9919 (2003).
- Pashkovskii, E. E., and Litvina, T. G., Twist viscosity coefficient of a dilute solution of the main-chain mesogenic polymer in a nematic solvent: an estimation of the anisotropy and the rotational relaxation time of polymer chains, *J. Phys. II*, **2**, 521–528 (1992a).
- Pashkovskii, E. E., and Litvina, T. G., Temperature dependences of the twist viscosity coefficient for solutions of comb-like mesogenic polymer in a nematic solvent: an estimation of the anisotropy and the rotational relaxation time of chains, *J. Phys. II*, **2**, 1577–1587 (1992b).
- Phillies, G. D. J., Hydrodynamic scaling of viscosity and viscoelasticity of polymer solutions, including chain architecture and solvent quality effects, *Macromolecules*, **28**, 8198–8208 (1995).
- Phillies, G. D. J., Self-consistency of hydrodynamic models for the zero-shear viscosity and the self-diffusion coefficient, *Macromolecules*, **35**, 7414–7418 (2002a).
- Phillies, G. D. J., Low-shear viscosity of nondilute polymer solutions from a generalized Kirkwood–Riseman model, *J. Chem. Phys.*, **116**, 5857–5866 (2002b).
- Phillies, G. D. J., and Quinlan, C. A., Analytic structure of the solutionlike–meltlike transition in polymer dynamics, *Macromolecules*, **28**, 160–164 (1995).
- Pochard, I., Boisvert, J.-P., Malgat, A., and Daneault, A., Donnan equilibrium and the effective charge of sodium polyacrylate, *Colloid Polym. Sci.*, **279**, 850–859 (2001).
- Raspaud, E., Lairez, D., and Adam, M., On the number of blobs per entanglement in semidilute and good solvent solution: melt influence, *Macromolecules*, **28**, 927–933 (1995).
- Rice, S. A., and Kirkwood, J. G., On an approximate theory of transport in dense media, *J. Chem. Phys.*, **31**, 901–908 (1959).
- Rouse, P. E., Jr., A theory of the linear viscoelastic properties of dilute solutions of coiling polymers, *J. Chem. Phys.*, **21**, 1272–1280 (1953).
- Roy-Chaudhury, P., and Deuskar, V. D., Rheological properties of concentrated polymer solutions: polybutadiene in good and theta solvents, *J. Appl. Polym. Sci.*, **31**, 145–161 (1986).
- Sato, T., Takada, Y., and Teramoto, A., Dynamics of stiff-chain polymers in isotropic solution. flexibility effect, *Macromolecules*, **24**, 6220–6226 (1991).

- Sato, T., Hamada, M., and Teramoto, A., Solution viscosity of a moderately stiff polymer: cellulose tris(phenyl carbamate), *Macromolecules*, **36**, 6840–6843 (2003).
- Shida, K., Ohno, K., Kimura, M., Kawazoe, Y., and Nakamura, Y., Dimensional and hydrodynamic factors for flexible star polymers in the good solvent limit, *Macromolecules*, **31**, 2343–2348 (1998).
- Shida, K., Ohno, K., Kawazoe, Y., and Nakamura, Y., Hydrodynamic factors for linear and star polymers on lattice under the theta condition, *Polymer*, **45**, 1729–1733 (2004).
- Simha, R., The influence of Brownian movement on the viscosity of solutions, *J. Phys. Chem.*, **44**, 25–34 (1940).
- Simha, R., A Treatment of the viscosity of concentrated suspensions, *J. Appl. Phys.*, **23**, 1020–1024 (1952).
- Simha, R., and Chan, F. S., Corresponding state relations for the Newtonian viscosity of concentrated polymer solutions: temperature dependence, *J. Phys. Chem.*, **75**, 256–267 (1971).
- Simha, R., and Somcynsky, T., The viscosity of concentrated spherical suspensions, *J. Colloid Sci.*, **20**, 278–281 (1965).
- Stockmayer, W. H., and Fixman, M., Dilute solutions of branched polymers, *Ann. N. Y. Acad. Sci.*, **57**, 334–352 (1953).
- Sunthar, P., and Prakash, J. R., Dynamic scaling in dilute polymer solutions: the importance of dynamic correlations, *Europhys. Lett.*, **75**, 77–83 (2006).
- Takahashi, Y., Isono, Y., Noda, I., and Nagasawa, M., Zero-shear viscosity of linear polymer solutions over a wide range of concentrations, *Macromolecules*, **18**, 1002–1008 (1985).
- Tanner, D. W., and Berry, G. C., Properties of cellulose acetate in solution: I. Light scattering, osmometry, and viscometry on dilute solutions, *J. Polym. Sci. Polym. Phys. Ed.*, **12**, 941–975 (1974).
- Texeira, R. E., Babcock, H. P., Shaqfeh, E. S. G., and Chu, S., Shear thinning and tumbling dynamics of single polymers in the flow gradient plane, *Macromolecules*, **38**, 581–592 (2005).
- Timasheff, S. N., Control of protein stability and reactions by weakly interacting cosolvents: the simplicity of the complicated, *Adv. Protein Chem.*, **51**, 355–432 (1998).
- Tominaga, Y., Suda, I., Osa, M., Yoshizaki, Y., and Yamakawa, H., Viscosity and hydrodynamic radius expansion parameters of oligo- and poly( $\alpha$ -methylstyrenes) in dilute solution, *Macromolecules*, **35**, 1381–1388 (2002).
- Utracki, L. A., and Simha, R., Corresponding state relations for the viscosity of moderately concentrated polymer solutions, *J. Polym. Sci. A*, **1**, 1089–1098 (1963).
- Utracki, L. A., and Simha, R., Viscosity of polymer solutions: scaling relationships, *J. Rheol.*, **25**, 329–350 (1981).
- Veerapaneni, S., and Wiesner, M. R., Hydrodynamics of fractal aggregates with radially varying permeability, *J. Colloid. Interface Sci.*, **177**, 45–57 (1996).
- Vega, D. A., Sebastian, J. M., Russel, W. B., and Register, R. A., Viscoelastic properties of entangled star polymer melts: comparison of theory and experiment, *Macromolecules*, **35**, 169–177 (2002).
- Wetzel, F. H., Elliot, J. H., and Martin, A. F., Variable shear viscometers for cellulose intrinsic viscosity determination, *Tappi J.*, **36**, 564–571 (1953).
- Yamakawa, H., *Modern Theory of Polymer Solutions*, Harper & Row, New York, 1971. [www.molsci.polym.kyoto-u.ac.jp/archives/redbook.pdf](http://www.molsci.polym.kyoto-u.ac.jp/archives/redbook.pdf).

- Yamakawa, H., Viscoelastic properties of straight cylindrical macromolecules in dilute solution, *Macromolecules*, **8**, 339–342 (1975).
- Yamakawa, H., *Helical Wormlike Chains in Polymer Solutions*, Springer-Verlag, Berlin, 1997.
- Yamakawa, H., and Fujii, M., Intrinsic viscosity of wormlike chains: determination of the shift factor, *Macromolecules*, **7**, 128–135 (1974).
- Yamakawa, H., and Fujii, M., Statistical mechanics of helical wormlike chains: I. Differential equations and moments, *J. Chem. Phys.*, **64**, 5222–5228 (1976).
- Yamakawa, H., and Yoshizaki, T., Effects of fluctuating hydrodynamic interaction on the hydrodynamic radius expansion factor of polymer chains, *Macromolecules*, **28**, 3604–3608 (1995).
- Yao, N., and Jamieson, A. M., Electrorheological behavior of side-chain liquid-crystal polysiloxanes in nematic solvents, *Macromolecules*, **30**, 5822–5831 (1997).
- Yao, N., and Jamieson, A. M., Transient shear flow behavior of dilute solutions of side-chain liquid-crystalline polysiloxanes in 4,4'-(*n*-pentyloxy)cyanobiphenyl, *Macromolecules*, **31**, 5399–5406 (1998).
- Yoshizaki, T., Nitta, I., and Yamakawa, H., Transport coefficients of helical wormlike coils: 3. Intrinsic viscosity, *Macromolecules*, **13**, 633–643 (1980).
- Yoshizaki, T., Nitta, I., and Yamakawa, H., Transport coefficients of helical wormlike coils: 4. Intrinsic viscosity of the touched-bead model, *Macromolecules*, **21**, 165–171 (1988).
- Zackrisson, M., and Bergenholtz, J., Intrinsic viscosity of core–shell particles, *Colloids Surf. A*, **225**, 119–127 (2003).
- Zhao, Y., Dong, S., Jamieson, A. M., Hu, X., Lal, J., Nazarenko, S., and Rowan, S. J., Rheological properties and conformation of a side-chain liquid crystal polysiloxane dissolved in a nematic solvent, *Macromolecules*, **38**, 5205–5213 (2005).
- Zimm, B. H., Dynamics of polymer molecules in dilute solution: viscoelasticity, flow birefringence and dielectric loss, *J. Chem. Phys.*, **24**, 269–278 (1956).
- Zimm, B. H., and Kilb, R. W., Dynamics of branched polymer molecules in dilute solution, *J. Polym. Sci.*, **37**, 19–42 (1959).
- Zimm, B. H., and Stockmayer, W. H., The dimensions of chain molecules containing branches and rings, *J. Chem. Phys.*, **17**, 1301–1314 (1949).

